REPUBLIC OF TURKEY
YILDIZ TECHNICAL UNIVERSITY
GRADUATE SCHOOL OF NATURAL AND APPLIED SCIENCES

INVESTIGATION OF ORTHOTROPIC STEEL DECK DESIGN USING FEM

ABDULLAH FETTAHOĞLU

PhD. THESIS
DEPARTMENT OF CIVIL ENGINEERING
PROGRAM OF STRUCTURAL ENGINEERING

ADVISER
ASSIST. PROF. DR. SERKAN BEKİROĞLU

İSTANBUL, 2015

REPUBLIC OF TURKEY
YILDIZ TECHNICAL UNIVERSITY
GRADUATE SCHOOL OF NATURAL AND APPLIED SCIENCES

INVESTIGATION OF ORTHOTROPIC STEEL DECK DESIGN USING FEM

A thesis submitted by Abdullah FETTAHOĞLU partial fulfillment of the requirements for the degree of **DOCTOR OF PHLOSOPHY** is approved by the committee on 01.07.2015 in Department of Structural Engineering, Civil Engineering Program.

Thesis Adviser
Assist. Prof. Dr. Serkan BEKİROĞLU
Yıldız Technical University

Approved By the Examining Committee
Assist. Prof. Dr. Serkan BEKİROĞLU
Yıldız Technical University ______________________

Prof. Dr. Yusuf AYVAZ, Member
Yıldız Technical University ______________________

Assoc. Prof. Dr. Barış SEVİM, Member
Yıldız Technical University ______________________

Assist. Prof. Dr. İ. Engin BAL, Member
İstanbul Technical University ______________________

Assist. Prof. Dr. Eleni SMYROU, Member
İstanbul Technical University ______________________

ACKNOWLEDGEMENTS

I would like to thank to my adviser Assist. Prof. Dr. Serkan BEKİROĞLU for his supports to this thesis during and till the end of my Ph.D. education. Special thanks given to my parents for their patience and spiritual permanent support during my Ph.D. education. Finally, I would like to thank as well to every member of examining committee composed of Prof. Dr. Yusuf AYVAZ, Assoc. Prof. Dr. Barış SEVIM, Assist. Prof. Dr. Engin BAL and Assist. Prof. Dr. Eleni SMYROU.

July, 2015

Abdullah FETTAHOĞLU

TABLE OF CONTENTS

LIST OF SYMBOLS

α	slope of rib web
ε_x	(Normal) strain in X direction
ε_y	(Normal) strain in Y direction
ε_z	(Normal) strain in Z direction
ε_{xy}	(Shear) strain in YZ plane and in Y direction
ε_{yz}	(Shear) strain in XZ plane and in Z direction
ε_{xz}	(Shear) strain in YZ plane and in Z direction
ε_e	Equivalent strain
I_R	Rib moment of inertia
N_i	Endurance stress range $\Delta\sigma_i$
σ_x	(Normal) stress in X direction
σ_y	(Normal) stress in Y direction
σ_z	(Normal) stress in Z direction
σ_{xy}	(Shear) stress in YZ plane and in Y direction
σ_{yz}	(Shear) stress in XZ plane and in Z direction
σ_{xz}	(Shear) stress in YZ plane and in Z direction
σ_e	Equivalent (v.- Mises) stress
$\Delta\sigma_{E,2}$	Equivalent constant amplitude stress range related to N_{max}
$\Delta\sigma_C$	Referece fatigue strength at $2x10^6$ cycles (normal stress)
γ_{Ff}	Partial factor for fatigue load intensity
γ_{Mf}	Partial factor for fatigue strength

LIST OF ABBREVIATIONS

APDL Ansys Parametric Design Language
EC Eurocode
EN European Norm
EPTOX (Normal) strain in X direction
EPTOY (Normal) strain in Y direction
EPTOZ (Normal) strain in Z direction
EPTOXY (Shear) strain in YZ plane and in Y direction
EPTOYZ (Shear) strain in XZ plane and in Z direction
EPTOXZ (Shear) strain in YZ plane and in Z direction
EPTOEQV Equivalent strain
FEA Finite Element Analysis
FEM Finite Element Method
MNMinimum
MXMaximum
RHPC Reinforced High Performance Concrete
SEA Sonlu Eleman Analizi
SEM Sonlu Eleman Metodu
SX (Normal) stress in X direction
SY (Normal) stress in Y direction
SZ (Normal) stress in Z direction
SXY (Shear) stress in YZ plane and in Y direction
SYZ (Shear) stress in XZ plane and in Z direction
SXZ (Shear) stress in YZ plane and in Z direction
SEQV Equivalent (v.- Mises) stress
UHPC Ultra High Performance Concrete
UMAX Maximum Displacement Vector Sum
USUM Displacement Vector Sum
UX Displacement in X direction
UY Displacement in Y direction
UZ Displacement in Z direction
YTU Yildiz Technical University

LIST OF FIGURES

Page

LIST OF TABLES

ABSTRACT

INVESTIGATION OF ORTHOTROPIC STEEL DECK DESIGN USING FEM

Abdullah FETTAHOĞLU

Department of Civil Engineering

PhD. Thesis

Adviser: Assist. Prof. Dr. Serkan BEKIROGLU

There are many orthotropic steel highway bridges in the world including damages, which are induced by either qualitative or quantitative reasons. Qualitative reasons of damages can be inadequate design, workmanship or material, whereas quantitative reasons are in general increased traffic loads and dimensions of load bearing structures. Most of these bridges especially built in Germany in 1960s show damages as a result of constantly increasing traffic density in heavy traffic lanes. In this thesis the quantitative reasons of damages in steel highway bridges will be assessed under conservative static wheel loads by changing one chosen unique dimension, while keeping other costants. So as to make this investigation possible, all dimensions and spans of orthotropic steel bridge are defined as variables in well known commercial FE- method programme ANSYS by means of APDL (Ansys Parametric Design Language).

In the first introductory chapter the history of orthotropic steel deck is summarized and famous bridges possessing orthotropic steel deck are given. Afterwards, the general design of orthotropic steel deck together with its load carrying components are introduced. Finally the methods used to analyse deck structure to obtain the internal forces and stresses are briefly explained.

In the second chapter, the ductility of steel ever known as non- linear material property, which causes stress relief with plastic hinge formation and increases the load carrying capacity of structures made of steel, and its contribution to stress calculations are investigated by means of Finite Element Method (FE- method). The ductility of steel is considered in stress calculations either as a simplification in calculations or directly incorporated into calculations as non- linear material property. For instance the stress calculation of truss structures is reduced in calculation of only normal forces aligned with members’ direction, due to plastic hinge formations, which indeed is consequence

of steel ductility. In case the form of structure composed of steel load- bearing components is complex because of geometry, not like truss members, the ductility of steel shall be taken into account by incorporating material non- linearity into stress calculations. The phenomenon, incorporating the complex geometry of steel components and material non- linearity in stress calculations can be achieved by means of FE- method. Steel orthotropic highway bridges, which are composed of deck- plate, longitudinal stiffeners going through cross – beams, cross- beams with cut- outs, main girders, bridge extensions for pedestrians, are extremely complex in geometry and are made of steel, which is ductile in nature. As a result, stress calculation of orthotropic steel bridge using FE- method is a perfect example for the investigation of ductility induced stress relief. The traditional constructional details and their dimensions of steel orthotropic highway bridges are given in Eurocode 3 Part 2. In the scope of this thesis, based on dimensions recommended in Eurocode 3 Part 2 and kinematic hardening material property of steel material, a FE- model of steel highway bridge is prepared. Results of calculations with and without material non- linearity are presented and compared with each other in order to demonstrate the decrease in stress because of steel ductility.

In the scope of the third chapter wearing coarse on deck plate is considered as uniformly distributed dead load. The dimensions of steel orthotropic bridge are chosen depending on Eurocode 3 Part 2 and a FE- model of orthotropic steel highway bridge will be prepared to analyze the effect of deck plate thicknesses of 12, 14 and 16 mm. Results of calculations will be presented and compared with each other in order to demonstrate the effect of deck plate on strain amplitudes, which are indicators of damages developed in structural parts of orthotropic steel deck.

In the fourth chapter, effects of cross beam web thickness and cross beam spacing on orthotropic steel bridge are assessed by means of a parameter study. Consequently, dimensional and constructional recommendations in association with cross beam thickness and spacing are presented.

In the fifth chapter, fatigue lives of four fatigue sensitive structural parts of orthotropic steel bridge are calculated. These are critical section in web of cross girder due to cut-outs, weld connecting deck plate to trapezoidal rib, continuous longitudinal stringer and deck plate. Finally, required thicknesses and spacings of these structural parts depending on their fatigue lives and design categories are given.

In the sixth chapter, moment of inertia of longitudinal stiffeners depending on cross-beam spacing is chosen as recommended in Eurocode 3 Part 2. The results of FE-analyses performed in this thesis state a numerical proof and validity for recommendations of Eurocode 3 Part 2 regarding longitudinal stiffener and cross beam spacing.

In the seventh chapter, it is focused on trapezoidal ribs, since they are dominantly used in industry. Three different slopes of trapezoidal rib web are assessed using FE- method, while rib width, height, spacing, span and thickness are kept constant. Results show that stresses especially in cross- beam and deflections of deck plate change depending on slope of trapezoidal stiffener webs.

In the eight chapter, effect of Elastic moduli, Poisson ratio and thickness of wearing surface on the stresses emerged in steel deck and wearing surface itself is investigated,while wearing surface is modeled by 3D finite elements, instead of considering as dead load.

In the ninth chapter, rib width to height and rib spacing to deck plate thickness ratios are assessed by means of the stresses developed under different ratios of these parameters. Afterwards necessary FE-analyses are performed to reveal the stresses developed under different rib width to height and rib spacing to deck plate thickness ratios. Based on the results obtained in this thesis, recommendations regarding these ratios are provided for orthotropic steel deck occupying trapezoidal ribs.

In the last section results and discussions obtained so far are restated and a summary of all chapters is given.

Key words: FEM, orthotropic steel deck, highway bridges, kinematic hardening, ductility, cross- beam, deck plate, fatigue, logitudinal stiffener,stress analysis, wearing surface, bonding layer, Eurocode 3.

ÖZET

ORTOTROPİK ÇELİK TABLİYE TASARIMININ SEM KULLANILARAK İNCELENMESİ

Abdullah FETTAHOĞLU

İnşaat Mühendisliği Anabilim Dalı

Doktora Tezi

Tez Danışmanı: Yrd. Doç. Dr. Serkan BEKİROĞLU

Dünyada nicel veya nitel nedenlerden dolayı hasarlı bir çok ortotropik çelik karayolu köprüsü mevcuttur. Nicel nedenler arasında uygunsuz veya yanlış dizayn, işçilik veya malzeme kullanımı sayılırken, nitel nedenler olarak genelde trafik yükünde meydana gelen artış ve köprünün taşıyıcı sisteminin boyutlandırılması sayılır. Çoğunluğu 1960' lı yıllarda Almanya' da yapılmış olan bu köprülerde artan trafik/ taşıt yoğunluğu nedeniyle özellikle ağır taşıt şeritinde hasarlar görülmektedir. Bu çalışmada çelik karayolu köprülerinde hasar oluşumuna sebeb olan nitel nedenler konservatif statik tekerlek yükleri kullanılarak araştırılmaktadır. Araştırma esnasında köprü taşıyıcı sisteminin bir boyutu sürekli değiştirilirken diğer tüm boyutlar sabit tutulmaktadır. Bu araştırmayı yapabilmek için ortotropik çelik köprüyü oluşturan taşıyıcı elemanların her birinin boyut ve açıklıkları ANSYS- SEM (Sonlu Eleman Metodu) programında değişken olarak tanımlanmaktadır. Bunun için APDL (ANSYS Parametrik dizayn kodu) kullanılarak bir algoritma yazılmıştır.

Giriş bölümünde ortotropik çelik tabliyelerin tarihsel gelişimi özetlenerek tanınmış ortotropik çelik köprülerden örnekler verilmiştir. Daha sonra, ortotropik çelik tabliyelerin genel dizaynı taşıyıcı sistem elemanlarıyla birlikte tanıtılmaktadır. En sonunda ise ortotropik çelik tabliyedeki iç kuvvet ve gerilmeleri elde etmek için kullanılan analiz metodları verilmektedir.

İkinci bölümde çeliğin sünekliği, yani doğrusal olmayan malzeme davranışı (bünye deklemi) SEM ile incelenmektedir. Çeliğin sünek savranışı plastik mafsal oluşumuna sebeb olarak gerilme değerlerinin azalmasına ve yapı elemanlarının taşıma gücününartmasına neden olmaktadır. Gerilme hesaplarında çeliğin sünekliği ya

hesaplarda basitleştirmeler yapılarak ya da doğrusal olmayan bünye denklemleri vasıtasıyla göz önüne alınmaktadır. Örneğin çelik kafeslerin gerilme hesabında çeliğin sünek davranışı çubukların birleşim noktalarında mafsallı oldukları varsayımıyla işlemlerin basitleştirilmesi olmaktadır. Çelik taşıyıcı sistemin bu basitleştirmeye olanak vermeyecek derecede karmaşık bir geometriye sahip olması durumunda, çeliğin sünekliğini hesaplarda göz önüne alabilmek için doğrusal olmayan bünye denklemleri doğrudan hesaplarda göz önüne alınmaktadırlar. Çelik taşıyıcı sistem elemanlarının karmaşık geometrilerini ve doğrusal olmayan malzeme davranışını gerilme hesaplarında bir arada göz önüne almak ancak SEM ile mümkün olmaktadır. Tabliye levhası, enleme kirişlerin içiden geçen boyuna nervürler, oyuk enleme kirişler, ana taşıyıcı kirişler ve yayaların geçişine olanak sağlayan köprü eklentilerinin oluşturduğu ortotropik çelik köprüler hem sünek davranış gösteren çelik malzemeden yapılmışlardır hem de karmaşık bir geometriye sahiptirler. Sonuç olarak, ortotropik çelik köprülerin gerilme hesabı çeliğin sünek davranışı nedeniyle gerilme azalması konusunu incelemek için mükemmel bir örnek teşkil etmektedir. Ortotropik çelik karayolu köprülerinin geleeksel detay ve boyutları Eurocode 3 Kısım 2 de verilmektedir. Bu çalışmanın kapsamında Eurocode 3 Kısım 2' de önerilen boyutlara ve çeliğin doğrusal olmayan malzeme davranışını temsil eden bünye denklemlerine dayanılarak köprünün bir SE- modeli hazırlanmaktadır. Süneklik nedeniyle gerilmelerde oluşan azalmanın gösterilmesi için hesaplar doğrusal ve doğrusal olmayan malzeme davranışları gözetilip tekrarlanmakta ve bulunan sonuçlar birbirleriyle karşılaştırılmaktadırlar.

Bölüm 3 kapsamında ortotropik çelik tabliye kaplaması üniform yayılı yük olarak idealize edilmektedir. Ortotropik çelik köprünün boyutları Eurocode 3 Kısım 2' ye göre seçilerek köprü analizi için tasarlanmış bir SE- modeli ile incelenmiştir. Bu incelemede ortotropik çelik tabliye levhası kalınlığının 12, 14 ve 16 mm olması durumlarının sonuçlara etkileri araştırılmaktadır. Tabliye levhasının genleme değerleri üzerindeki etkisini ortaya koymak amacıyla hesap sonuçları birbirleriyle karşılaştırılarak sunulmaktadırlar. Bu genleme değerleri çelik köprünün taşıyıcı elamanlarında ortaya çıkan hasar büyüklüğünün göstergesi niteliğindedirler.

Bölüm 4' de enleme kirişin gövde et kalınlığı ve açıklığının gerilme sonuçlarına etkisi araştırılmaktadır. Sonuç olarak enleme kirişin et kalınlığı ve açıklığına bağlı olarak boyutsal ve konstrüktif kurallar verilmektedir.

Bölüm 5' de köprünün yorulma mukavemeti açısından hasar oluşumuna hassas dört bölgesi için yorulma ömrü hesaplanmaktadır. Bu bölgeler enleme kirişin oyulmuş kesiti, tabliye lavhasını boyuna nervüre bağlayan kaynaklar, boyuna nervürlerin kendileri ve tabliye levhasının kendisidir. En sonunda bu dört bölgenin yorulma ömürleri ve dizayn kategorilerine bağlı olarak sahip olmaları gereken boyut ve açıklıklar verilmektedir.

Bölüm 6' da enleme kiriş açıklığına bağlı olarak boylama nervürlerin atalet momentleri Eurocode 3 Kısım 2' de önerildiği gibi seçilmektedir. Bu çalışmada yapılan Sonlu Eleman Analizleri (SEA) sonuçları Eurocode 3 Kısım 2' de verilen önerileri doğrulamaktadırlar.

Bölüm 7' de trapez boyuna nervürlere yoğunlaşılmaktadır, çünkü trapez boyuna nervürler endüstride sıkça kullanılmaktadırlar. Trapez boyuna nervürlerin gövde eğiminin sonuçlara etkisi diğer boyutlar sabit tutularak SEM ile incelenmektedir. Sonuçlar göstermektedir ki, özellikle enleme kirişlerde ortaya çıkan gerilmeler ve tabliye levhasında gerçekleşen deplasmanlar trapez nervürlerin gövde eğimlerine bağlı olarak değişmektedirler.

Bölüm 8' de tabliye levhası ve üstündeki kaplama içindeki gerilmelerdeki değişim kaplamanın elastik modulü, Poison oranı ve kalınlığına bağlı olarak incelenmektedir.

Bölüm 9' da boylama nervürün genişliğinin yüksekliğine ve nervürler arası mesafenin tabliye levhası kalınlığına oranları, bu parametrelerin farklı değerleri için ortaya çıkan gerilmeler aracılığıyla incelemektedir. Bu çalışmada elde edilen sonuçlara dayanılarak trapez nervürlere sahip ortotropik çelik tabliyeler için önerilerde bulunulmaktadır.

Son bölümde bulunan tüm sonuçlar belirtilerek üzerlerinde tartışılmakta ve tüm bölümlerin özeti verilmektedir.

Anahtar Kelimeler:SEM, ortotropik çelik tabliye, karayolu köprüleri, kinematik pekleşme, süneklik, enleme kiriş, tabliye levhası, yorulma mukavemeti, boyuna nervür, gerilme analizi, tabliye üst kaplaması, bağ katmanı, Eurocode 3.

CHAPTER 1

INTRODUCTION

1.1 Literature Review

Construction of orthotropic decks with deck plate, cross-beams and trapezoidal ribs going through the cut-outs in cross beam webs started approximately in 1965 and is still widely used in industry [1]. Orthotropic deck structure is a common design, which is used worldwide in fixed, movable, suspension, cable-stayed, girder, etc. bridge types. In Japan, Akashi Kaikyo suspension bridge, Tatara cable-stayed bridge [2], Trans-Tokyo Bay Crossing steel box-girder bridge [3], which are among the longest bridges in the world, have orthotropic deck structure. In France Millau viaduct has a box girder with an orthotropic deck with trapezoidal stiffeners [4]. In England, Germany and Netherlands there are a lot of steel highway bridges having orthotropic decks [1]. In USA San Francisco Oakland Bay Bridge, Self Anchored Suspension Span in California and in Italy Strait of Messina Bridge are examples of orthotropic steel bridges. In Turkey, the Golden Horn Bridge, First Bosphorus Bridge and Fatih Sultan Mehmet Bridge are also examples of orthotropic steel bridges [5]. In Troitsky [6], Huang et al. [7], Hoorpah [9], Korniyiv [9], and Choi et al. [10], Design Manual of Orthotropic Bridge- 2[11] examples of bridges, in which orthotropic deck is used, are given in detail. Moreover, a lot of researchs are completed with respect to this subject since 1950s [12- 21]. The spacings of longitudinal stringer and cross beam are in general 300 mm and 3 m to 5 m respectively. In addition to orthotropic deck structure, wearing surface lying on deck plate and main girders transmitting load to supports are two important components of orthotropic bridges. While wearing surface might be of asphalt or concrete, main girder might be of a girder, a truss, a cable-stayed or a tied arch system.Orthotropic decks resist against corrosion by means of traditional anti-corrosive paintings used in industry.

The top of the orthotropic deck is covered by wearing course and individual ribs are sealed with end plates to prevent moisture from entering the interior of the rib [11].Deck plate forms the flanges of ribs, cross-beams and main girders, hence leads an integral behavior of whole orthotropic deck and results in fewer material use. The closed ribs became dominant on open ribs in industry, because they have much more torsional, buckling rigidities, distribute wheel loads much better on deck plate, require half amount of welding than open ribs, provide less steel material needed in bridge orthotropic deck and so lighter dead load, which makes them also cost effective against orthotropic decks of open ribs. As a result they have become inevitable part of orthotropic decks to span long distances. In Figure 1.1 types of closed ribs are given as trapezoidal, U-shaped and V-shaped forms, in which trapezoidal ribs became paramount in time.

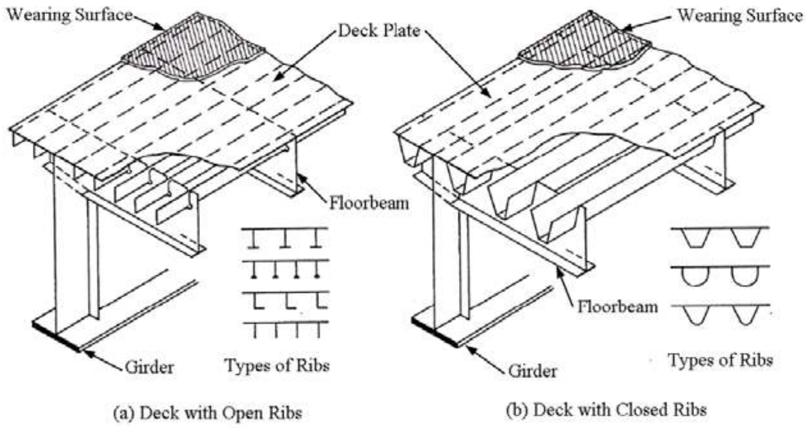

Figure 1.1 Orthotropic deck with open and closed ribs [11, 22].

Experienced cracks in orthotropic bridges revealed that the design of orthotropic decks should be performed with respect to fatigue analysis because of repetitive wheel loads varying in type and magnitude. Therefore the fatigue strengths of orthotropic deck details are provided by engineering standard, Eurocode 3 Part 1-9 [23]. To calculate stresses developed under wheel loads the solution method chosen shall enclose the entire bridge geometry, which can be achieved today using FE- method instead of conventional analytical and numerical methods used in the history in the absence of FE-method. In addition to the correct analysis and correct design of orthotropic decks, their fabrication, shipping to construction area and workmanship should be done flawlessly with care to obtain the desired service life. For that reason all steps until and during the construction of orthotropic decks require necessary quality control measures so as to provide the required service life. Because of their higher initial costs, if orthotropic steel decks are produced under permanent surveillance of quality control measures, they can supply a 100 year service life, which is demonstrated by laboratory studies [11].

After this introductory first chapter, considering kinematic hardening in stress calculation of orthotropic steel decks is handled in chapter 2. Afterwards, effect of deck plate thickness on structural behavior of steel orthotropic deck is investigated in chapter 3. Then, in chapter 4effect of cross- beam on stresses revealed in orthotropic steel deck is evaluated. Next, arranging thickesses and spacings of orthotropic deck for desired fatigue life and design category is researced in chapter 5. In chaper 6, a FE- analysis study conforming recommendations of Eurocode 3 Part 2 regarding rib dimensions and cross- beam spacing is performed. In chapter 7, an assessment on web slope of trapezoidal rib in orthotropic decks using FE- method [24- 44] is done. Subsequently, recommended properties of elastic wearing surfaces on orthotropic steel decks are investigated in chapter 8. In chapter 9, optimizing rib width to height and rib spacing to deck plate thickess ratios in orthotropic decks is investigated. Consequently, results and discussions are provided in the last chapter 10.

1.2 Objective of the Thesis

There are many orthotropic steel highway bridges in the world including damages, which are induced by either qualitative or quantitative reasons. Qualitative reasons of damages can be inadequate design, workmanship or material, whereas quantitative reasons are in general increased traffic loads and dimensions of load bearing structures. Most of these bridges especially built in Germany in 1960s show damages as a result of constantly increasing traffic density in heavy traffic lanes. The aim of this thesis is to investigate the quantitative reasons of damages in steel highway bridges under conservative static wheel loads using FE- method by changing one chosen unique dimension, while keeping others costant. So as to make this investigation possible, all dimensions and spans of orthotropic steel bridge are defined as variables in well known commercial FE- method programme ANSYS by means of APDL (Ansys Parametric Design Language).

1.3 Hypothesis

A lot of research and study are done worldwide so far related to steel orthotropic bridges. However still analysis and design methods of steel orthotropic deck are not completely clear and effect of all dimensions of steel orthotropic deck on the stresses developed in itself is not completely and in detail known. Hence, this thesis searches and provides magnitude of the dimensional effects on the stresses of steel orthotropic bridge and makes analysis and design method of it as celar as possible. For that reason, several FE- analyses are performed in this thesis and the design method of a steel orthotropic bridge to supply 100 years servive life is summarized in the last chapter.

1.4 Conventional Calculation Methods

Bridges possessing orthotropic steel decks are subjected to fluctuating wheel loads of different magnitudes. Wheel loads are first dispersed by wearing course and introduced in deck plate. Subsequently, longitudinal stringers transmit wheel loads to cross beams. Finally wheel loads are transferred from cross beams over main girders to the supports. Although an orthotropic deck forms an integrated structure to resist against wheel loads, the assumed load transmitting scheme is generally accepted as given in Figure1.2.

System	Action	Figure	Result
1	Local deck plate deformation	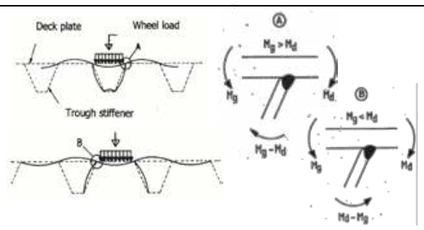	Transverse flexural stress in deck plate and rib.
2	Panel deformation	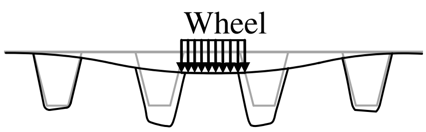	Transverse deck stress from rib differential displacements

Figure 1.2 (cont'd)

3	Rib longitudinal flexure	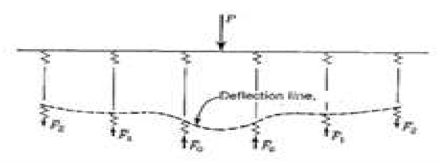	Longitudinal flexure and shear in rib acting as a continuous beam on flexible floorbeam supports
4	Cross-beam in-plane flexure	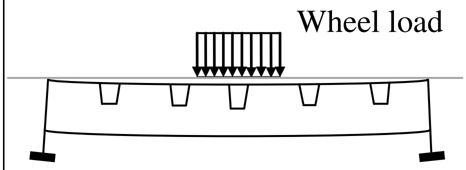	Flexure and shear in cross-beam acting as beam spanning between rigid girders
5	Cross-beam distortion	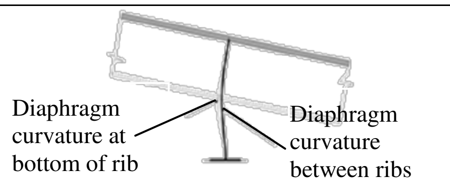	Out-of-plane flexure of cross-beam web at rib due to rib rotation
6	Rib distortion	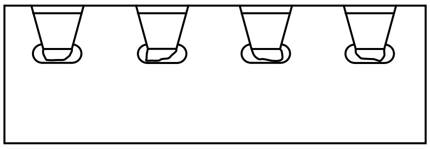	Local flexure of rib wall due to cross-beam cut- out
7	Global	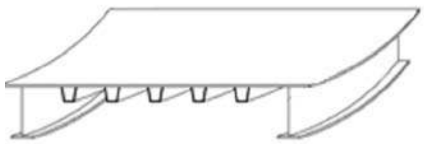	Axial, flexural, and shear stresses from supporting girder deformations.

Figure 1.2 Decomposing of orthotropic bridge deck into subsystems [11].

1.5 Analysis of Orthotropic Deck using FE- Method

So as to compare stresses developed under different structural thicknesses, spacings and spans, all dimensions of the bridge shall be defined as variables in ANSYS [45]. Therefore an algorithm to provide this condition is written by means of APDL (Ansys Parametric Design Language). Afterwards thicknesses, spacings and spans of structural parts, which are of interest, are entered in ANSYS using this algorithm. Stresses developed under different parameter values are given in the subsequent sections. The FE-model of the bridge is generated using SHELL 181, which is illustrated in Figure1.3. In Chapter 8, in addition to SHELL 181, which is used to model steel load carrying members of the bridge, SOLID 185, which is given in Figure1.4, is also used to model wearing course on steel deck.

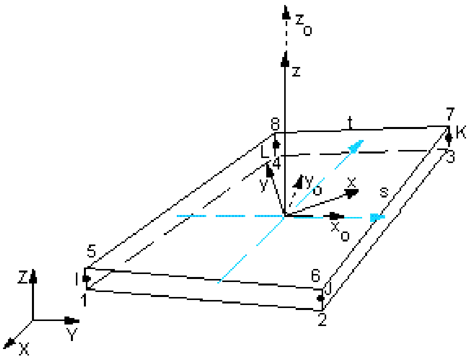

x_o = Element x- axis , if x is not defined by user.

x = Element x-axis, which is defined by user.

Figure 1.3 SHELL 181 finite element, which is used in this thesis to model steel load carrying members [45].

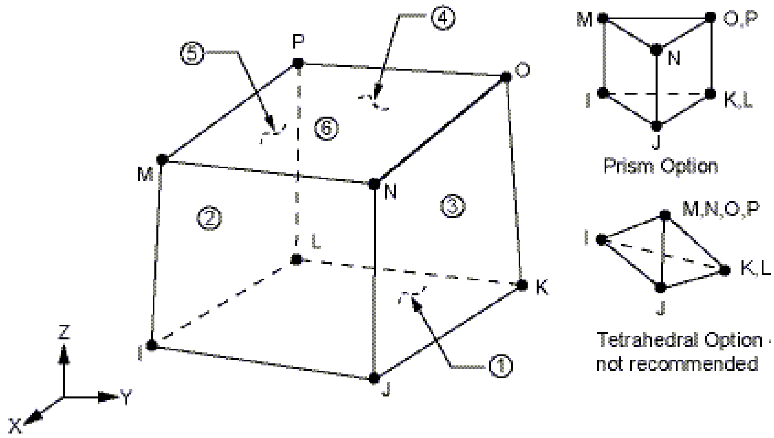

Figure 1.4 SOLID 185 finite element, which is used in this thesis to model linear elastic wearing course on steel deck [45].

The FE-model of Huurman et al. [46] inspired the researcher to create FE-model of the bridge used in this research [47- 51]. However, in the FE-model, which is generated using ANSYS [45] and used in this thesis, stiffened main girder and pedestrian road are also generated, which are not included in the FE-model of Huurman et al. [46] (See Figure1.5 and 1.6). Because of mesh refinement process the number of nodal unknowns increase excessively and as a result spans of the bridge used in this research are chosen as short as possible. Figure1.7 depicts the perspective front view of the whole orthotropic steel bridge, whereas Figure1.8 presents the conservative static wheel loading employed in chapter 3 through chapter chapter 9. To decrease further the number of nodal unknowns solely the quarter of the bridge shown in Figure1.9 is modeled by applying the necessary boundary conditions and used in chapter 3 through chapter 9. As necessary conditions, it is meant first the symmetry resraints applied on the mid lines passing through the bridge' longitudinal and transversal directions. On the bridge' s mid line aligned on global Y- axis all rotations as to Y and Z- axes and displacements along X- axis are set to zero. Similarly, on the bridge's mid- line aligned on global X- axis all rotations as to X and Z- axes and displacements along Y axis are set to zero. Second, the restraints applied on the physical point of the bridge, which is in contact with the real support in practice are set to zero. These are displacements in global Z- axis and and all rotations at the bridge support point, which is depicted in

Figure 1.9. In chapter 2, a different traffic loading is used and is presented relevantly in this chapter. Width of pedestrian road and deck plate in transverse direction are 1.1 m and 6.3 m respectively, while width of deck plate changes, when rip width and/ or spacing changes.

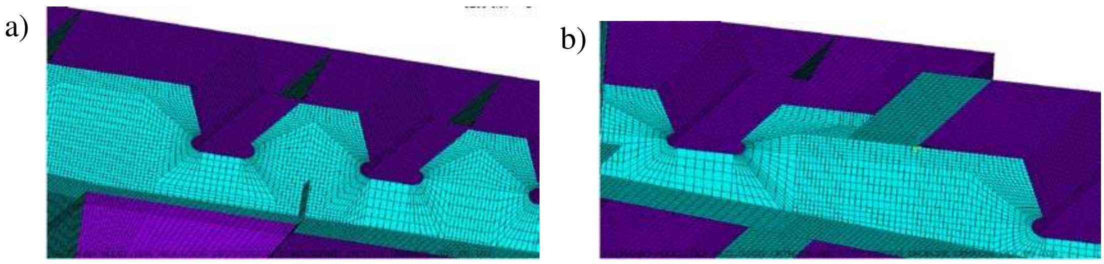

Figure 1.5 a) Connection of cross-beam to main girder. b) Connection of deck plate to pedestrian road.

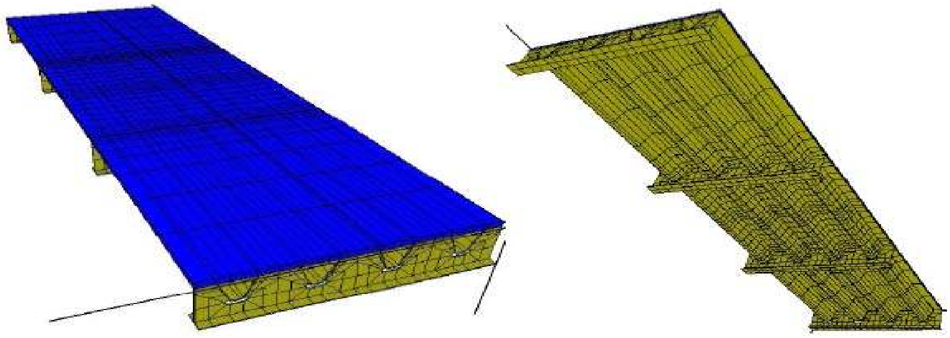

Figure 1.6 Huurman's FE- model for orthotropic steel bridge [46].

The bridge analyzed in this thesis spans 6 m in longitudinal direction and has two stiffened main girders at supports, one normal main girder at field (outside support areas), 2 exterior ribs at each side, 5 interior ribs in the middle, 1 rib in each main girder and 1 rib in each pedestrian road. The initial height, width and spacing of the ribs used in orthotropic deck are 275 mm, 300 mm and 300 mm respectively. However, one of these parameters is changed in FE-analyses to evaluate its effect on results, while number of ribs and other dimensions are kept constant.

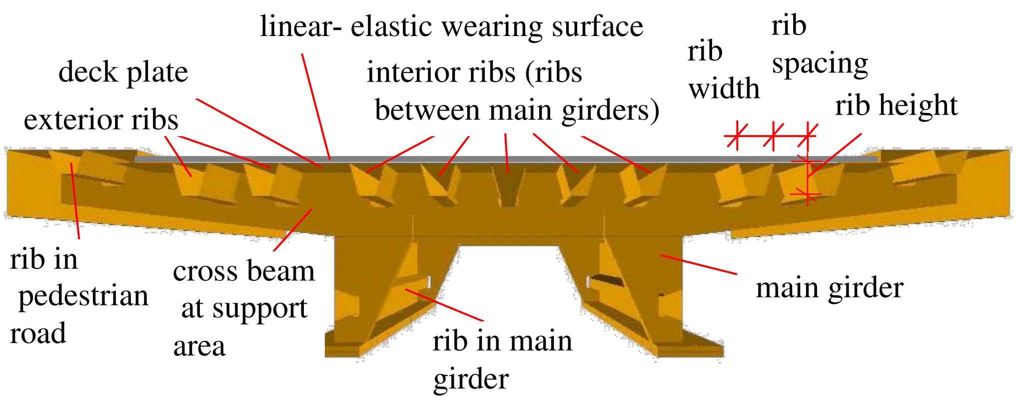

Figure 1.7 Traditional orthotropic steel bridge as to Eurocode 3 Part 2 [52].

According to Capital 3.2 of Eurocode 3 Part 1.1 [53] material properties of the selected steel material (S 355H) are given in Table 1.1. The characteristic yield strength given in Table 1.1 is used only in some cases in the FE- analyses to identify the stressed points of the structure, which are beyond the yield point. In general, since all stress, strain and displacement results are compared with each other to identify the effect of one unique dimension on the stresses, strains and displacements of the structure, the characteristic yield strength is not used for assessment of results. Some of the FE-analyses are based on geometric and material non-linear theories, details of which can be found in Fettahoglu and Bekiroglu [47] and in chapter 2.

Table 1.1 Material properties

Yield strength of steel (f_y)	355 N/mm^2	Shear module (G)	81 000 N/mm^2
Ultimate strength (f_u)	510 N/mm^2	Poisson ratio (υ)	0.3
Elasticity module (E)	210 000 N/mm^2	Density (ρ_{steel})	78.5 kN/m^3

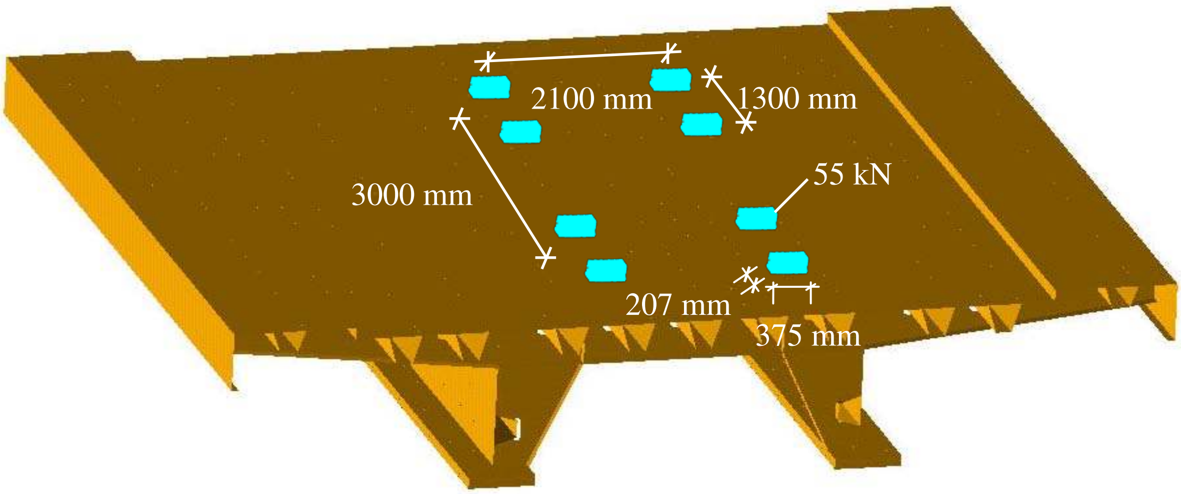

Figure 1.8 Wheel loads used in the FE-analyses

According to Capital 3 of Eurocode 3 Part 1.1 [53] a distributed load of 0.24 kN/ m² per cm of wearing surface having 75 mm thickness, which lies on deck plate, is assumed in the analyses done in all chapters except chapter 8. Because wearing surface is directly incorporated in FE- model and therefore its density is entered in ANSYS as a material property in chapter 8.

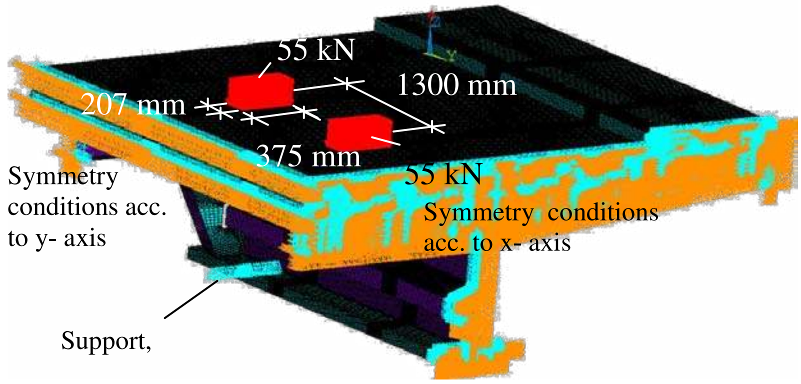

Figure 1.9 FE-model and boundary conditions of bridge quarter.

In this thesis first the solid model of FE- model is established based on the recommendations of Huurman et al. [46] and experience of the researcher. Second, the line element sizes, according to which number of elements and nodes in FE- model changes, are determined in chapter 2. As apparent from the Table 2.1, line element sizes determined relying on Mesh 4 results are edequate to be used throughout this thesis. The line element size determined in global X- axis is 6 mm. In global Y- axis the determined line element sizes are 25 mm and 6.25 mm outside wheel areas and inside wheel areas respectively. To explain the relationship between line element sizes and number of elements assume a plate, whih is formed with 4- node SHELL 181 finite elements and has sizes 4 m in global X- direction and 9 m in global Y- direction and mesh this plate as per line elements size of 10 mm in global X- direction and line element size of 20 mm in global Y- direction. The number of elements produces after meshing is calculated as (4000 / 10) x (9000 / 20) = 180 000. The number of nodes in this instance is calculated as ((4000 / 10)+1) x ((9000 / 20)+1) = 180 851. As a result if the loading is not changed, number of elements and nodes used with the same line element sizes are always same. The number of elements and nodes of the FE- model (See Figure 1.9) employed in all chapters except chapter 2 and chapter 9 are 284 010 and 293 491 respectively. In chapter 2 a mesh optimization is performed under different loading to specify the line sizes of solid model of FE- model. All meshes used in following subsequent chapters are based on this aforementioned line sizes. In chapter 9, the number of elements and nodes are 1 469 148 and 1 535 833 respectively, since the modeling of wearing surface with SOLID 185 brick elements causes huge increase of finite element and node numbers.

1.6 Determination of Most Unsuitable Wheel Load and Area for FE- analyses

The simulations done in all chapters except chapter 2 are performed using the most unsuitable wheel load and area for dimensioning of orthotropic decks. In this subchapter, the determination stages of this loading is explained. Table 1.2 indicates the footprints for the tyre named as 315/ 80 R22.5, which is used in front axle or used in rear axles instead of tandem wheels in heavy truck vehicles. The footprints of this wheel load is obtained considering different wheel load and tyre pressure [54].

Table 1.2 Comparison of footprints for tyre 315/80 R22.5 considering different tyre pressures.

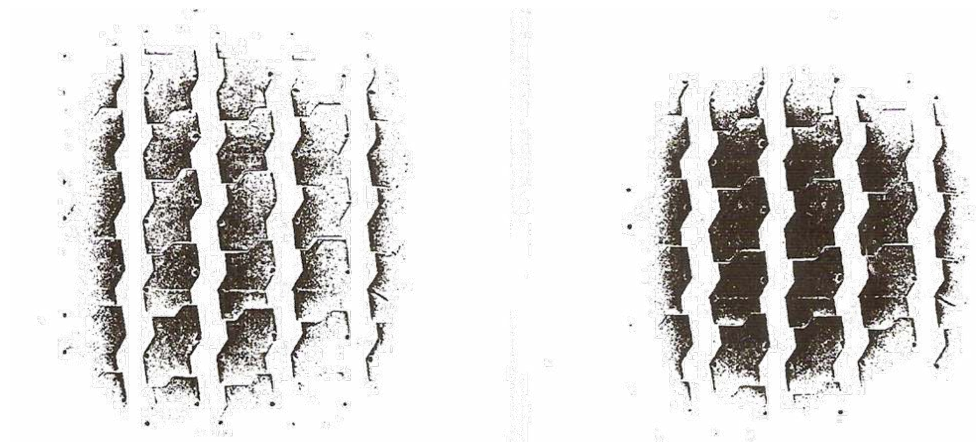

The different gray levels indicate the amount of contact pressure, left uniform distributed pressure, right concentration of pressure in the middle.

Tyre pressure	
5.0 bar	8.3 bar
Footprints area	
37 627 mm^2	26 107 mm^2
Wheel load	
25 286 N	27 883 N
Averaged contact pressure	
0.67 N/mm^2	1.07 N/mm^2
Maximum contact pressure	
2.78 N/mm^2	3.05 N/mm^2

Table 1.3 provides a comparison of wheel load areas with wheel load areas as per Eurocode 1 Part 3 [55], Table 4.8 for fatigue load model 2 and 4[56]. The comparison of wheel areas, which are of interest, is provided in Table 1.3.

Table 1.3 Comparison of tyre contact areas.

<table>
<tr><td colspan="3">Tyre 315/80 R22.5</td></tr>
<tr><td>Eurocode 1, Part 3
Table 4.8
Tyre art A</td><td>Tyre inflation 5.0 bar
Wheel load 2.53 t</td><td>Tyre inflation 8.3 bar
Wheel load 2.78 t</td></tr>
<tr><td>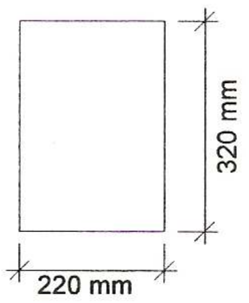
</td><td>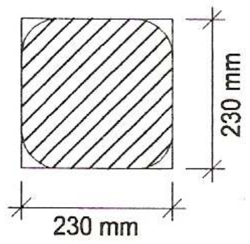
</td><td>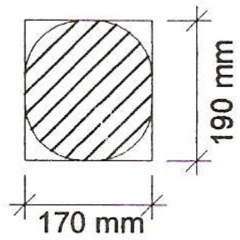
</td></tr>
</table>

Usage of tyre types in heavy truck vehicles is provided by Table 1.4 with respect to Eurocode 1 Part 3 [55].

Table 1.4 Usage of Tyre types in heavy truck vehicles.

Tyre type	Usage amount (%)
425/65 R22.5	1%
385/65 R22.5	34%
365/80 R20	12%
315/80 R22.5	8%
295/80 R22.5	8%
275/70 R22.5	2%

Usage of so called wide base tyres 425 or 385 is limited to be placed only in the nonmotorized rear axles so far. The permissible axle weight for rear axle is determined as 9 ton. The future vehicles are however is produced using single tyre called as 495/ 45

R22.5 (super single) for the motorized axle. The tyre 495/ 45 R.22.5 possesses a smaller wheel contact area than the tandem tyres called as 2x315/80 R22.5. Hence the wheel contact breadth reduces from 540 mm in 400 mm[57]. The tyre contact pressure depends generally on wheel load, tyre inflation, evironmental temperature and vehicle speed. [58] supplies wheel contact pressure depending on temperature and vehicle speed.In the scope of this thesis, effects of temperature and vehicle speed on tyre contact pressure and tyre contact area are ignored. Figure 1.10 proves that the static wheel loads are more conservative than dynamic transient wheel loads. Therefore, stresses and strains calculated in this thesis stay on the safe side, which is demonstrated in Figure 1.10, that vehiches rolling with slower speed lead to higher strains and stresses.

a)

b)

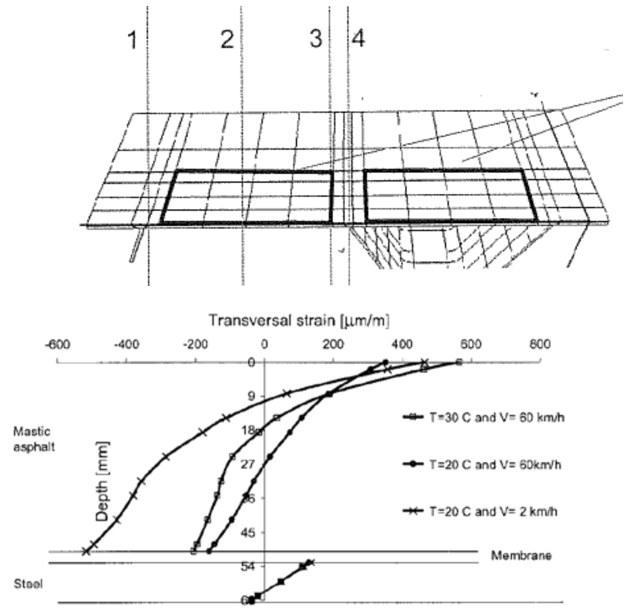

Figure 1.10 a) Wheel footprints. b) Stress state and damage at 20°C and different vehicle speeds (Dual- wheel load in the mid point of crossbeam).

Figure 1.11 Replacing of dual tyres with a super single tyre.

As mentioned before the aim of this subchapter is to determine the most unsuitable wheel loading according to Eurocode [55]. As a result Fatigue Load Model 2, which is a combination of idealized group of frequently employed heavy truck vehicles. These so called frequently used heavy truck vehicles are defined by,

- Axle number and distance between axles (Table 1.6, column 1 and 2),
- Frequently applied axle load(Table 1.6, column 3),
- Wheel load area and transversal distance between wheel loads (Column 4 of Table 1.6 and Table 1.5).

The maximum and minimum stresses shall be determined from the worst conditions of different heavy truck vehicles. Different heavy truck vehicles shall be considered seperately, that is every heavy truck vehicle rolls alone on its traffic lane. If one of heavy truck vehicle among all of them forms the worst (most suitable for FE- analyses) conditions, other vehicles are allowed not to be taken into account.

Table 1.5 Wheel contact areas.

Type of wheel area and axle	Geometry
A	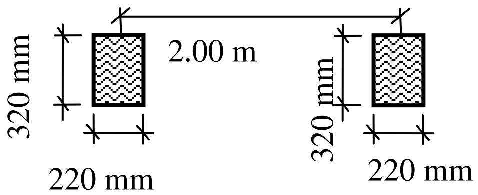
B	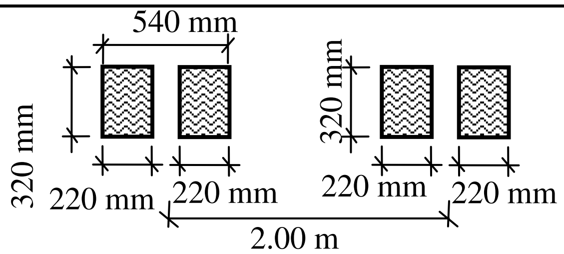
C	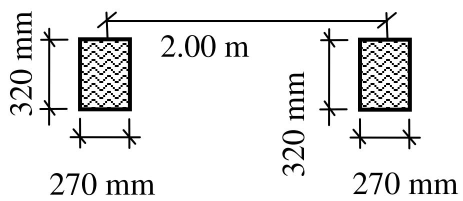

Table 1.6 Group of frequently used heavy truck vehicles.

1	2	3	4
View of heavy truck vehicle	Axle distance (m)	Frequently used axle load (kN)	Tyre type
	4.50	90	A
		190	B
	4.20	80	A
	1.30	140	B
		140	B
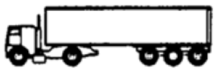	3.20	90	A
	5.20	180	B
	1.30	120	C
	1.30	120	C
		120	C
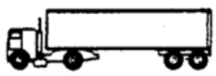	3.40	90	A
	6.00	190	B
	1.80	140	B
		140	B
	4.80	90	A
	3.60	180	B
	4.40	120	C
	1.30	110	C
		110	C

By means of symmetries in x and y axes solely the quarter of bridge geometry is modeled using finite elements. Conveniently, wheel loads and the arrangement of wheel areas must be chosen symmetrical according to X- and Y- axis. Nevertheless, arrangement of wheel loads given in Table 1.6 does not fulfil this symmetry condition. As a solution to this symmetry issue, only the wheels of nonmotorized rear axles are considered to build the wheel load arrangement of quarter FE- model, which means that the wheel loading used to reflect the effect of heavy truck vehicle is composed of expansion of wheel loads on quarter FE- model. The first three rows of Table 1.6 provide the arrangement of aferomentioned wheel loads on quarter FE- model. In this thesis only the arrangement (distances between wheel areas and axles) given in tables here is used in the FE- analyses of this thesis. Complying with this arragement the wheel contact areas and pressures are obtained by comparing the contact pressure values given in Table 1.7 with tyre types supplied by Eurocode [55, 56].

Table 1.7 Comparison of wheel areas with areas given in Eurocode.

<table>
<tr>
<td>ENV 1991 T 3
Tyre type B
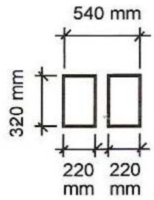

FLM 2 190 kN ≈ 0.675 N/mm^2</td>
<td>495/45 R 22.5
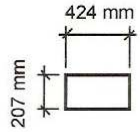

(Super Single tyre- NEW)
Motorized axle 110 kN 0.627 N/mm^2</td>
</tr>
<tr>
<td>ENV 1991 T 3
Tyre type B
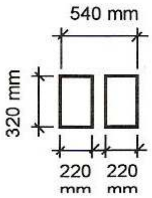

FLM 2 190 kN ≈ 0.675 N/mm^2</td>
<td>2 * 315/80 R 22.5
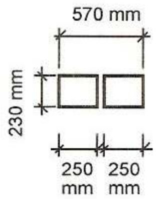

(Dual tyres- OLD)
Motorized axle 110 kN 0.478 N/mm^2</td>
</tr>
<tr>
<td>ENV 1991 T 3
Tyre type B
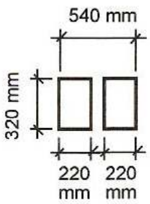

FLM 2 190 kN ≈ 0.675 N/mm^2</td>
<td>2 * 295/60 R 22.5
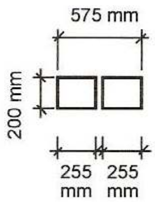

Motorized axle 110 kN 0.539 N/mm^2</td>
</tr>
</table>

Table 1.7 (cont'd)

ENV 1991 T 3 Tyre type C 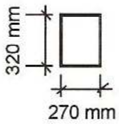 FLM 2 120 kN ≈ 0.694 N/mm^2	385/65 R 22.5 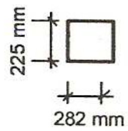 Motorized axle 90 kN 0.709 N/mm^2

As mentioned before, edges of wheel areas of FE- model in transverse direction must be dividable by 75 mm, because of the element mesh sizes contemplated at the initial phase of FE- modeling. Therefore the wheel areas given in Table 1.7 shall be replaced by adaptating wheel areas and using tyre type 3 as given in Table 1.8.

Table 1.8 Wheel loads and areas employed in FE- analyses.

385/65 R 22.5 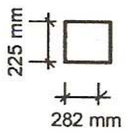 Motorized axle 90 kN 0.709 N/mm^2	Selected wheel load area for FE- model as tyre type C 225 mm 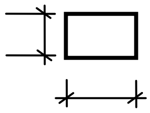 300 mm Motorized axle 90 kN ≈ 0.667 N/mm^2

Based o the wheel loading given in Table 1.7 it is decided that Super Single tyresare the most suitable tyres for FE- analyses. The super single tyres are started to be employed in traffic recently, but its usage is increasing. Nevertheless, it is seen from Table 1.4 that the percentage of using by dual tyres in traffic is 8%. As a result, these two types of tyres are selected for the most suitable wheel load area of tyre type B.Possible wheel loads for FE- model as tyre type B are gathered in Table 1.9 below.

Table 1.9 Possible wheel loads for FE- model as tyre type B.

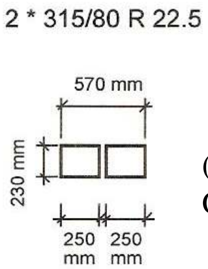 (Dual tyres- OLD) Motorized axle 110 kN ≈ 0.478 N/mm^2	Dual tyres- 1 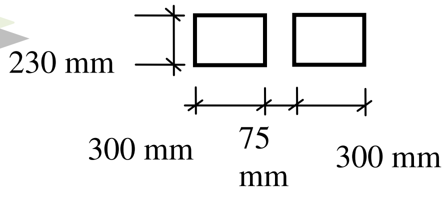 Motorized axle 110 kN ≈ 0.399 N/mm^2
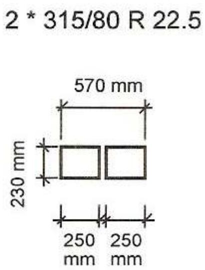 (Dual tyres- OLD)) Motorized axle 110 kN ≈ 0.478 N/mm^2	Dual tyres- 2 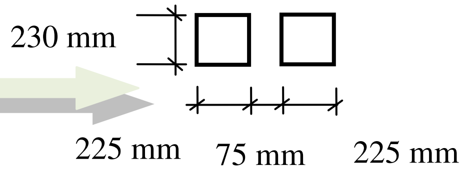 Motorized axle 110 kN ≈ 0.531 N/mm^2
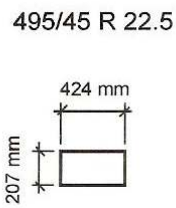 (Super Single tyres- NEW) Motorized axle 110 kN ≈ 0.627 N/mm^2	Super Single tyres- 1 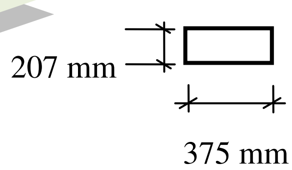 Motorized axle 110 kN ≈ 0.709 N/mm^2
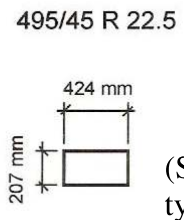 (Super Single tyres- NEW) Motorized axle 110 kN ≈ 0.627 N/mm^2	Super Single tyres- 2 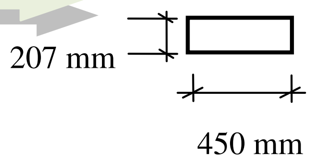 Motorized axle 110 kN ≈ 0.590 N/mm^2

In the FE- analyses done to determine the most unsuitable wheel load, weight induced by wearing surface on steel deck is ignored, since it is uniformly distributed over deck plate and very small in comparison to weight of steel structural parts.

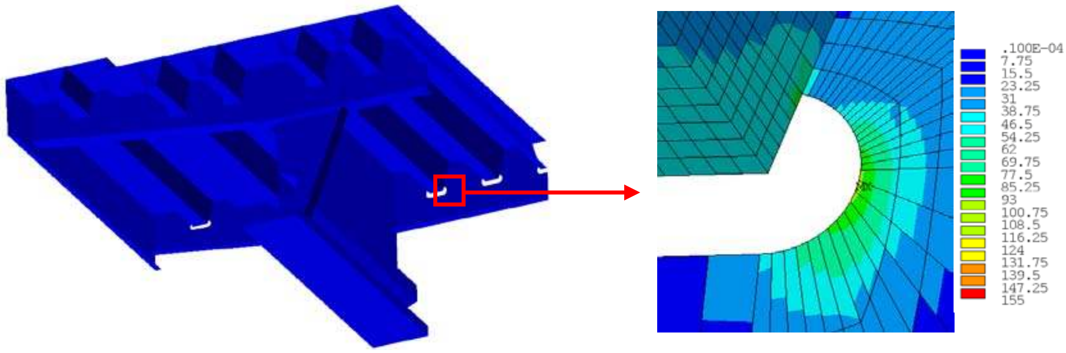

Figure 1.12 Distribution of v.- Mises- Stresses under dual tyre- 1. Maximum Stress is 98.467 MPa, while max. resultant displacement is 1.212 mm.

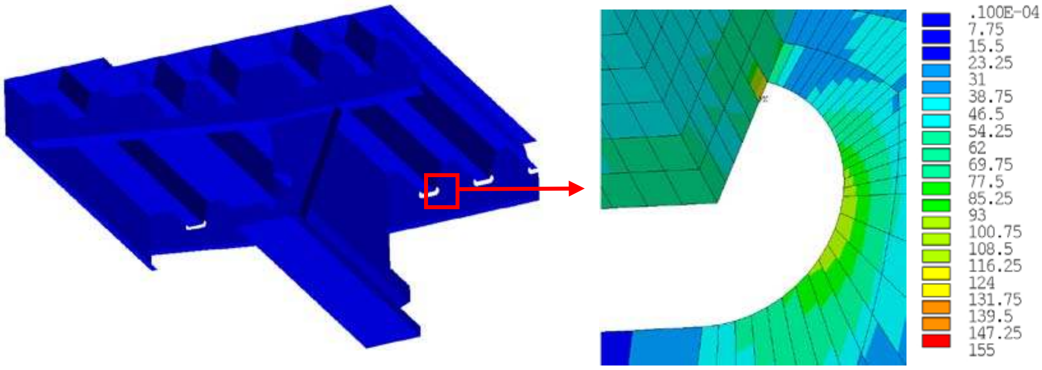

Figure 1.13 Distribution of v.- Mises- Stresses under dual tyre- 2. Maximum Stresses is 130.969MPa, while max. resultant displacement is 1.454 mm.

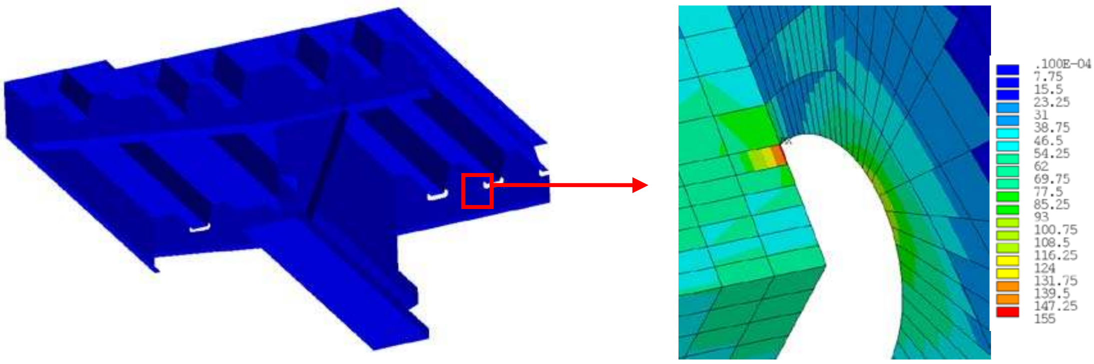

Figure 1.14 Distribution of v.- Mises- stresses under Super Single tyre- 1. Maximum Stress is 150.669 MPa, while max. resultant displacement is 1.450 mm.

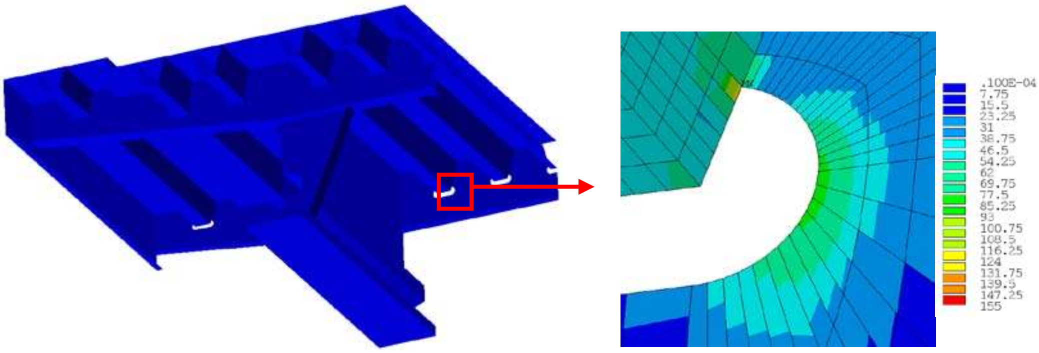

Figure 1.15 Distribution of v.- Mises- stresses under Super Single tyre- 2. Maximum Stress is 125.645 MPa, while max. resultant displacement is 1.216

It is apparent from evaluating of Figures 1.12- 1.15 that the most suitable wheel loading is Super Single tyre- 1 complying with tyre type B. Consequently, Super Single tyre is used with wheel (or tyre) areas of tyre type B in the FE- analyses. After determination of wheel areas, FE- analyses are performed as per Table 1.10.

Table1.10 FE- Model- loadings to obtain the most suitable loading for dimensioning of orthotropic steel deck.

View of heavy truck vehicle	FE- model- loading using nonmotorized axles
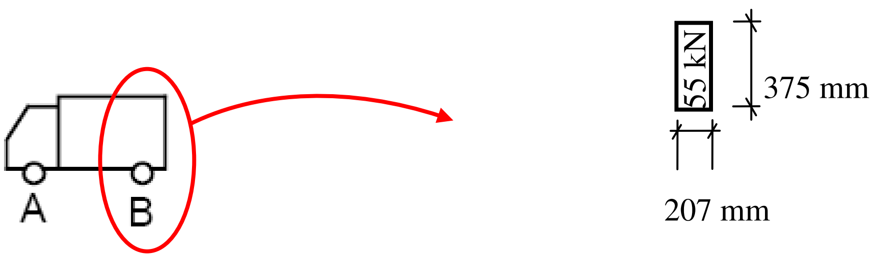	Simulation name = Super Single tyre- 1
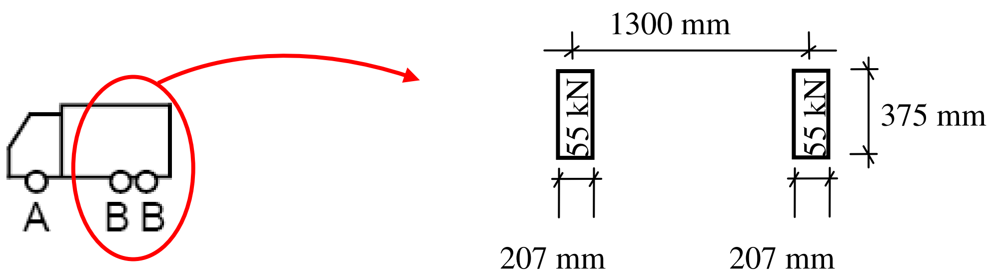	Simulation name = BB

Table 1.10 (cont'd)

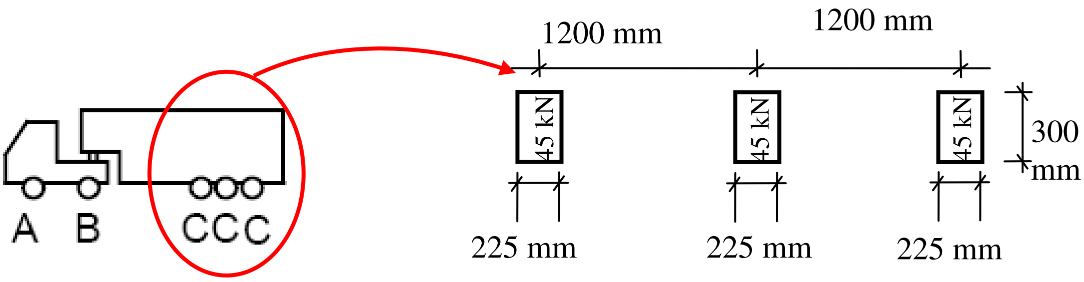	Simulation name = CCC. Here due to numerical obstacles (and due to small cross- beam spacing, 3m) axle spacing is reduced from 1.3 m in 1.2 m.

After simulations (FE- analyses) named as BB and CCC are performed, the loading of simulation BB is selected as the most suitable wheel loading to be used in the rest of this thesis, since the maximum deformation and v.- Mises- stress developed in simulation BB are higher than the values obtained from simulation CCC. Maximum deformation and stress obtained from BB are 1.729 and 255.279 MPa respectively, while the maximums obtained from CCC are 1.564 mm and 248.340 MPa respectively. To illustrate stress and deformation distribution obtained from the mentioned simulations Figure 1.16 and 1.17 are given below. Finally, the second row of Table 1.10 (BB) indicates the most suitable wheel loading, which is used in the rest of FE- analyses for investigation of dimensions of steel deck regarding stresses and strains developed in deck.

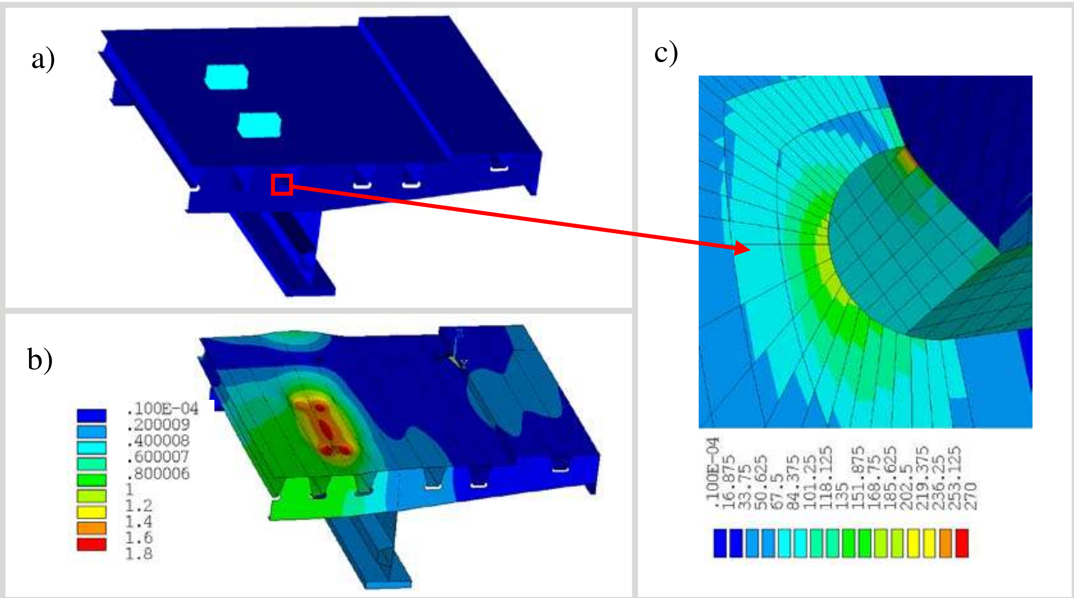

Figure 1.16 a) FE- model of simulation BB. b) Distribution of resultant displacement. c) Distribution of v.- Mises- stress.

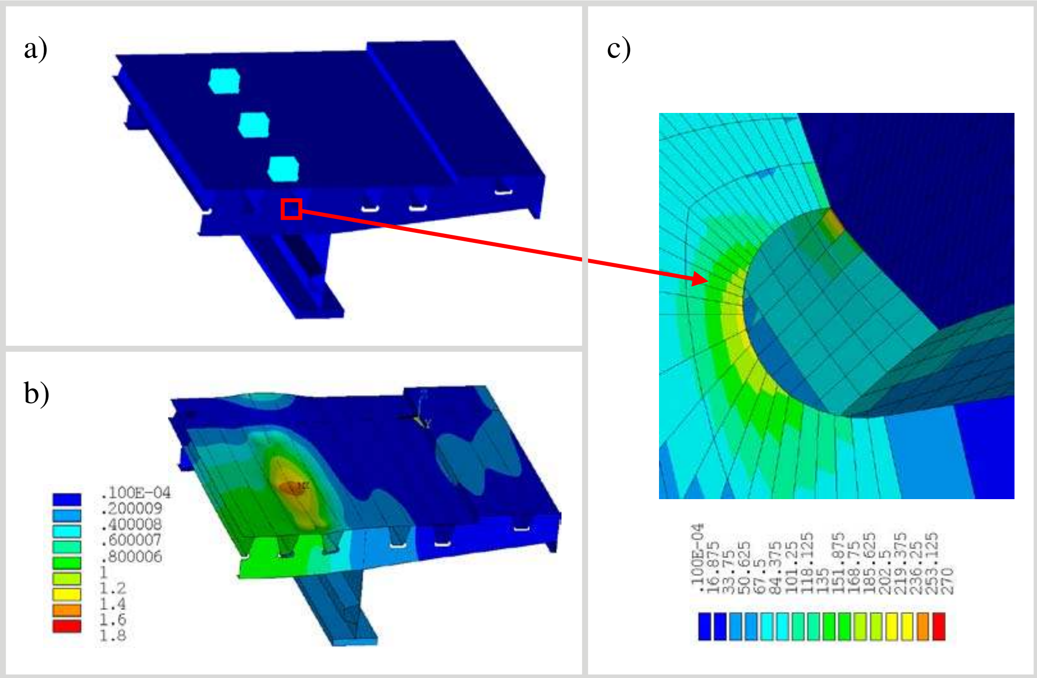

Figure 1.17 a) FE- model of simulation CCC. b) Distribution of resultant displacement. c) Distribution of v.- Mises- stress.

CHAPTER 2

EFFECT OF CONSIDERING KINEMATIC HARDENING IN STRESS CALCULATIONS

Effect of kinematic hardening in stress calculations is evaluated using the structural geometry of steel highway orthotropic bridge. Steel highway bridges are really adequate examples for kinematic hardening, since most of these bridges are today overloaded according to their initial design loads. Most of these bridges were designed especially in Germany in years 1960s. From that time to so far the number and weight of vehicles passing over these bridges increased heavily, so that the load bearing parts of the bridges are subject to more loads and more frequently than they are designed for. To indicate the effect of kinematic hardening, which is a property of structures made of steel, the bridge FE- model is loaded beyond its material yield point.

2.1 Geometric Nonlinearity

Since the finite element SHELL 181 embedded in ANSYS enables considering both geometric and material nonlinearities, it is used to model steel parts of bridge in this thesis. In this research the geometric nonlinearity is taken into account by means of Newton Raphson Method [45]. A brief explanation of method is explained hereafter, The general equation of nodal unknowns is given as,

$$[K]\cdot\{u\}=\{F^a\} \tag{2.1}$$

whereas,

$[K]$ = Stiffness matrix,

$\{u\}$ = Displacements (nodal unknowns) vector,

$\{F^a\}$ = Load vector.

If $[K]$ is a function of $\{u\}$, (2.1) becomes a nonlinear equation. The Newton- Raphson-Method makest the iterative solution of nonlinear equation system possible and given as, [59]

$$\left[K_i^T\right]\cdot\{\Delta u_i\}=\{F^a\}-\{F_i^{nr}\} \tag{2.2}$$

$$\{u_{i+1}\}=\{u_i\}+\{\Delta u_i\} \tag{2.3}$$

whereas,

$[K_i^T]$ = Tangential stiffness matrix,

i = Number of current iteration,

$[F_i^{nr}]$ = Vector of internal element forces derived from stresses.

$[K_i^T]$ and $[F_i^{nr}]$ are functions of $\{u_i\}$. The right side of (2.2) is residual- load vector. This vector is the measure of loads, which remains out of equilibrium.

2.2 Material Nonlinearity

The material nonlinearity of steel is incorporated into FE- model simulations using "Bilinear- Kinematic- Hardening" law, which conforms to Eurocode 3 Part 1-5, Figure C2.c: Modelling of Material Behavior, as illustrated in Figure 2.1. This theory comprises yield function, hardening and flow rules. Here just a summary of method is given. For details please see Mendelson, Cook et al., Simo and Taylor [60- 62]. The yield criterion proposes a stress state, after which material starts to yield. This criterion is a yield function of stress tensor and equals to equivalent (v.- Mises) stress with Kinematic Hardening,

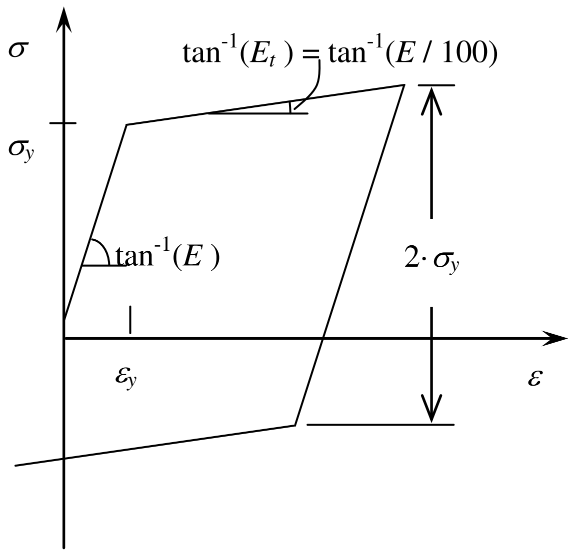

Figure 2.1 Stress strain relationship of steel.

$$\sigma_e = \left[\frac{3}{2} (\{s\} - \{\alpha\})^T [M] (\{s\} - \{\alpha\}) \right]^{1/2} \tag{2.4}$$

whereas,

$\{s\}$= deviatoric stress vector

$\{\alpha\}$= backstress or displacement vector of yield surface.

$$\{s\} = \{\sigma\} - \sigma_m [1 \quad 1 \quad 1 \quad 0 \quad 0 \quad 0]^T = [\{s_\sigma\} \quad \{s_\tau\}]^T \tag{2.5}$$

$$\{\alpha\} = C \int d\{\varepsilon^{pl}\} = [\{\alpha_\sigma\} \quad \{\alpha_\tau\}]^T \tag{2.6}$$

The unknowns in (2.5) and (2.6) mean,

$$\{\sigma\} = \text{Stress vector} = \begin{bmatrix}\sigma_x & \sigma_y & \sigma_z & \tau_{xy} & \tau_{yz} & \tau_{xz}\end{bmatrix}^T \tag{2.7}$$

$$\sigma_m = \text{Hydrostatic stress} = \frac{1}{3}\left(\sigma_x + \sigma_y + \sigma_z\right) \tag{2.8}$$

$$C = \frac{2}{3}\frac{E \cdot E_T}{E - E_T} \tag{2.9}$$

As per v.- Mises- yield criterion yielding does not depend on hydrostatic stress. When the equivalent stress becomes equal to the uniaxial yield stress (σ_{yield}) , the material starts to yield. As a result the yield surface is as in Figure 2.2 and yield criterion is as given,

$$F = \left[\frac{3}{2}(\{s\} - \{\alpha\})^T [M](\{s\} - \{\alpha\})\right]^{1/2} - \sigma_{yield} = 0 \tag{2.10}$$

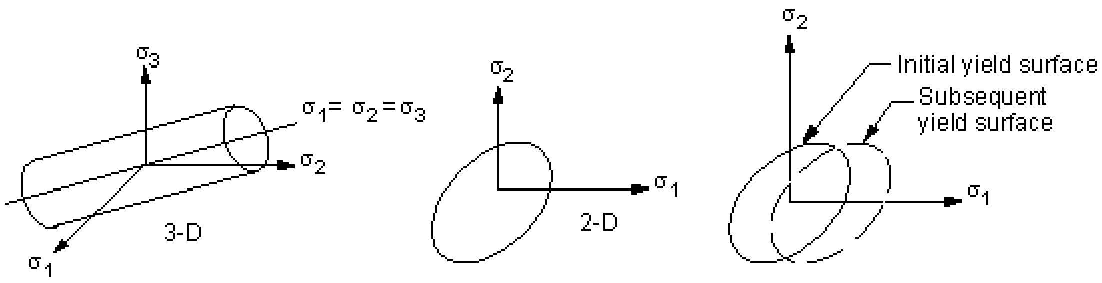

Figure 2.2 Yield surface according to "Kinematic Hardening".

The direction and amplitude of plastic strain are using flow rule given as,

$$\left\{d\varepsilon^{pl}\right\} = \lambda\left\{\frac{\partial Q}{\partial \sigma}\right\} \tag{2.11}$$

Whereas,

λ = Plastic constants, which sets the value of plastic strain.

Q = Plastic potential function, which sets the direction of plastic strain.

Here,Q is equal to yield function given in (2.10) and plastic strain develops perpendicular to yield surface. Therefore this flow rule is called as "Associative Flow Rule".

Now to be able to calculate plastic strain,λ hast to be calculated. The transform of (2.10) results in,

$$F(\{\sigma\}, \{\alpha\}) = 0 \tag{2.12}$$

The first derivation of yield function results in,

$$dF = \left\{\frac{\partial F}{\partial \sigma}\right\}^T [M]\{d\sigma\} + \left\{\frac{\partial F}{\partial \alpha}\right\}^T [M]\{d\alpha\} = 0 \tag{2.13}$$

Whereas, $$[M]=\begin{bmatrix}1&0&0&0&0&0\\0&1&0&0&0&0\\0&0&1&0&0&0\\0&0&0&2&0&0\\0&0&0&0&2&0\\0&0&0&0&0&2\end{bmatrix} \quad (2.14)$$

If (2.6) is differentiated for once, it results in,

$$\{d\alpha\}=C\{d\varepsilon^{pl}\} \quad (2.15)$$

The increment of stresses can be calculated using the relationship between elastic stresses and strains.

$$\{d\sigma\}=[D]\{d\varepsilon^{el}\} \quad (2.16)$$

$$\{d\varepsilon^{el}\}=\{d\varepsilon\}-\{d\varepsilon^{pl}\} \quad (2.17)$$

whereas,

$[D]$ = Stresss- Strain Matrix

ε^{el} = Elastic Strains

ε^{pl} = Plastic Strains

When (2.15) and (2.16) are together with (2.17) replaced in (2.13), the following equation is obtained,

$$\left\{\frac{\partial F}{\partial \sigma}\right\}^T [M][D]\{d\varepsilon\}=\left(-C\left\{\frac{\partial F}{\partial \alpha}\right\}^T [M]+\left\{\frac{\partial F}{\partial \sigma}\right\}^T [M][D]\right)\{d\varepsilon^{pl}\} \quad (2.18)$$

In (2.18) $\{d\varepsilon^{pl}\}$ is replaced with (2.11) under consideration of equation, $Q = F$.

$$\lambda=\frac{\left\{\frac{\partial F}{\partial \sigma}\right\}^T [M][D]\{d\varepsilon\}}{-C\left\{\frac{\partial F}{\partial \alpha}\right\}^T [M]\left\{\frac{\partial F}{\partial \sigma}\right\}+\left\{\frac{\partial F}{\partial \sigma}\right\}^T [M][D]\left\{\frac{\partial F}{\partial \sigma}\right\}} \quad (2.19)$$

As a result, increment in plastic strains depends on the total strain increment, the current stress state and the form of yield function. Subsequently, λ can be calculated and the plastic strain increment results using (2.11) in,

$$\left\{\frac{\partial F}{\partial \sigma}\right\}=\left(\frac{3}{2\cdot\sigma_y}\begin{bmatrix}\{s_\sigma\}-\{\alpha_\sigma\}\\0\end{bmatrix}+\frac{3}{\sigma_y}\begin{bmatrix}0\\\{s_\tau\}-\{\alpha_\tau\}\end{bmatrix}\right) \quad (2.20)$$

The algorithm is as follows:

The stresses are calculated based on a test strain $\{\varepsilon^{tr}\}$, which is the total strain minus the plastic strain from the previous time point.

$$\{\varepsilon_n^{tr}\} = \{\varepsilon_n\} - \{\varepsilon_{n-1}^{pl}\} \tag{2.21}$$

n stands for the current time point. Then the test stress yields in,

$$\{\sigma_n^{tr}\} = [D]\{\varepsilon_n^{tr}\} \tag{2.22}$$

Using (2.4) the equivalent stress is calculated. If $\sigma_e$is smaller than σ_{yield}, then material behaves elastic and no calculation of plastic strain increment is required.

As long as the equivalent stress excesses yield point, λ is calculated using Local-Newton- Raphson- Iteration- Process [62].

$\{\Delta\varepsilon^{pl}\}$ is calculated using (2.11).

The current plastic strain is calculated.

$$\{\varepsilon_n^{pl}\} = \{\varepsilon_{n-1}^{pl}\} + \{\Delta\varepsilon^{pl}\} \tag{2.23}$$

Subsequently the elastic strain is calculated.

$$\{\varepsilon^{el}\} = \{\varepsilon^{tr}\} - \{\Delta\varepsilon^{pl}\} \tag{2.24}$$

Consequently the stress vector is again calculated using elastic strains and then the iterations are repeated until the convergency is satisfied.

$$\{\sigma\} = [D]\{\varepsilon^{el}\} \tag{2.25}$$

The difference in position of yield surface is calculated using (2.15), whereas n-1 depends on the value of previous time point.

$$\{\alpha_n\} = \{\alpha_{n-1}\} + \{\Delta\alpha\} \tag{2.26}$$

2.3 Bridge Loads as per Eurocode 1 Part 2

The traffic load group 1 is applied on the bridge according to Eurocode 1 Part 2 [63].

The traffic road, on which vehicles pass, are divided into numerical traffic lanes.

Road width = w = 6.3 m,

Width of numerical traffic lanes = w_l = 3.0 m

Number of numerical traffic lanes = n_l = Int(w /3) = 2,

Width of remaining surface within of road = $w_R = w - w_l \cdot n_l = 6.3\text{-}2\cdot3 = 0.3$ m

Finally, traffic road is consist of two numerical traffic lanes of 3 m,each of which will be under load values given in the next pharagraph.

According to Eurocode 1 Part 2 [63] traffic load group 1 comprises characteristic load values of dominant load model 1 and reduced values of pedestrian loads. Because, loading is chosen to be applied as to symmetry planes, considerig pedestrian loads is inconvenient. As a result no pedestrian load is taken into account in the FE- model of the bridge. The load values are as follows,

Wheel load on main traffic lane = 180 kN

Equally distributed load on main traffic lane = 13.5 kN/ m²

Equally distributed load on remaining road surface = 3.75 kN/ m²

Weight of wearing surface = 0.324 kN/m² per cm thickness

ρ_{steel} = 10.5975 t /m³

2.4 Optimization of Mesh and Substeps

The optimization of mesh refinement and substeps are done under traffic load group 1 according to Eurocode 1 Part 2 [63] for limit state of load carrying capacity. In addition asphalt course thickness is assumed as 7.5 cm so as to consider its dead load. Therefore the wheel load area is expanded from 0.4x0.4m^2 to 0.562x0.562m^2. (Here 0.562 m = 0.4 m (width of wheel area) + 2*0.075m (thickness of asphalt) + 2*0.006m (half of deck plate thickness)). However because of the limitation caused by finite elements' side sizes in model, the width of wheel area has to be any times of 75 mm, which is determined as per mesh refinement study given in Table 2.1. Subsequently, the width of wheel load area is set as 0.525 m. The traffic loading is as illustrated in Figure 2.3.

It is searched the optimal mesh refinement for FE- model of bridge under consideration. Two criteria are important for this issue. First, the correctness of results, second number of elements/ nodal unknowns and iterations (time required for FE- analyses). At the beginning of optimization process mesh refinement is chosen with experience of researcher. Since the number of substeps and mesh refinement are separately analyzed, geometric and material non- linearities are ignored in mesh refinement analyses. Under these assumptions five simulations are performed and their results are tabulated in Table 2.1. As per assessment of results, Mesh 4 is chosen as adequate mesh for FE- model of bridge.

Exceptmin. σ_{xy} , min. ε_{xy} developed in the rib of main girder, and min. σ_{yz} , min. ε_{yz} developed in the bottom flange of main girder web, all deviations between Mesh 4 and Mesh 5 are smaller than 6 %. Since not main girder, but deck plate, cross- beam and longitudinal stiffener are investigated in this thesis and main girder is solely modeled to include its boundary effect on orthotropic steel deck, the aferomentined max. stress and strain values are not taken into account for mesh refinement purposes. Moreover all stress vales are much smaller than yield stress. As a result Mesh 4 provides stresses and strains within enough tolerance for this research.

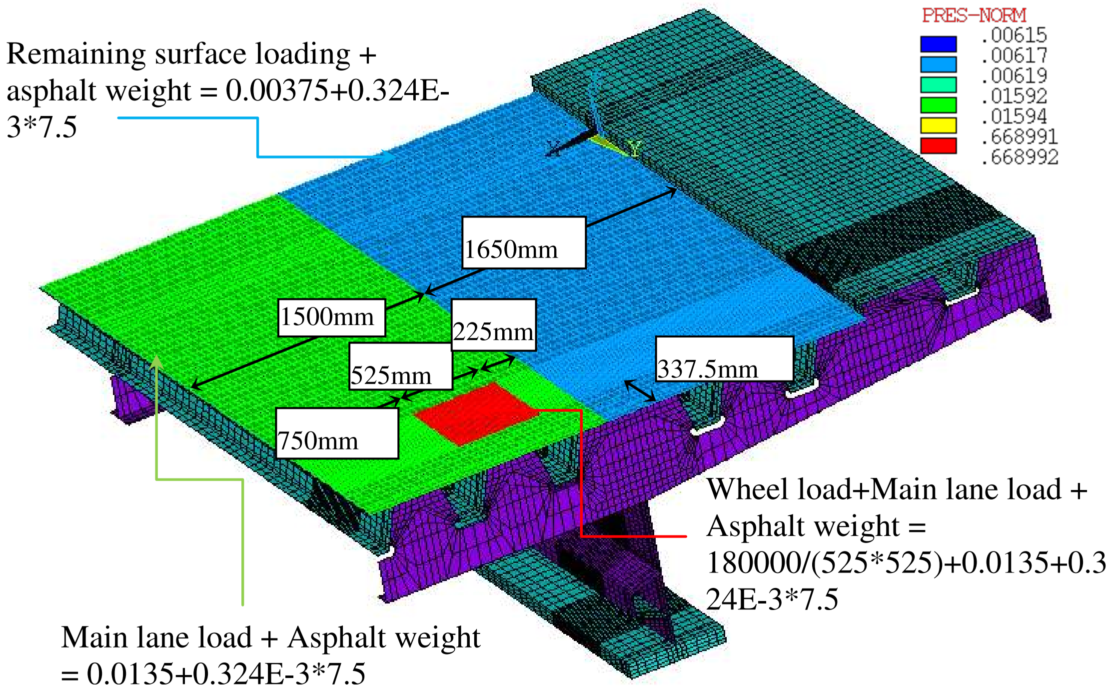

Figure 2.3 Traffic loading used in this chapter.

Table 2.1. Number of elements, stresses and strains as per mesh refinement*

		Mesh 1	Mesh 2	Mesh 3	Mesh 4	Deviation (%)	Mesh 5
Number of elements		29194	123288	197300	300282	49.27	448217
UMAX		3.276	3.313	3.318	3.324	0.06	3.326
σ_e		340.811	447.555	474.723	493.657	3.49	510.907
σ_x	comp.	-149.676	-191.998	-202.247	-217.881	3.32	-225.115
	ten.	211.383	283.732	300.268	311.536	2.56	319.505
σ_y	comp.	-175.329	-200.493	-204.560	-221.599	1.22	-224.298
	ten.	104.559	154.831	159.656	188.834	1.38	191.435
σ_z	comp.	-372.416	-474.806	-501.148	-517.904	2.09	-528.745
	ten.	225.191	296.616	314.405	347.377	3.19	358.470

Table 2.1 (cont'd)

σ_{xy}	comp.	-29.838	-38.785	-44.041	-55.47	7.54	-59.655
	ten.	34.205	39.335	40.003	41.638	3.77	43.206
σ_{yz}	comp.	-44.871	-49.162	-50.44	-66.276	9.00	-72.243
	ten.	69.991	82.527	84.422	91.290	0.60	91.838
σ_{xz}	comp.	-116.337	-158.462	-173.985	-184.413	4.80	-193.263
	ten.	90.568	107.776	116.876	123.881	5.88	131.165
ε_e		0.001623	0.002131	0.002261	0.002351	3.49	0.002433
ε_x	comp.	-0.000665	-0.000850	-0.000897	-0.000961	3.33	-0.000993
	ten.	0.000798	0.001131	0.001222	0.001289	3.57	0.001335
ε_y	comp.	-0.000812	-0.000860	-0.000863	-0.000902	0.33	-0.000905
	ten.	0.000671	0.000808	0.000856	0.000881	1.36	0.000893
ε_z	comp.	-0.001641	-0.002137	-0.002271	-0.002359	2.50	-0.002418
	ten.	0.001091	0.001409	0.001482	0.001613	2.85	0.001659
ε_{xy}	comp.	-0.000369	-0.000480	-0.000545	-0.000687	7.57	-0.000739
	ten.	0.000423	0.000487	0.000495	0.000516	3.68	0.000535
ε_{yz}	comp.	-0.000556	-0.000609	-0.000625	-0.000821	8.89	-0.000894
	ten.	0.000867	0.001022	0.001045	0.001130	0.62	0.001137
ε_{xz}	comp.	-0.00144	-0.001962	-0.002154	-0.002283	4.82	-0.002393
	ten.	0.001121	0.001334	0.001447	0.001534	5.87	0.001624

* The symbols used in table are element normal and shear stress/ strains. ANSYS uses following abbreviations instead of symbols used in Table 2.1. Here, *UMAX* is max. displacement vector sum. **SEQV** = σ_e , **SX** = σ_x , **SY** = σ_y , **SZ** = σ_z , **SXY** = σ_{xy} , **SYZ** = σ_{yz} , **SXZ** = σ_{xz} ,**EPTOEQV** = ε_e , **EPTOX** = ε_x , **EPTOY** = ε_y , **EPTOZ** = ε_z , **EPTOXY** = ε_{xy} , **EPTOYZ** = $\varepsilon_{yz,}$ **EPTOEXZ** = ε_{xz}

Using Mesh 4 refinement, three simulations are performed, when substep number is 5, 8 and 10 respectively. Assessment of these results emerges that even 5 substepsare enough to obtain results in convergence tolerance. Anyway in this research substep number of 8 is used to display the results.

Table 2.2. Stresses and strains as per number of substeps

		Simulation 1	Deviation(%)	Simulation 2	Deviation (%)	Simulation 3
Number of Substeps		5	60	8	25.00	10
Number of Iterations		16	19	19	26.32	24
UMAX		3.344	0.00	3.344	0.00	3.344
σ_e		404.026	0.00	404.010	0.00	404.005
σ_x	comp.	-219.675	0.00	-219.676	0.00	-219.676
	ten.	311.243	0.00	311.230	0.00	311.226
σ_y	comp.	-220.591	0.00	-220.591	0.00	-220.592
	ten.	189.223	0.00	189.225	0.00	189.226
σ_z	comp.	-401.416	0.01	-401.441	0.00	-401.451
	ten.	343.998	0.00	343.994	0.00	343.994
σ_{xy}	comp.	-55.020	0.00	-55.020	0.00	-55.020
	ten.	41.899	0.00	41.899	0.00	41.899
σ_{yz}	comp.	-66.229	0.00	-66.228	0.00	-66.228
	ten.	90.386	0.00	90.386	0.00	90.386
σ_{xz}	comp.	-184.727	0.00	-184.720	0.00	-184.717
	ten.	122.590	0.00	122.589	0.00	122.588
ε_e		0.002572	0.12	0.002569	0.16	0.002565
ε_x	comp.	-0.000969	0.00	-0.000969	0.00	-0.000969
	ten.	0.001289	0.00	0.001289	0.00	0.001289
ε_y	comp.	-0.000899	0.00	-0.000899	0.00	-0.000899
	ten.	0.001241	0.89	0.001230	0.00	0.001230
ε_z	comp.	-0.002554	0.20	-0.002549	0.00	-0.002549
	ten.	0.001597	0.00	0.001597	0.00	0.001597
ε_{xy}	comp.	-0.000681	0.00	-0.000681	0.00	-0.000681
	ten.	0.000519	0.00	0.000519	0.00	0.000519

Table 2.2 (cont'd)

ε_{yz}	comp.	-0.000820	0.00	-0.000820	0.00	-0.000820
	ten.	0.001119	0.00	0.001119	0.00	0.001119
ε_{xz}	comp.	-0.002287	0.00	-0.002287	0.00	-0.002287
	ten.	0.001518	0.00	0.001518	0.00	0.001518

2.5 Results& Discussion

Results obtained neglecting nonlinearities shows that the nonlinearity has to be considered in the simulation, since some stress values excess the yield point (355 MPa). Figure 2.4 displays the effect of considering kinematic hardening in stress calculations. According to solution neglecting kinematic hardening the structure fails at some points. However considering kinematic hardening in stress calculations proves that the structure does not fail and continues to carry load thanks ductile material property of steel, while plastic strains develop. This result coincides with the experiences of structural steel, that keeps on carrying loads beyond its yield point. While local vertical displacement under wheel load and v.- Mises strain increase 0.60 % and 9.27 % respectively, v.- Mises stress decreases 18.16 %. The plastic strain develops just in the cross- beam to longitudinal rib connection as shown in Figure 2.5.

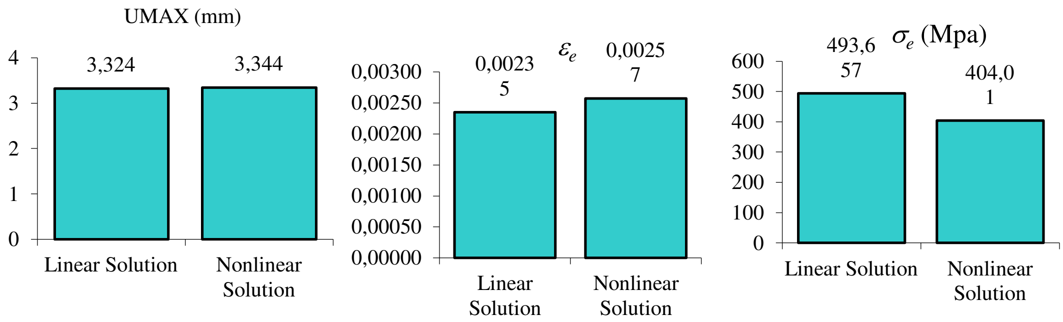

Figure 2.4 Effect of considering kinematic hardening in stress calculations.

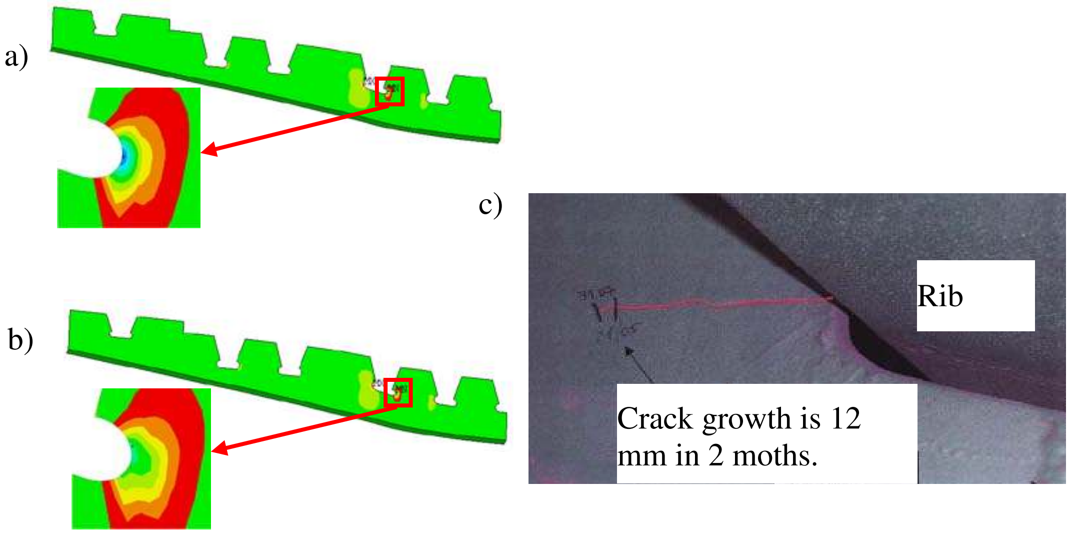

Figure 2.5 a) Distribution of σ_z (here vertical bending stress) on cross- beam with neglecting nonlinearity. b) Distribution of σ_z on cross- beam with considering nonlinearity. c) Yield line (or crack growth) on the material emerged in a real orthotropic steel bridge, that exists in industry [17].

CHAPTER 3

EFFECT OF DECK PLATE THICKNESS ON THE STRUCTURAL BEHAVIOR OF STEEL ORTHOTROPIC HIGHWAY BRIDGES

Deck plate thicknesses of 12, 14 and 16 mm are chosen and three FE- analyses are done in this chapter. Results of calculations will be presented and compared with each other in order to demonstrate the effect of deck plate on strain amplitudes, which are indicators of damages developed in structural parts of steel bridge.

3.1 Parameter Study of Deck Plate Thickness

This section presents the results of the parameter study of deck plate thickness, which emerges the effect of this thickness on the stress and displacements developed in steel structural parts. All dimensions of the bridge defined in FE- model are kept constant, while deck plate thickness increases. Deck plate thicknesses of simulations, which are DBD12, DBD14 and DBD16, are 12, 14 and 16 mm respectively. The results of simulations are given with figures, in which max. v.- Mises stress and displacement values on load bearing steel parts are presented. In the following figures deformed shape is given at left side, whereas v.- Mises stress values are given at right side. In the left figure vertical deformations are given based on nodal (averaged) values. Here MX means max. vertical displacement, whereas MN means min. vertical displacement. The symbol UZ is the vertical displacement value of point where max. v.- Mises stress occurs. For instance in Figure 3.1, UZ = -1.413 mm is the vertical displacement of the point, at which max. v.- Mises stress occurs. In this figure start point of arrow shows the place of max. v.- Mises stress, whereas end point of arrow shows the value and distribution of v. –Mises stress on deck plate. At the right side of Figure 3.1 max. v.- Mises stress value (126.652 MPa) is given based on element results (non averaged value). Briefly, the place and elevation of max. v.- Mises stress are given at the left side and value of this v.- Mises stress is given at the right side of Figure 3.1. The global load bearing structure withstands under applied wheel loads well. Distinctive are the local (or discretized) behavior of deck plate, ribs and cross- beam web. Wheel loads are transferred respectively by deck plate, ribs, cross- beams and main girder to supports, while these mentioned load bearing structures deform and subject to stress (See Figure 3.4). The main girder prevents the deformations passes to the other as acting like a support. That means the exterior ribs deforms less than the interior ribs located direct under wheel loads. As a result of this support like behavior of main girder the load is not carried by the whole structural frame (See Figure 3.4). In comparison transverse stresses are much higher than longitudinal stresses in deck plate analysis. As a result the transverse stresses play the distinctive role in the analysis of deck plate thickness regarding stress values developed under wheel loads. The max. values of v.- Mises stresses are the indicators of potential damages, so that these values are used in the assessment of results. The wheel loads are located direct on one web of interior rib, which exists next to main girder. On the other web of interior rib there is no load. That leads bending and twisting of this rib, which is welded to cross- beam at lateral sides, to deck plate at top and goes through cut- out of cross- beam at the bottom. The max. v.- Mises stress rises at this cut- out of cross- beam. Results of FE- analyses are depicted in Figure 3.1 to Figure 3.10.

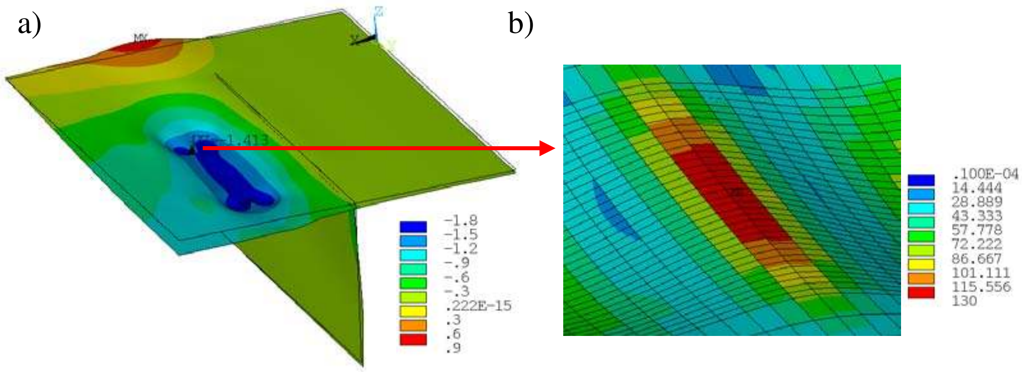

Figure 3.1 a) Distribution of vertical displacement on deck plate and main girder, when deck plate thickness is 12 mm. b) Distribution of v.- Mises- stress on deck plate, when deck plate thickness is 12 mm.

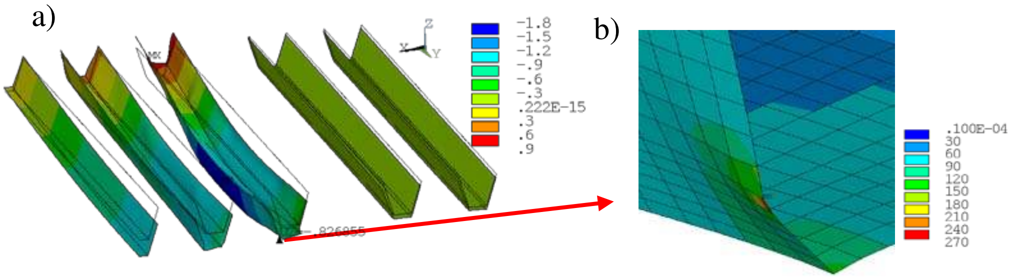

Figure 3.2 a) Distribution of vertical displacement on ribs, when deck plate thickness is 12 mm. b) Distribution of v.- Mises- stress on ribs, when deck plate thickness is 12 mm.

Figure 3.3 a) Distribution of vertical displacement on cross- beam, when deck plate thickness is 12 mm. b) Distribution of v.- Mises- stress on cross- beam, when deck plate thickness is 12 mm.

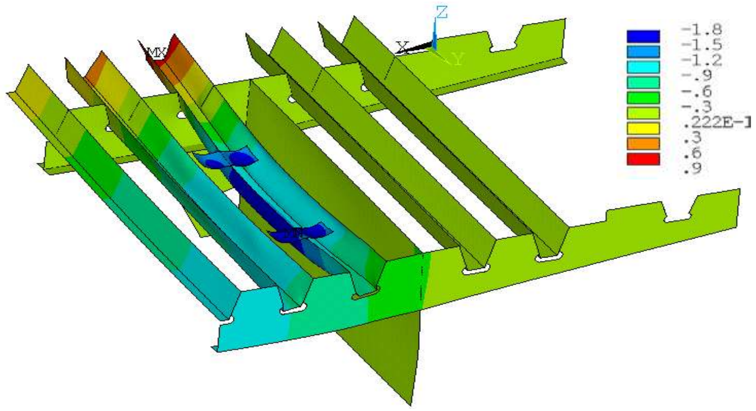

Figure 3.4 The picture of load transferring from wheels, over deck plate, ribs, cross- beams and main girder to supports.

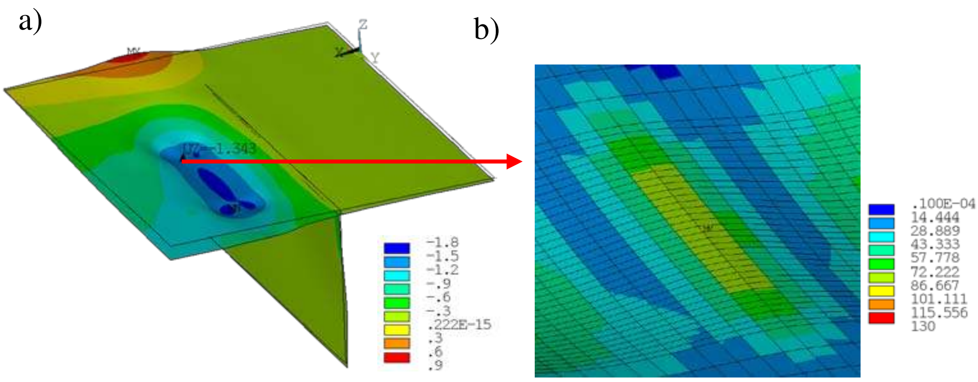

Figure 3.5 a) Distribution of vertical displacement on deck plate and main girder, when deck plate thickness is 14 mm. b) Distribution of v.- Mises- stress on deck plate, when deck plate thickness is 14 mm.

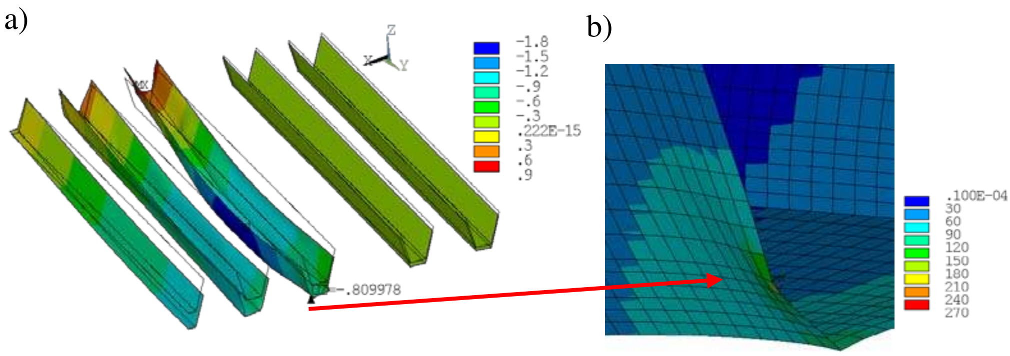

Figure 3.6 a) Distribution of vertical displacement on ribs, when deck plate thickness is 14 mm. b) Distribution of v.- Mises- stress on ribs, when deck plate thickness is 14 mm.

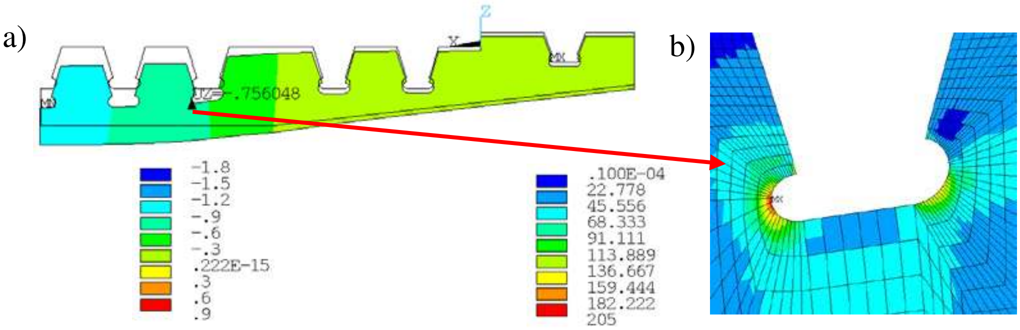

Figure 3.7 a) Distribution of vertical displacement on cross- beam, when deck plate thickness is 14 mm. b) Distribution of v.- Mises- stress on cross- beam, when deck plate thickness is 14 mm.

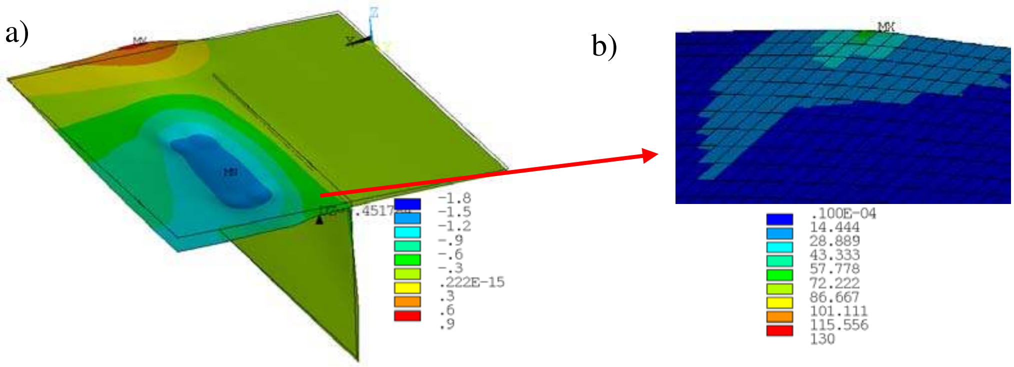

Figure 3.8 a) Distribution of vertical displacement on deck plate and main girder, when deck plate thickness is 16 mm. b) Distribution of v.- Mises- stress on deck plate, when deck plate thickness is 16 mm.

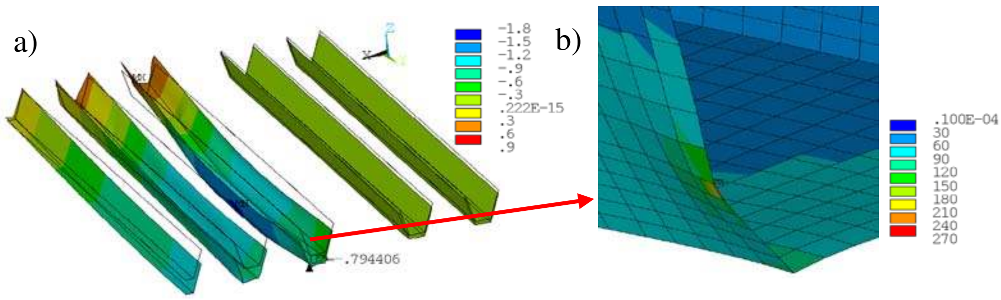

Figure 3.9 a) Distribution of vertical displacement on ribs, when deck plate thickness is 16 mm. b) Distribution of v.- Mises- stress on ribs, when deck plate thickness is 16 mm.

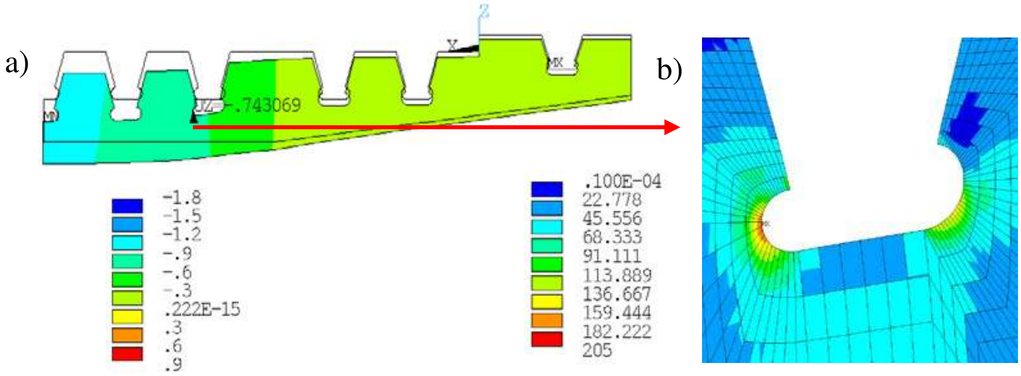

Figure 3.10 a) Distribution of vertical displacement on cross- beam, when deck plate thickness is 16 mm. b) Distribution of v.- Mises- stress on cross- beam, when deck plate thickness is 16 mm.

3.2 Results &Discussion

Former studies revealed that the complex geometry of orthotropic bridges has better to be taken into account for the correct stress analysis of deck plate, longitudinal stiffeners, cross- beams, main girder… etc, briefly all structural parts of orthotropic bridge [1 and 46]. It is understood that the classical solution methods derived so far can not reflect the real stresses, which assume simplifications in the geometry of orthotropic bridge structure, since the damages appeared in deck plate, ribs, cross- beam, etc… should not have been developed in years after bridge is constructed as per these classical calculation methods. The aim of this thesis is not developing a simple calculation method for orthotropic steel bridges. However this thesis aims to find out dimensional constructional conservative facts and rules like minimum thickness of deck plate. By means of this thesis a FE- model is generated to comprise the complex geometry of orthotropic bridge. Differing from Huurman's et. al. [46] FE- model pedestrian road, main girder, exterior ribs and connections of these structural parts, which are complex in geometry, are also modeled in the FE- model used in this thesis. It is seen from the results of this thesis that, instead of FE- modeling of main girder, it can be included as a support in the FE- model for the stress analysis of deck plate, longitudinal stiffeners and cross- beams. From the results it is seen that main girder act as a support in vertical direction, whereas rib- webs behave as vertical springs in transverse direction (See

Figures 3.2, 3.6 and 3.9). Because the ribs between main girder are stressed, but the exteriors ribs are almost not affected from wheel loads,the main girder prevents the deformations and loads passes to the other side as acting like a support in transverse direction. According to Eurocode 3 Part 2 [52] the recommended deck plate thickness (*t*) is 12 mm, nevertheless*t* must be higher than 14 mmfor asphalt wearing course thickness higher than 40 mm. The recommendations of the standard bases on practical results and requires a numerical foundation. This thesis provides a numerical foundation to Eurocode 3 Part 2 [52] (recommendations for orthotropic steel bridges). It is seen from Figure 3.11 that, increasing deck plate thickness from 12 mm to 14 mm results in 31.5 % decrease in v.- Mises stress, whereas increasing deck plate thickness from 14 mm to 16 mm results in 10.6 % additional decrease in v.- Mises stress. So, the conventional 12 mm deck plate thickness can be 2 mm increased, where it is necessary, but it should be kept in mind that the additional 2 mm increases after 14 mm will always be less effective.

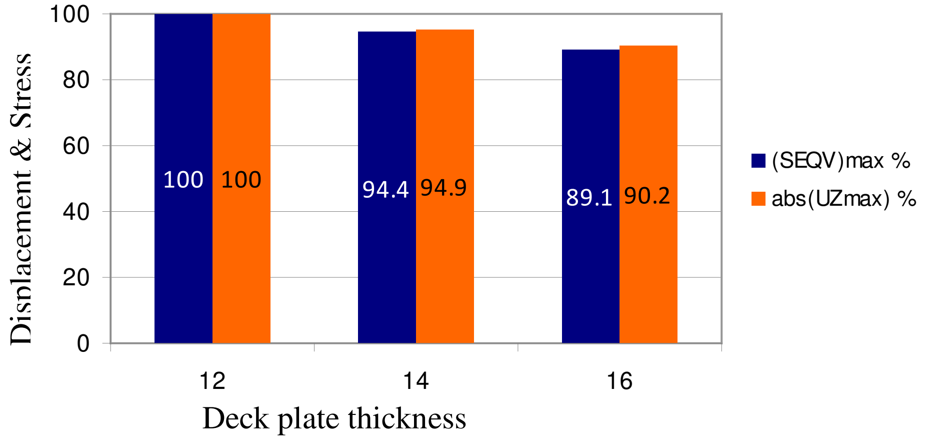

Figure 3.12 Variation of max. v.-Mises-stress and max. vertical displacement in ribs as per deck plate thickness.

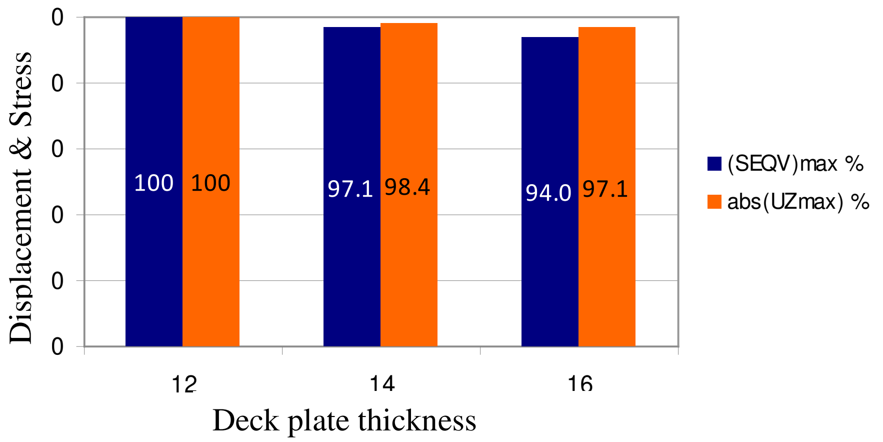

Figure 3.13 Variation of max. v.-Mises-stress and max. vertical displacement in cross- beam as per deck plate thickness.

For v.- Mises stress rises in deck plate, the critical component is σ_x. This transverse stress takes its maximum at the tension zone of deck plate, when deck plate thicknesses are 12 and 14 mm (see Figures 3.1 and 3.5). These extreme values develop direct under local wheel loads and over rib- webs, which act like a vertical spring. This phenomenon is depicted in Figure 3.14 below.

Figure 3.14 Distribution of σ_x under wheel load and over rib- web as per deck plate thickness.

The tension stress rises at top of deck plate in bridge transversal (see Figure 3.15) or longitudinal (see Figure 3.17) direction cause tension strains on top of the deck plate. These tension stresses are thought to be the one of major causes of cracks developed in bridges' deck plates. Cracks developed in deck plate asphalt conform to layout of longitudinal stiffeners and cross- beams as per practical findings shown in Figure 3.16.

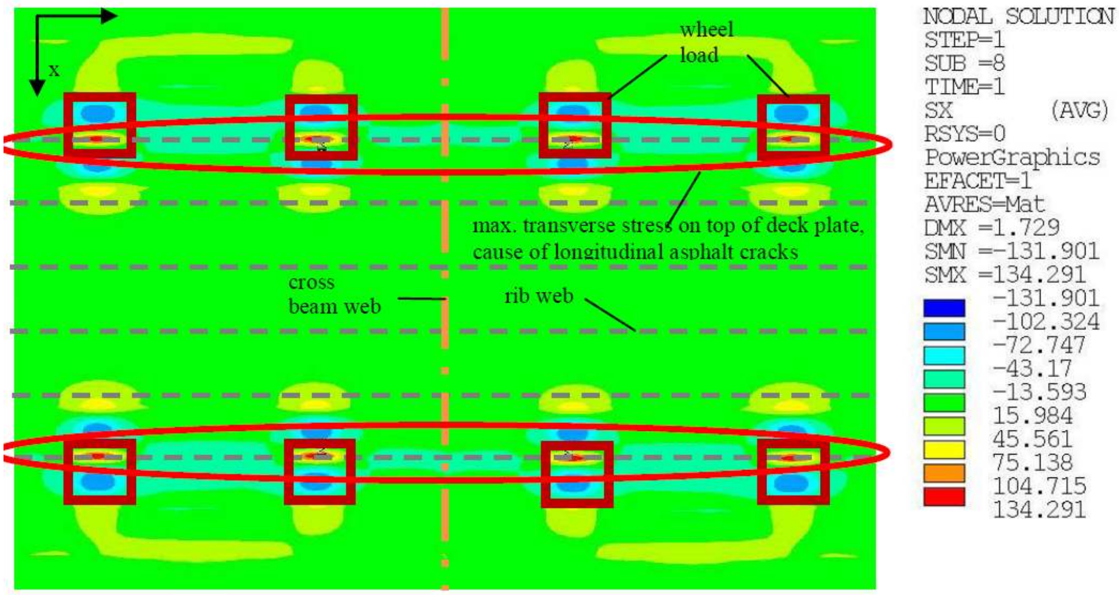

Figure 3.15 Max. transverse stresses at the top of extended deck plate.

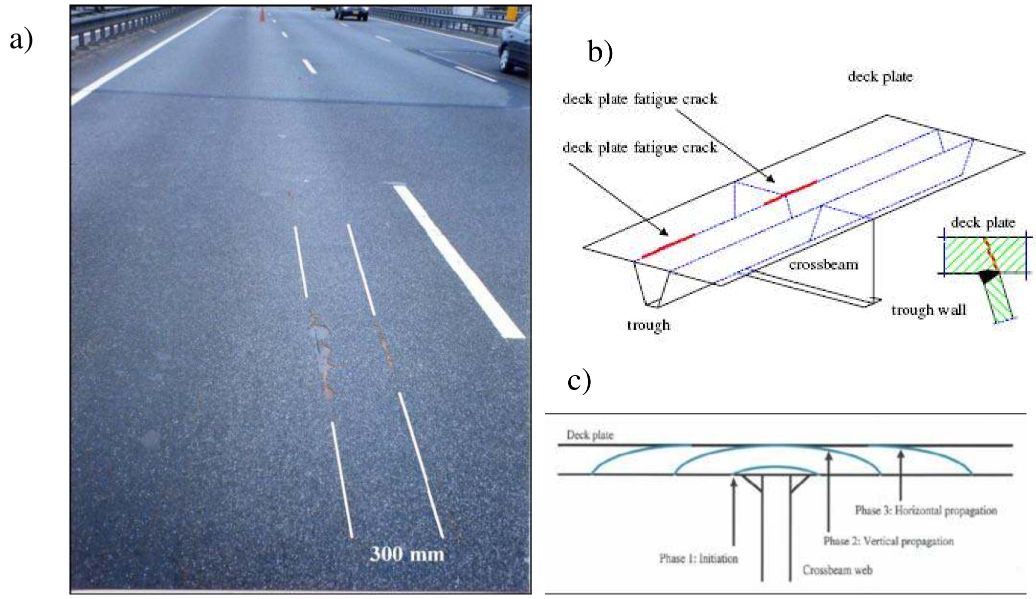

Figure 3.16 a) Visual observation of deck plate cracks in movable bridge. b) Potential deck plate cracks. c) Beginning phase of this phenomenon [1].

Figure 3.15 is the top view of extended FE- model, the quarter of which is used for stress analysis in this thesis. Here max. transverse tension stresses occurs under wheel load and over longitudinal stiffener web (trough in Figure 3.16). In this thesis static loads are used as wheel loads induced from vehicles. However, these wheel loads are continuous and repeating over longitudinal stiffener web and causes the longitudinal cracks in deck plates of steel highway orthotropic bridges (see Figure 3.16). As a result, the FE- model used in this thesis could successfully reflect the place and formation of this phenomenon in deck plates. Jong [1] explains this phenomenon of crack formation in deck plate as follows: The crack initiation is at the root of the longitudinal fillet weld between the trough web and the deck plate at the intersection of the cross-beam and the continuous closed trapezoidal stiffeners (troughs). After the initiation phase the crack growth is in the vertical direction from the underside to the top of the deck plate. After the crack has grown through the deck plate its growth is in the horizontal/longitudinal direction. When the crack lengthens it threatens the safety of the structure. Figure 3.16 left is a photograph of the visually observed cracks in the Van Brienenoord Bridge in summer 1997. Damage to the epoxy surfacing in the wheel tracks of the heavy vehicle lane is the first indication of deck plate cracks. The locations of the trough webs under the deck plate at a centre-to-centre distance of 300 mm are clearly visible. Also visible is the crack in the steel deck plate. Deformation of the steel deck plate at the crack location is the reason for this visibility. The length of the crack shown is approximately 50 cm [1].

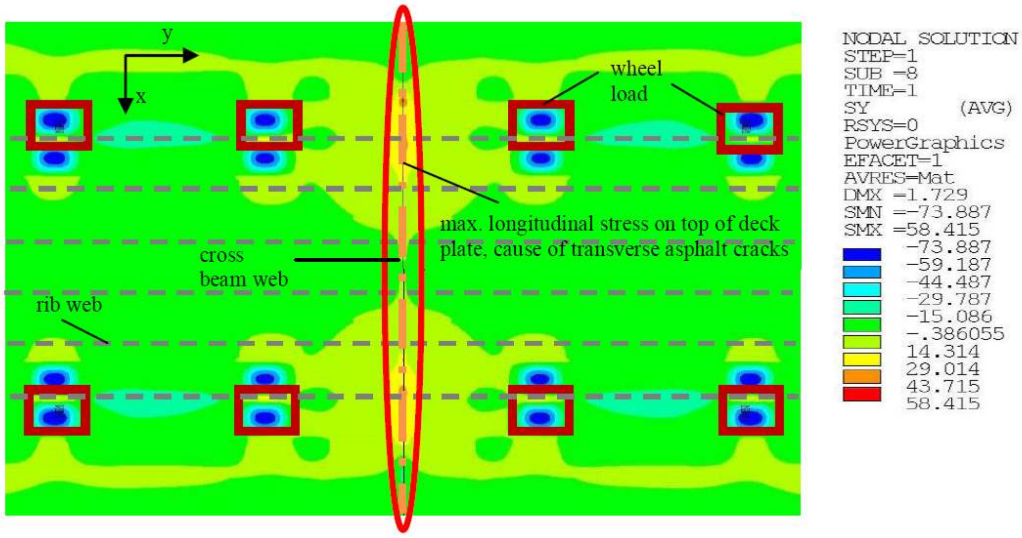

Figure 3.17 Max. longitudinal stresses at the top of extended full bridge.

In addition to rib web to deck plate connection, cross- beam web to deck plate connection is the second potential crack formation place because of longitudinal tension stresses in deck plate. Figure 3.17 illustrates the distrubition of longitudinal stresses at the top of deckplate of extended full bridge geometry used in this thesis. It is apparent from the results of this thesis and the results in the literature that, in general transverse cracks on deck plate occur after longitudinal cracks and over cross-beam webs. The places of cracks in bridge asphalts comply with constructive pattern, which is determined by webs of ribs (longitudinal stiffeners), cross beams and main girders. There are sufficient practical results, which indicates that the high tension strains develop at top of deck plate yield to longitudinal and transversal cracks in deck plate and its overlying asphalt [64].In conclusion of analyses, increasing deck plate thickness from 12 mm to 14 mm reduces v.-Mises stress 31.5 %. However, increasing deck plate thickness from 14 mm to 16 mm reduces v.-Mises stress only 10.6 %. Therefore, increase in deck plate thickness does not linearly reduce v.-Mises stress. The extreme tension stress pattern revealed on deck plate surface in the FE-model comply with the real crack formation as per findings in practice.

CHAPTER 4

EFFECT OF CROSS- BEAM ON STRESSES REVEALED IN ORTHOTROPIC STEEL BRIDGES

In the scope of this thesis first, spacing of cross- beam varies, while other dimensions remain constant. Second, cross- beam web thickness varies, as other dimensions remain constant. By this way, the quantitative causes of damages; thin cross- beam web and cross beam of long spacing, are analyzed. It is important to mention that geometric and material nonlinearities are both considered in this chapter.

4.1 Effect of Cross- Beam Spacing on Stresses

This chapter presents the results of the parameter study of cross- beam spacing, which emerges the effect of this spacing on the stress and displacements developed in steel structural parts. All dimensions of the bridge (except cross- beam spacing) defined in FE- model are kept constant, while cross- beam spacing increases. Cross- beam spacings of simulations QABST2000, BB, QABST4000 and QABST5000 are 2, 3, 4 and 5 m respectively. The results of simulations are given in figures, in which max. v.- Mises stress and displacement values on load bearing steel parts are presented. In figures deformed shape is given at the left side, whereas v.- Mises stress values are given at the right side. In the left figure vertical deformations are given based on nodal (averaged) values. Here MX means max. vertical displacement, whereas MN means min. vertical displacement. The symbol UZ designates the point where max. v.- Mises stress occurs. Briefly, the place and elevation of max. v.- Mises stress is pictured in the left figure and the value of this v.- Mises stress is given in the right figure. Max. values of v.- Mises stresses are the indicators of potential damages, so that these values are used in the assessment of results. The wheel loads are located direct on one web of interior rib adjacent to main girder. On the other web of interior rib there is no load. This loading condition leads bending and twisting of this rib, which is welded to cross- beam at lateral sides, to deck plate at top and goes through cut- out of cross- beam at the bottom. From the whole assessment of results obtained in this chapter, max. v.- Mises stress rises at this cut- out of cross- beam. Results of these FE- analysis are given below in Figure4.1 to Figure4.12.

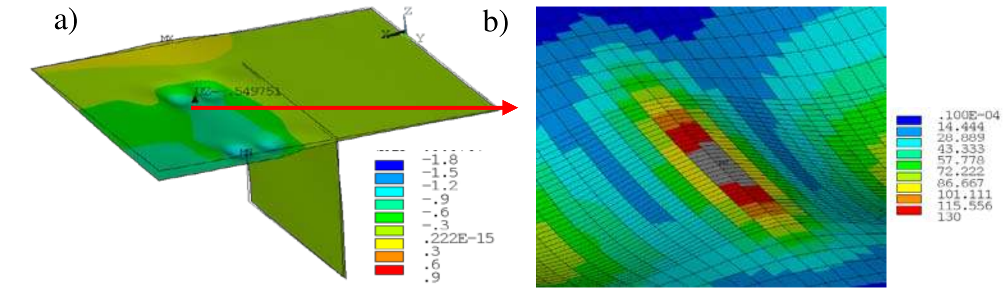

Figure 4.1 a) Distribution of vertical displacement on deck plate and main girder. when cross- beam spacing is 2 m. b) Distribution of max. v.-Mises on deck plate.

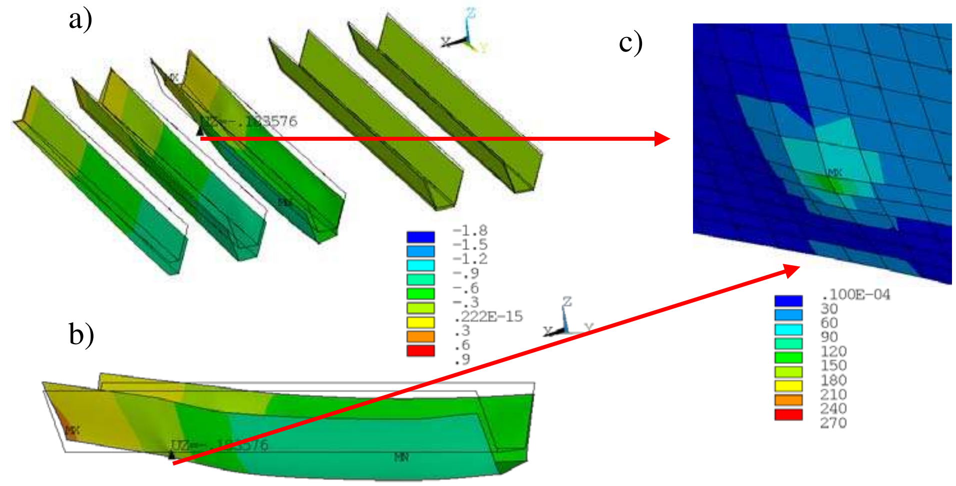

Figure 4.2 a) Distribution of vertical displacement in ribs, when cross- beam spacing is 2 m. b) Close- up view of rib, in which max. vertical displacement develops, when cross- beam spacing is 2 m. c) Distribution of max. v. Mises stress in rib, when cross- beam spacing is 2 m.

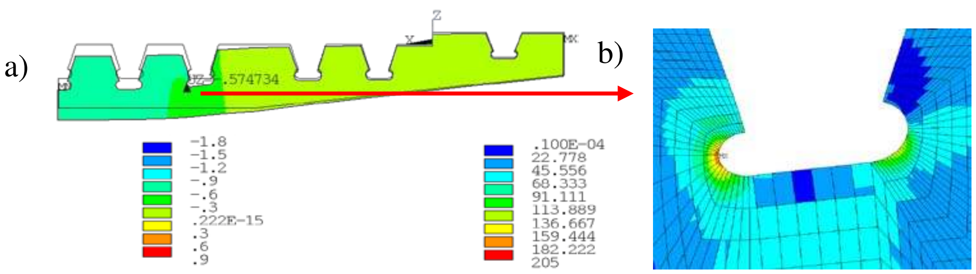

Figure 4.3 a) Distribution of vertical displacement in cross- beam, when cross- beam spacing is 2 m. b) Distribution of v. Mises stress, when cross- beam spacing is 2 m.

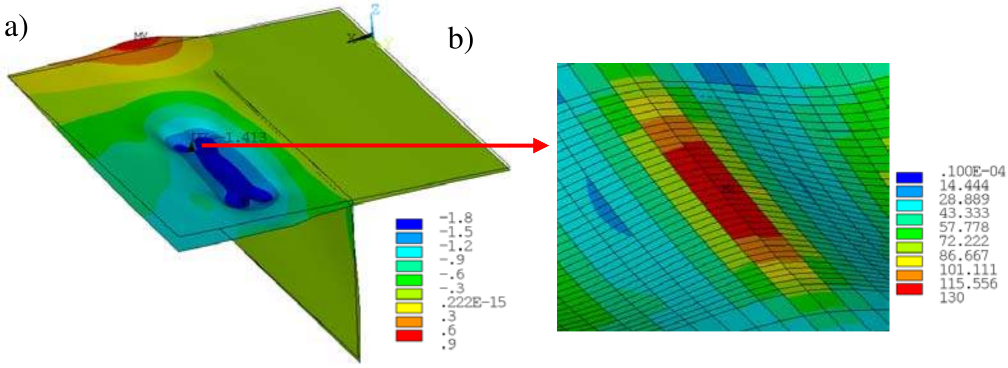

Figure 4.4 a) Distribution of vertical displacement in deck plate and main girder, when cross- beam spacing is 3 m. b) Distribution of v.- Mises- stress in deck plate, when cross- beam spacing is 3 m.

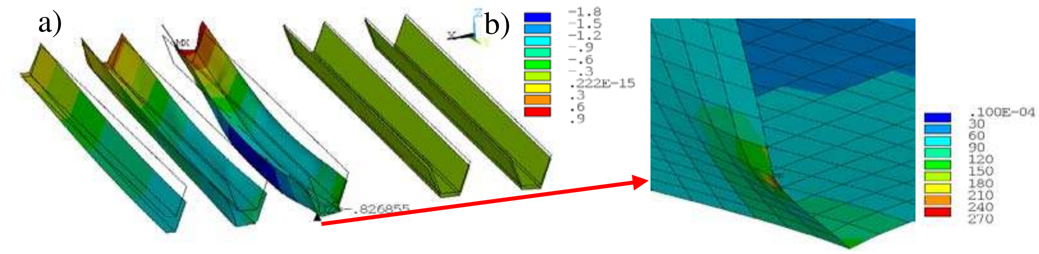

Figure 4.5 a) Distribution of vertical displacement in ribs, when cross- beam spacing is 3 m. b) Distribution of v.- Mises- stress in ribs, when cross- beam spacing is 3 m.

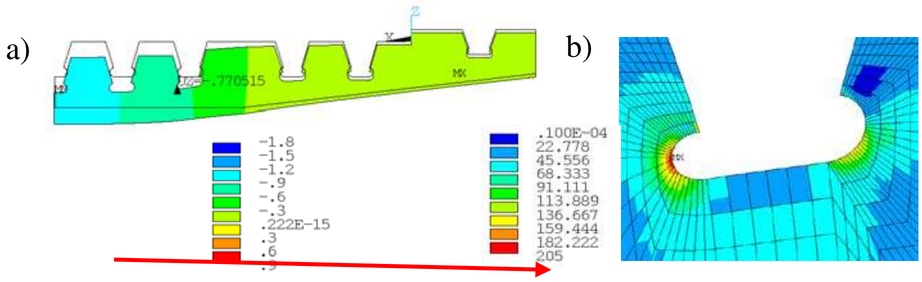

Figure 4.6 a) Distribution of vertical displacement in cross- beam, when cross- beam spacing is 3 m. b) Distribution of v.- Mises- stress in cross- beam, when cross- beam spacing is 3 m.

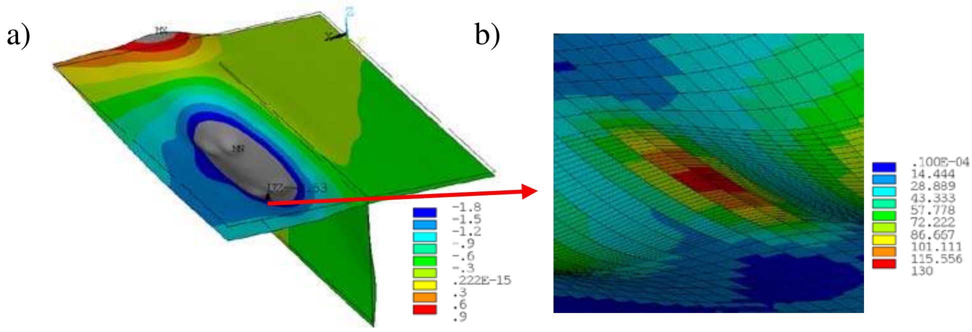

Figure 4.7 a) Distribution of vertical displacement in deck plate and main girder, when cross- beam spacing is 4 m. b) Distribution of v.- Mises- stress in deck plate, when cross- beam spacing is 4 m.

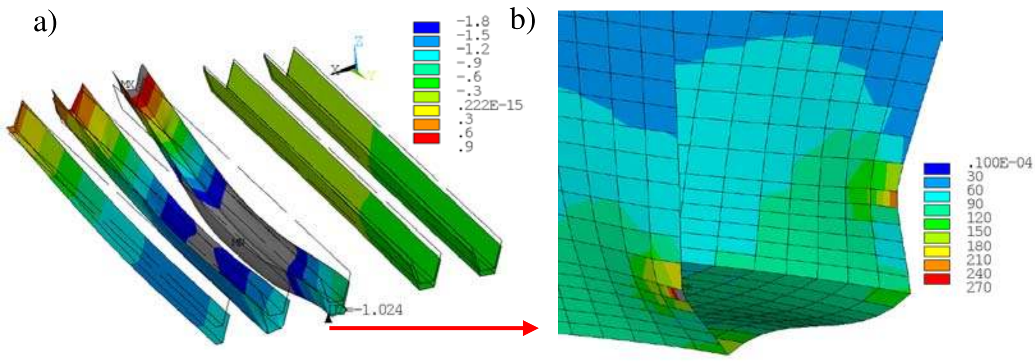

Figure 4.8 a) Distribution of vertical displacement in ribs, when cross- beam spacing is 4 m. b) Distribution of v.- Mises- stress in ribs, when cross- beam spacing is 4 m.

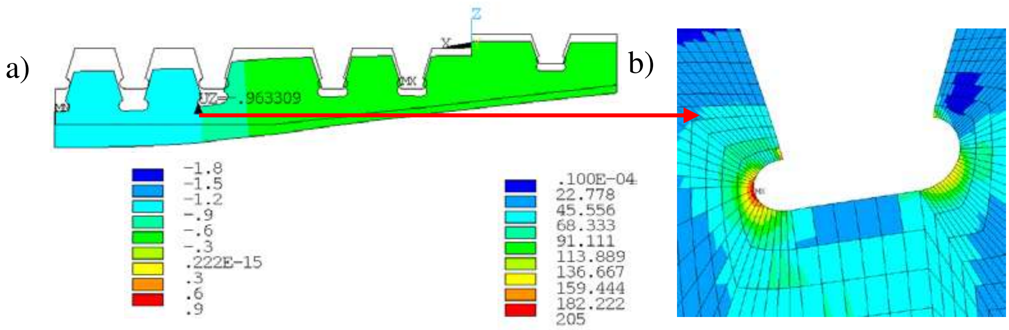

Figure 4.9 a) Distribution of vertical displacement in cross- beam, when cross- beam spacing is 4 m. b) Distribution of v.- Mises- stress in cross- beam, when cross- beam spacing is 4 m.

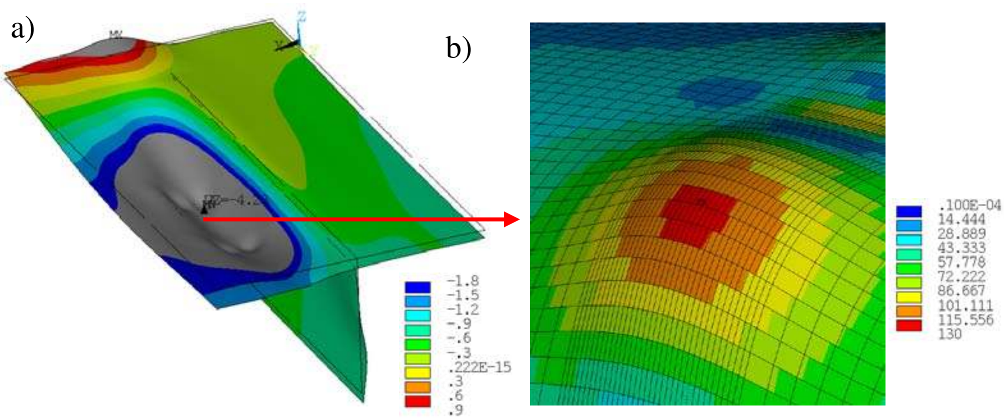

Figure 4.10 a) Distribution of vertical displacement in deck plate and main girder, when cross- beam spacing is 5 m. b) Distribution of v.- Mises- stress in deck plate, when cross- beam spacing is 5 m.

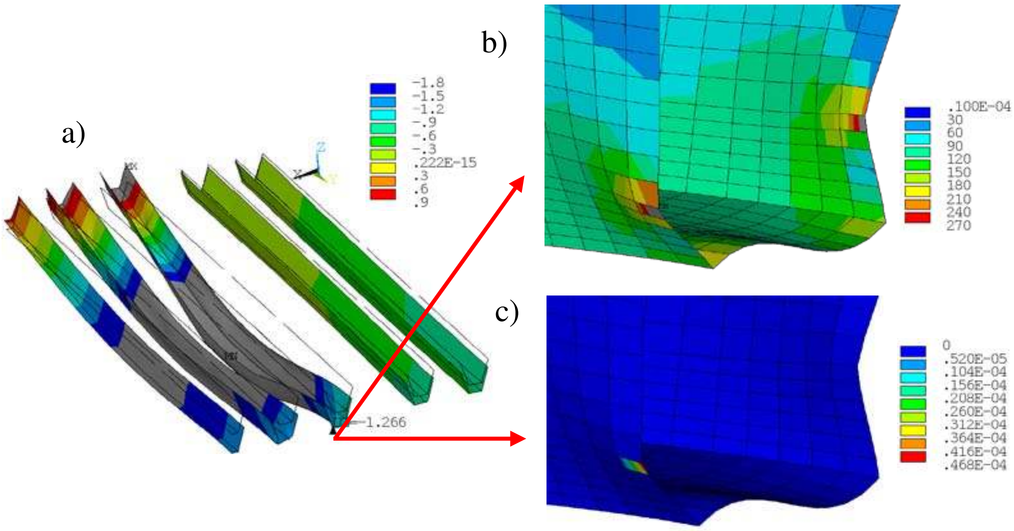

Figure 4.11 a) Distribution of vertical displacement in ribs, when cross- beam spacing is 5 m. b) Distribution of v.- Mises- stress in ribs, when cross- beam spacing is 5 m. c) Distribution of plastic strain in ribs.

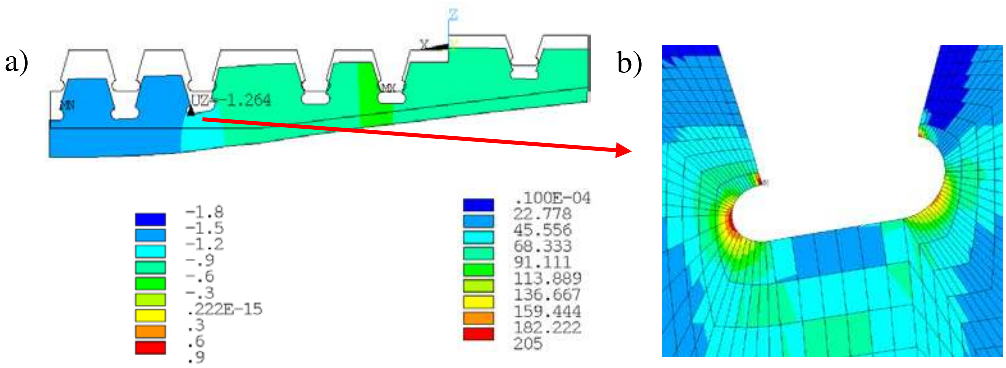

Figure 4.12 a) Distribution of vertical displacement in cross- beam, when cross- beam spacing is 5 m. b) Distribution of v.- Mises- stress in cross- beam, when cross- beam spacing is 5 m.

4.2 Effect of Cross- Beam Web Thickness on Stresses

This chapter investigates the change in stresses of steel structural parts, if cross- beam web thickness changes. For that reason, all other dimensions of the bridge defined in FE- model are kept constant, while cross- beam web thickness increases from 14 mm to 16, 18 and 20 mm respectively. Here the cross- beam spacing is always taken as 3 m in all simulations. Results show that any change in cross- beam web thickness has almost no effect on deck plate and rib stresses. The change of stresses in cross- beam itself are given in Figure 4.13 to Figure 4.16.

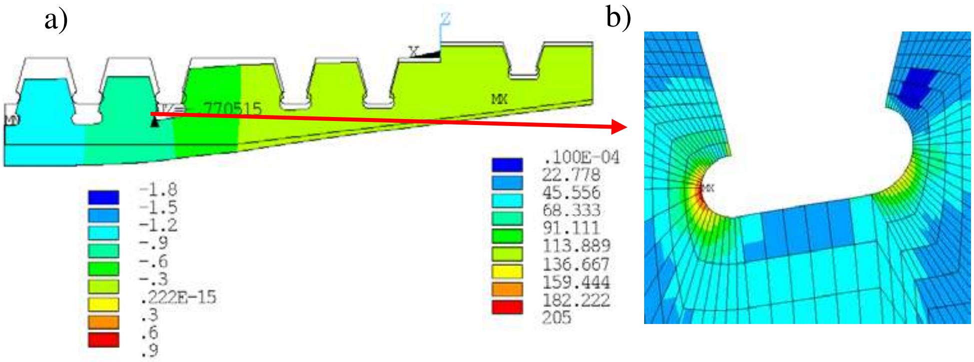

Figure 4.13 a) Distribution of vertical displacement in cross- beam, when cross- beam web thickness is 14mm. b) Distribution of v.- Mises- stress in cross- beam, when cross- beam web thickness is 14 mm.

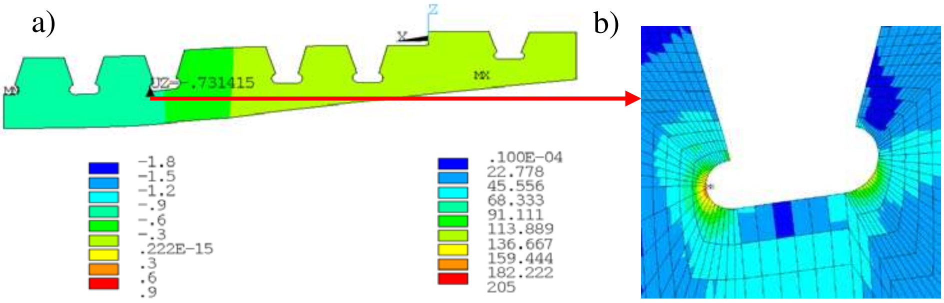

Figure 4.14 a) Distribution of vertical displacement in cross- beam, when cross- beam web thickness is 16 mm. b) Distribution of v.- Mises- stress in cross- beam, when cross- beam web thickness is 16 mm.

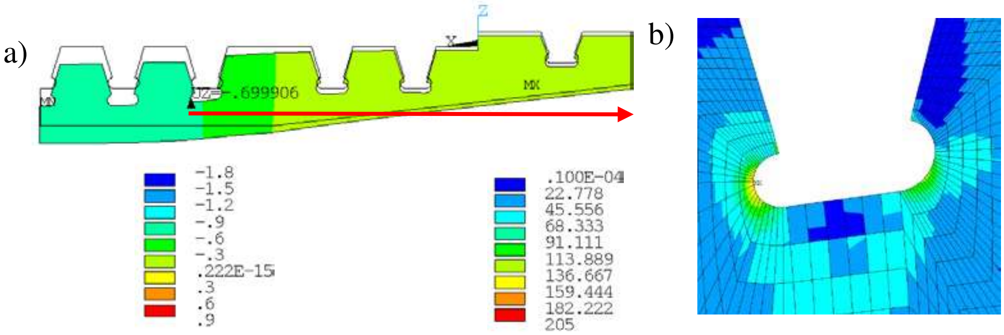

Figure 4.15 a) Distribution of vertical displacement in cross- beam, when cross- beam web thickness is 18 mm. b) Distribution of v.- Mises- stress in cross- beam, when cross- beam web thickness is 18 mm.

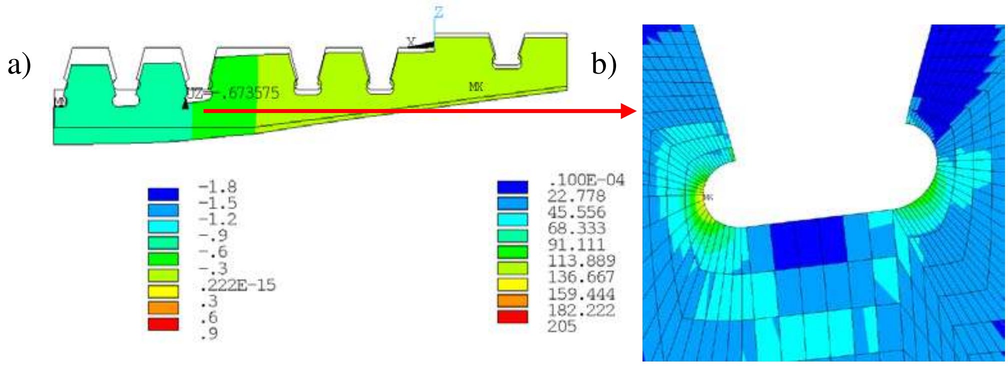

Figure 4.16 a) Distribution of vertical displacement in cross- beam, when cross- beam web thickness is 20 mm. b) Distribution of v.- Mises- stress in cross- beam, when cross- beam web thickness is 20 mm.

4.3 Results &Discussion

While cross- beam spacing increases, the deflections of deck plate, especially direct under wheel loads, increases heavily, nevertheless they still remain in elastic range. Max. v.- Mises- Stress emerges at the top face of deck plate, when cross- beam spacing is 2, 3 and 4 m. At cross- beam spacing of 5 m, max. v.- Mises- Stress emerges at the bottom face of deck plate direct under wheel loads. Stresses in deck plate decrease inverse proportional to cross- beam spacing, until it takes the value of 5 m. Apparently, the stresses in deck plate will increase proportional to cross- beam spacing after 5 m spacing value, since the sign of bending moment under wheel loading changes at 5 m spacing of cross- beam. As a result local effects (stresses & deflections) will be higher at cross- beam spacing of 6 m than cross- beam spacing of 5 m. With respect to stresses and deflections emerge in ribs, cross- beam spacing is of great importance, since the max. value of v.- Mises- Stress (indicator of damage) takes values from 150.785 MPa to 355.099 MPa, while cross- beam spacing rises from 2 to 5 m. As cross- beam spacing increases, twisting of the rib, which is under wheel load, becomes larger and results in higher stresses at rib to cross- beam connection. For instance at the cross- beam spacing of 2 m, twisting of the rib is very small, so that the bending is dominant on the deformed shape of the rib. This result can be obviously seen from the comparison of Figure4.2 and Figure4.11. Regarding cross- beam itself, increasing its spacing yields in increase of dead load on cross- beam and the moment arm of wheel loads. These effects cause slight increases of stresses and deflections in cross- beam itself.

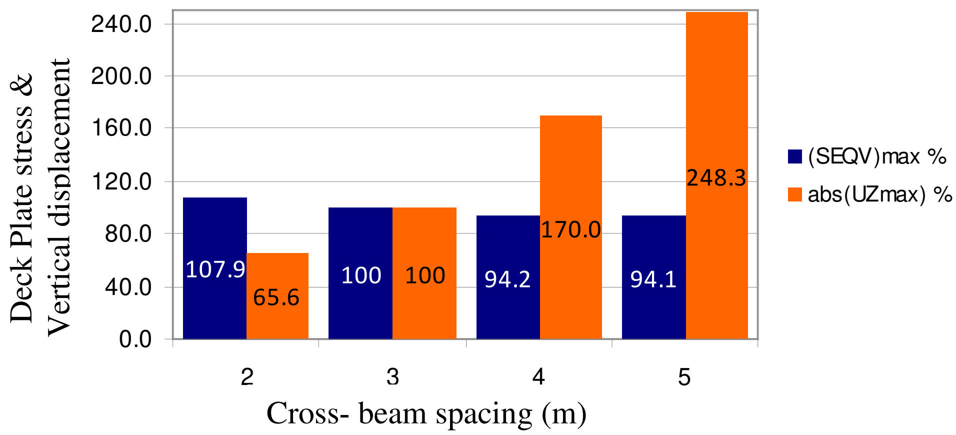

Figure 4.17 Variation of max. v.- Mises-Stress & vertical displacement in deck plate depending on cross- beam spacing.

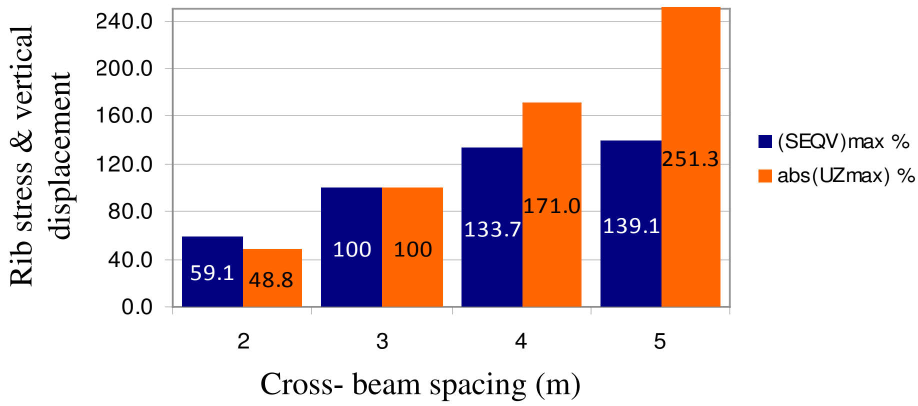

Figure 4.18 Variation of max. v.- Mises-Stress & vertical displacement in ribs depending on cross- beam spacing.

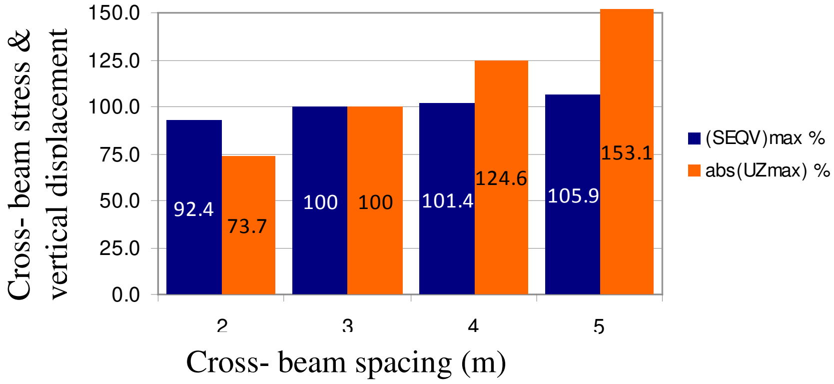

Figure 4.19 Variation of max. v.- Mises-Stress & vertical displacement in cross- beam depending on cross- beam spacing.

Because of increase in cross- beam web thickness, there exist almost no change in stresses and deflections developed in deck plate and ribs. The increase and so strengthening cross- beam web causes decreasing of shear force and so decreasing of tooth stresses in cross- beam web. The amount of this decrease in stress and deflection values is illustrated in Figure4.20 below.

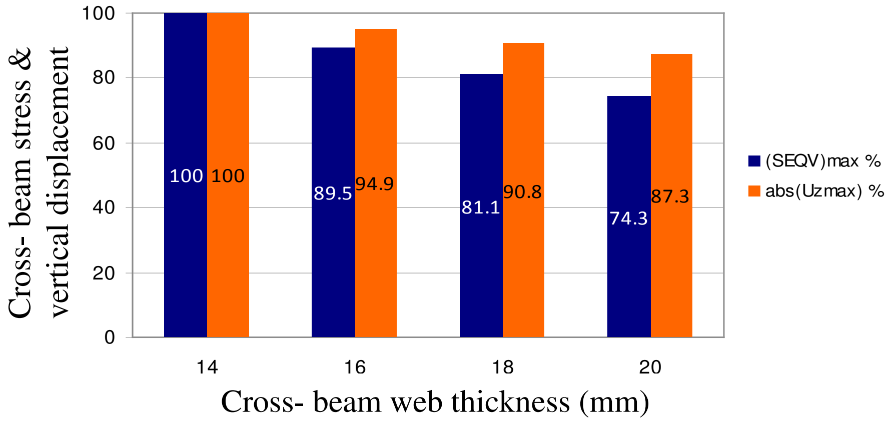

Figure 4.20 Variation of max. v.- Mises-Stress & vertical displacement in cross- beam depending on cross- beam web thickness.

It is seen from the results that the increase of cross- beam spacing from 2 m to 5 m causes very slight decrease of deck plate stresses, but heavily increase of deck plate deflections. With regard to steel load bearing parts of bridge all these stresses and deflections stay in elastic limits and have no hazard on the bridge. Nevertheless, the excessive deflections of deck plate can result in irreversible vertical displacements in wearing surfaces lying on deck plate and as a result rut formations can occur in wearing surface. In terms of longitudinal ribs, stresses and deflections are highly affected by cross- beam spacing. At 5 m of cross- beam spacing rib material starts to yield. A cross- beam spacing between 3 and 4 m is recommended for the bridge analyzed in this thesis. Too small cross- beam spacings like between 2 and 3 m are found to be very conservative under wheel loads. Regarding cross- beam itself, the increase of its spacing leads to slight increase of stresses and deflections in cross- beam. Therefore it is concluded that the stresses in cross- beam are allowed not to be considered, when determining cross- beam spacing of the bridge. As for cross- beam web thickness, it has no effect on the stresses developed in deck plate and ribs, but has effect on the stresses developed in cross- beam itself, as expected.

CHAPTER 5

ARRANGING THICKNESSES AND SPACINGS OF ORTHOTROPIC DECK FOR DESIRED FATIGUE LIFE AND DESIGN CATEGORY

When the orthotropic deck structure design was developed in 1960s, fatigue calculations were not considered in design principles [65]. In addition, fatigue strengths of structural parts forming orthotropic deck were also not known at that time. In time cracks have appeared and developed continuously in orthotropic decks, which shall not have been emerged in orthotropic deck according to design principles foreseen at that time. These cracks and improved fatigue theory of fluctuating variable loads reminded to calculate orthotropic decks as per fatigue strengths [6]. Afterwards, several research facilities have been started to obtain fatigue strengths of structural details of orthotropic decks [66-70]. Finally, Eurocode 3 Part 1-9[23] collects fatigue strengths of orthotropic deck details and is used throughout this thesis for the fatigue calculations. To simulate vehicle loads in traffic, static wheel loads and wheel load area, which comply with the wheels of vehicles used today in traffic, are selected. Since the number and weight of vehicles in traffic are increased in time since 1960's up to now, the frequency of wheel loads on the bridges, hence the design traffic category of many existing bridges changed. As a solution to this problem, thicknesses, spacings and spans of fatigue sensitive structural parts of bridge are determined under today' s valid wheel loads and design traffic category for desired fatigue life in the next section. These fatigue sensitive structural parts are the critical section in web of cross girder due to cut outs, weld connecting deck plate to trapezoidal rib, continuous longitudinal stringer and deck plate. Subsequently, results are assessed and conclusions of this thesis together with future work are given. Cross- beam spacing is always taken as 3 m in all FE- analyses except the FE- analysis named as Redesign- 2. Width of pedestrian road and deck plate in transverse direction are 1.1 m and 6.3 m respectively, while width of deck plate changes, when rip spacing changes. Nevertheless, length of deck plate is always equal to 6 m (bridge span distance), when cross- beam spacing changes. That is, number of cross beams differs for cross beam spacing of 3 m (3 cross- beams) and 2 m (4 cross-beams).

5.1 Critical Section in web of cross- girder due to cut- outs

In this structural part Vierendeel stresses play the distinctive role, when designing for desired fatigue life. Vierendeel stresses are basically described as linearly distributed bending stresses as given in Figure 5.2. Stress range at this part is calculated by means of the stress results of FE- analysis. Fatigue strength of this part is given in detail category 71 as per Eurocode 3 Part 1-9 (D) Table 8.8 [23]. Stress distribution in this critical part is depicted in Figure 5.1, in which web tickness of cross girder is determined by stresses due to Vierendeel effect. Because entire bridge geometry is incorporated in the FE- model, stress concenrations develop at the edge of cut outs, even though the material does not yield. If the concentration of stresses at cut out edge is ignored and the distribution of stresses are assumed linear, the traditional stresses due to Vierendeel effect result in the values given in Figure 5.2. Since stress ranges given in S- N curves are based on stresses calculated according to linear elasticity theory, the linear distributed stresses in Figure 5.2 shall be taken into account for fatigue calculations. Using stresses calculated based on elasticity theory, when using S- N curve is stipulated by Eurocode 3 Part 1- 9 [23].

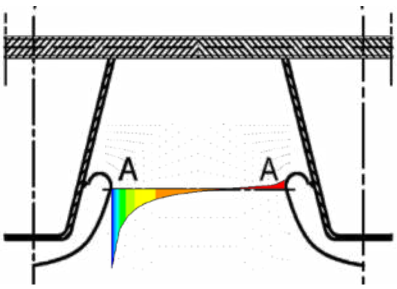

Figure 5.1 Stress distribution in cross girder in vicinity of cut outs. (Simulation "BB").

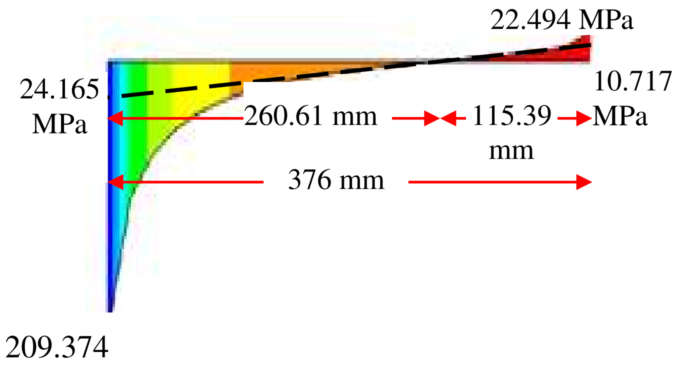

Figure 5.2 Stresses due to Vierendeel effect with and without concentration at edges. (Simulation "BB").

First, the stress range of this structural part for its fatigue calculation is simply the double of max. absolute stress at the edge of cut out. Second, the endurance of this structural part is calculated using fatigue strength (S- N curve), which is fatigue detail category 71 given in Figure 5.3. Third, the fatigue life of structural part is calculated using Table 4.5 in Eurocode 1 Part 2 as per different web thicknesses of cross girder. Table 5.1 shows Table 4.5 in Eurocode 1 Part 2 [63], which shows the occurance of stress range in a year according to bridge design traffic category.

Table 5.1 Number of vehicle passing per year for one traffic lane.

Design Traffic Category	Occurance of stress range per year for one traffic lane
1: Motorways and streets with 2 or more traffic lanes in every traffic direction and with high passing of trucks	$2x10^6$
2: Motorways and streets with average passing of trucks	$0.5x10^6$
3: Main streets with low passing of trucks	$0.125x10^6$
4: Local streets with low passing of trucks	$0.05x10^6$

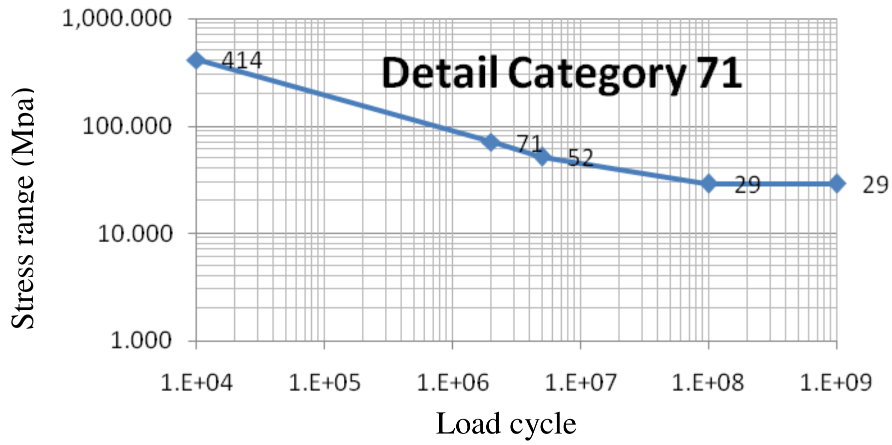

Figure 5.3 Fatigue strength curve 71.

$\Delta\ \sigma_{E,2}$ = 2x24.165 = 48.33 MPa

γ_{Ff} = 1.00

γ_{Mf} = 1.15 (According to Eurocode 3 Part 1-9: 2003 (D) Table 3.1: Damage tolerant assessment method with high consequence of failure [23]).

γ_{Ff} x $\Delta\sigma_{E,2}$ = 48.33 < 61.74 = 71 / 1.15 = 61.74 = $\Delta\sigma_C$ / γ_{Mf}

The fatigue calculation done above is repeated for increased web thicknesses of cross girder. There are totally 4 conditions; web thickness of 14 mm (simulation BB), 16 mm (simulation QSD16), 18 mm (simulation QSD18) and 20 mm (simulation QSD20).

Table 5.2 summarizes the results of fatigue calculation, namely fatigue lives as per chosen cross- beam web thickness and design traffic category.

Table 5.2 Fatigue life calculation of web of cross girder as per its thickness

Simulation's name	$\Delta\ \sigma_{E,2}$ (MPa)	N_i	Fatigue life (year) as per Design Traffic Category			
			1	2	3	4
BB	48.330	4 094 832	2.05	8.19	32.76	81.90
QSD16	42.808	6 574 653	3.29	13.15	52.60	131.49
QSD18	38.390	11 334 620	5.67	22.67	90.68	226.69
QSD20	34.770	18 598 335	9.30	37.20	148.79	371.97

According to Capital 4.6.1 General Issues 2(c) of Eurocode 1 Part 2 [63] service life of bridges shall be 100 years for all design traffic categories. Fatigue lives depending on design traffic categories are calculated for cross- beam web thicknesses of 14 mm, 16 mm, 18 mm and 20 mm respectively. Figure 5.4 shows that increasing cross- beam web thickness leads increasing of its fatigue life. As design category number of bridge increases, slope of the curve given in Figure 5.4 increases also. However, required service life of bridge (100 years) is obtained only for design traffic categories of 3 and 4. As a result, recommended cross- beam web thicknesses for bridges of design traffic category 3 and 4 are 20 mm and 16 mm respectively.

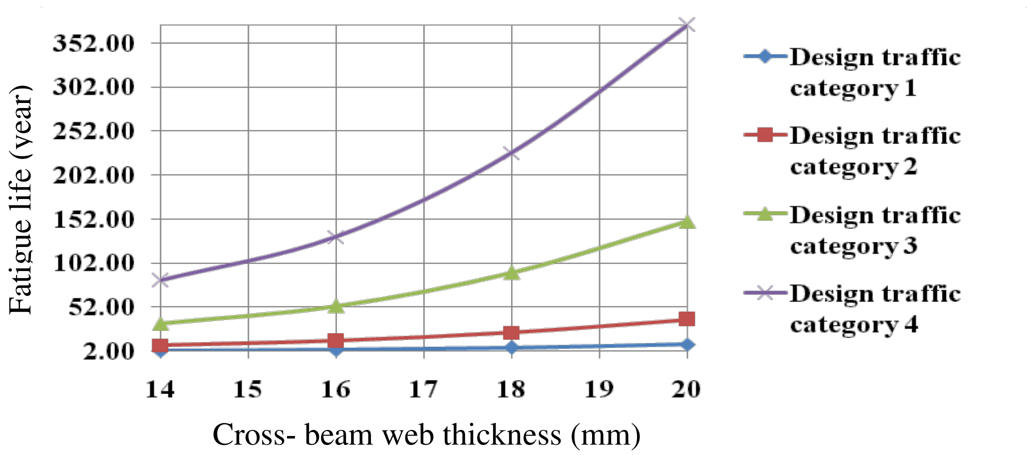

Figure 5.4 Fatigue lives of cross- beam web as to thickness and design traffic category.

5.2 Continuous Longitudinal Stringer, with Additional Cut-out in Cross Girder

The fatigue assessment of this structural part is based on the direct stress in the longitudinal stringer (see Figure 5.5). The fatigue strength of this structural part is determined by Fatigue Strength Curve 71 according to Eurocode 3 Part 1-9: 2003 (D) Table 8.8 [23]. Here Fatigue Strength Curve 71 is selected instead of Curve 80, since the thickness of cross beam web is 14 mm (higher than 12 mm).

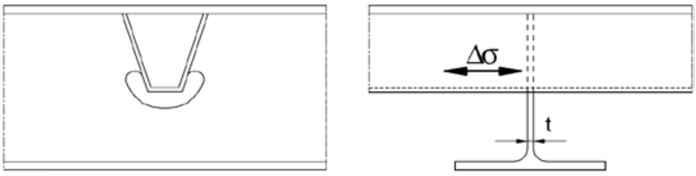

Figure 5.5 Fatigue sensitive structural part.

$\Delta\ \sigma_{E,2}$ = 2x82.162 = 164.324 MPa (See Figure 5.6)

γ_{Ff} = 1.00

γ_{Mf} = 1.00 (According to Eurocode 3 Part 1-9: 2003 (D) Table 3.1: Damage tolerant assessment method with low consequence of failure [23]).

γ_{Ff} x $\Delta\sigma_{E,2}$ = 164.324>71 = $\Delta\sigma_C$ / γ_{Mf}

The fatigue life of this structural part is very short even for design traffic category 4. Now 4 scenarios will be assessed, in which rib thicknesses are increased. These are the results of simulations having names of RD8NRV1, RD8NRV2, RD10NRV1 and RD10NRV2. In RD8NRV1, the thickness of one rib at both sides of main girder is increased from 6 mm to 8 mm. In RD8NRV2, the thickness of two ribs at both sides of main girder is increased from 6 mm to 8 mm. In RD10NRV1, the thickness of one rib at both sides of main girder is increased from 6 mm to 10 mm. In RD10NRV2, the thickness of two ribs at both sides of main girder is increased from 6 mm to 10 mm. Increasing rib thickness leads lengthening of structure' s fatigue life as seen in Table 5.3, nevertheless none of the fatigue lives provides a meaningful lifespan for structure.

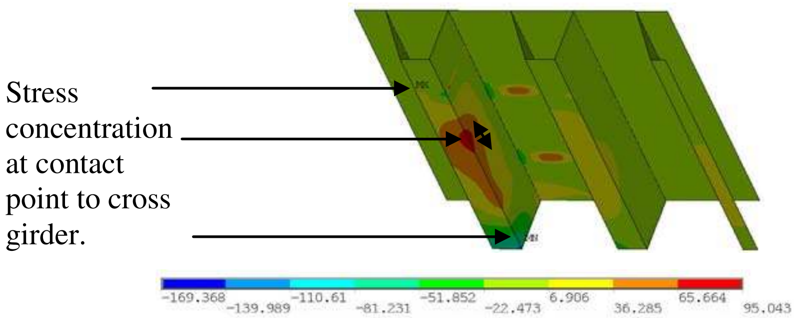

Figure 5.6 Extreme values of direct stresses in ribs. (Simulation "BB").

Table 5.3 Fatigue life calculation of rib as per its thickness.

Simulation name	$\Delta\ \sigma_{E,2}$ (Mpa)	N_i	Fatigue life (year) as perDesign Traffic Category			
			1	2	3	4
BB	164.324	158 444	0.08	0.32	1.27	3.17
RD8NRV1	122.860	379 095	0.19	0.76	3.03	7.58
RD8NRV2	120.638	400 431	0.20	0.80	3.20	8.01
RD10NRV1	97.620	755 725	0.38	1.51	6.05	15.11
RD10NRV2	94.682	828 281	0.41	1.66	6.63	16.57

Figure 5.7 illustrates the variation of fatigue life of continuous longitudinal stringer. Neither traditional rib web thickness of 6 mm nor increased rib web thickness values of 8 mm and 10 mm provides required bridge' s service life, 100 years. Max. fatigue life of this structural part even for design traffic category 4 and using 10 mm rib web thickness is very low, 16.57 years. So, not increasing rib web thickness, but may be decreasing rib spacing and / or cross- beam spacing can supply required fatigue stiffness to this structural detail.

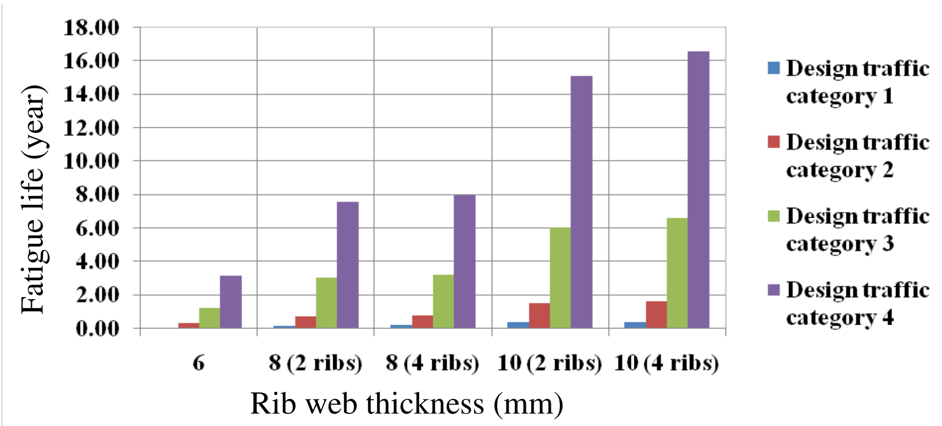

Figure 5.7 Fatigue lives of rib web as to thickness and design traffic category.

5.3 Weld connecting deck plate to rib

Weld connecting deck plate to rib is of importance as per fatigue strength on the basis of practical findings. Calculation of stress range depends on the moment in rib web (see Figure 5.8).

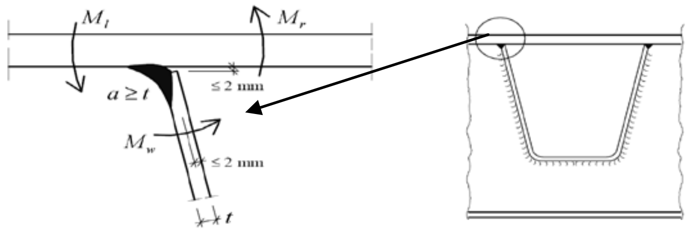

Figure 5.8 Weld connecting deck plate to rib.

According to Eurocode 3 Part 1-9: 2003 (E) Table 8.8 [23] assessment of fatigue life is based on direct stresses from bending of rib web. This direct stress is taken from the results of FE- analysis given in Table 5.4 (See also Figure 5.9).

$\Delta\ \sigma_{E,2}$ = 2x67.469 = 134.938 MPa

$\gamma_{Ff} = 1.00$

γ_{Mf} = 1.15 (According to Eurocode 3 Part 1-9: 2003 (D) Table 3.1: Damage tolerant assessment method with high consequence of failure [23]).

γ_{Ff} x $\Delta\sigma_{E,2}$ = 134.938 >71/ 1.15 = 61.74 = $\Delta\sigma_C$ / γ_{Mf}

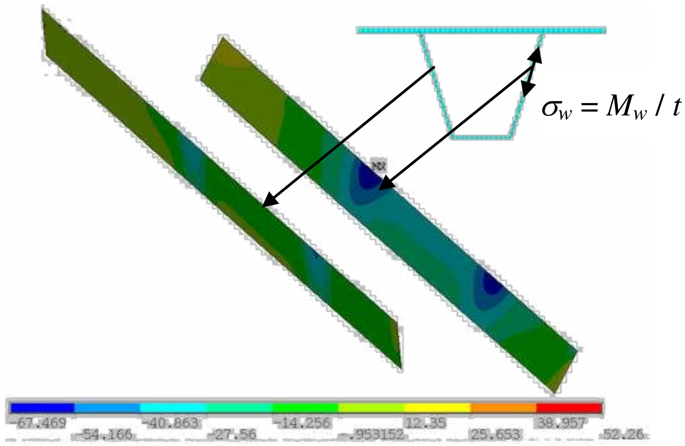

Figure 5.9 Direct stress values for fatigue assessment of weld. (Simulation "BB").

If it is assumed that the contact area between deck plate and rib carries the traffic load in case of pressure stresses, the max. tension stress is equal to the stress range for the fatigue calculation of weld.

γ_{Ff} x $\Delta\sigma_{E,2}$ = 52.26 <71/ 1.15 = 61.74 = $\Delta\sigma_C$ / γ_{Mf}

The fatigue lives of weld are given in Table 5.4. Unfortunately, according to the results given in Table 5.4 any increase of rib web has almost no effect on the fatigue life of weld.

Table 5.4 Fatigue life calculation of weld between rib and deck plate as per rib thickness.

Simulation's name	$\Delta\ \sigma_{E,2}$ (MPa)	N_i	Fatigue life (year) as per Design Traffic Category			
			1	2	3	4
BB	52.260	3 238 757	1.62	6.48	25.91	64.78
RD8NRV1	52.732	3 152 563	1.58	6.31	25.22	63.05
RD8NRV2	52.597	3 176 900	1.59	6.35	25.42	63.54
RD10NRV1	51.444	3 395 333	1.70	6.79	27.16	67.91
RD10NRV2	51.605	3 363 653	1.68	6.73	26.91	67.27

As given in Table 5.4 weld connecting deck plate to rib has not a fatigue life equals or higher than 100 years, when the thickness of rib 6 mm, 8 mm or 10 mm is. In addition, changing rib web thickness has almost no influence on fatigue life of weld connecting deck plate to rib.

5.4 Deck plate

The fatigue calculation of deck plate is done as per Fatigue Strength Curve 160, which is given in Figure 5.10. Therefore sharp edges, surface and rolling flaws on deck plate shall be improved by grinding, until smooth transition is achieved.

5.4.1 Deck plate part, which is on the rib web

$\Delta\ \sigma_{E,2}$ = 2x134.291 = 268.582 MPa (See Figure 5.11)

$\gamma_{Ff} = 1.00$

γ_{Mf} = 1.00 (According to Eurocode 3 Part 1-9: 2003 (D) Table 3.1: Damage tolerant assessment method with low consequence of failure [23]).

$\gamma_{Ff} \times \Delta\sigma_{E,2} = 268.582 > 160 = \Delta\sigma_C / \gamma_{Mf}$

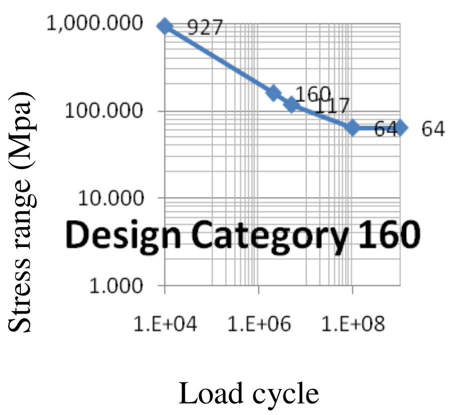

Figure 5.10 Fatigue Strength Curve 160.

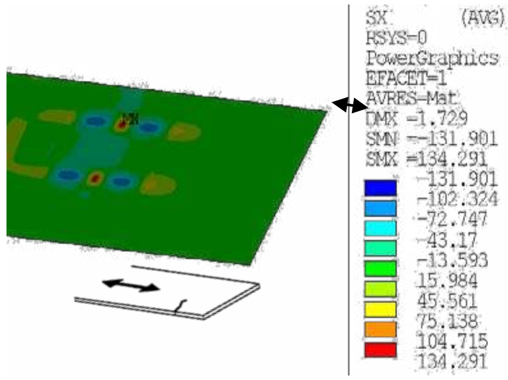

Figure 5.11 Direct stresses in deck plate for fatigue calculation. (Simulation "BB").

Results tabulated in Table 5.5 indicate that increasing deck plate thickness has a positive effect on increasing fatigue life, however this does not provide satisfied values. In Table 5.5 deck plate thicknesses in simulations BB, DBD14 and DBD16 are 12 mm, 14 mm and 16 mm respectively.

Table 5.5 Fatigue life calculation of deck plate on rib web as per deck plate thickness.

Simulation's name	$\Delta\ \sigma_{E,2}$ *(Mpa)*	N_i	Fatigue life (year) as per Design Traffic Category			
			1	2	3	4
BB	268.582	413 330	0.21	0.83	3.31	8.27
DBD14	179.170	1 392 296	0.70	2.78	11.14	27.85
DBD16	121.240	4 493 552	2.25	8.99	35.95	89.87

5.4.2 Deck plate part between rib webs

γ_{Ff} x $\Delta\sigma_{E,2}$ = 107.342 + 102.377 = 209.719 > 160 = $\Delta\sigma_C$ / γ_{Mf} (See Figure 5.12)

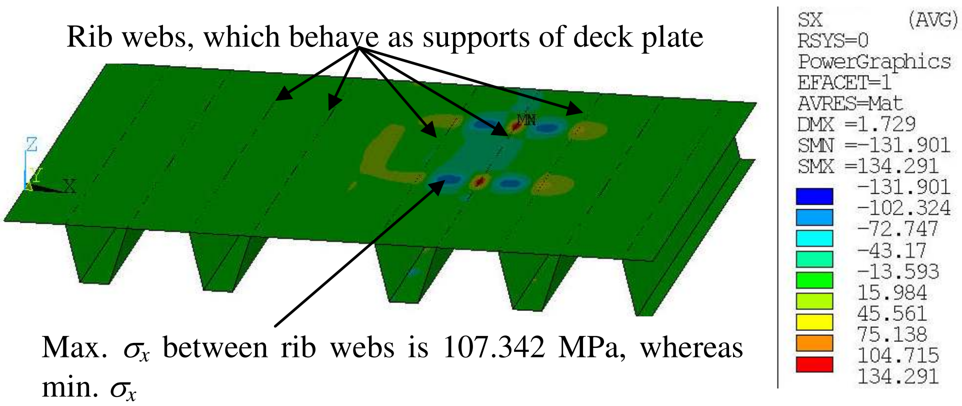

Figure 5.12 Stresses considered for fatigue calculation of deck plate between rib webs.

Table 5.6 tabulates the fatigue results , when deck plate thickness 12 mm (BB), 14 mm (DBD14) and 16 mm (DBD16) is.

Table 5.6 Fatigue lives of deck plate between rib webs as per deck plate thickness.

Simulation's name	Max. Stress	Min. Stress	$\Delta\ \sigma_{E,2}$ *(MPa)*	N_i	Fatigue life (year) as per Design Traffic Category			
					1	2	3	4
BB	107.342	102.377	209.719	868 189	0.43	1.74	6.95	17.36
DBD14	84.322	80.74	165.062	1 780 682	0.89	3.56	14.25	35.61
DBD16	69.226	66.492	135.718	3 203 430	1.60	6.41	25.63	64.07

It is seen from Figure 5.13 and Figure 5.14 that increasing deck plate thickness results in higher fatigue lives of this structural part, nevertheless never supplies the required service life, 100 years. Reducing rib spacing shall be a remedy for supplying the required service life of 100 years.

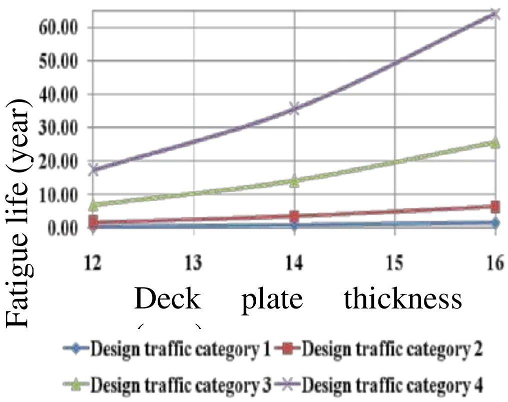

Figure 5.13 Fatigue lives of deck plate part between rib webs as to thickness and design traffic category.

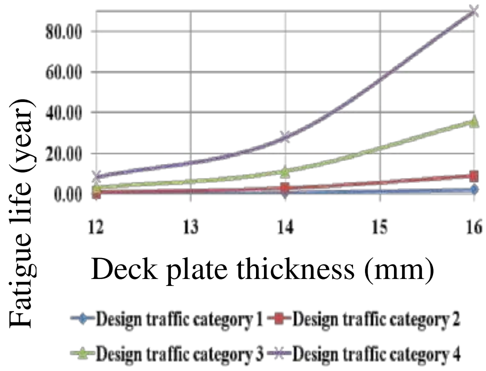

Figure 5.14 Fatigue lives of deck plate part on rib web as to thickness and design traffic category.

5.5 Redesign of Bridge Providing Necessary Fatigue Life

Because all of the structural parts of bridge do not simultaneously provide 100 years even for design traffic category 4, new designs of orthotropic bridge are required to be evaluated. Subsequently, two redesigns are considered according to the dimensions given in Table 5.7. Fatigue calculations of redesigned orthotropic deck structure are given in Table 5.8.

Table 5.7 Changed dimensions in FE- analyses, Redesign- 1 and -2.

Dimension definition	Redesign- 1	Redesign- 2
Cross- beam spacing (m)	3	2
Rib spacing (mm)	100	150
Deck plate thickness (mm)	18	18
Cross- beam web thickness (mm)	16	16

Table 5.8 Fatigue lives of redesigned bridge structures.

Simulation Name	Structural Part	$\Delta\ \sigma_{E,2}$ *(MPa)*	N_i	Fatigue Life (year) as per Desig Traffic Category			
				1	2	3	4
Redesign 1	Cross-beam	10.774		∞			
	Rib	16.616					
	Weld	9.251					
	Deck plate between rib webs	34.225					
	Deck plate on rib webs	77.04	40 388 858	20.19	80.78	323.11	807.78
Redesign 2	Cross-beam	6.951		∞			
	Rib	51.162	5 423 119	2.71	10.85	43.38	108.46
	Weld	16.373		∞			
	Deck plate between rib webs	105.94	8 214 847	4.11	16.43	65.72	164.30
	Deck plate on rib webs	65.492	90 982 538	45.49	181.97	727.86	1 819.65

In the first redesign of the bridge stress ranges appeared in cross- beam web, longitudinal stringer and weld connecting deck plate to rib are below cut- off limit. However stress range developed in deck plate part resting on rib web enforced bridge to be classified in design traffic category 3. If deck plate thickness is increased, design traffic category of bridge can be increased to 2 and 1 without changing other dimensions of bridge. Second redesign of bridge has a fatigue life of 108.46 years, when it is used as to design traffic category 4. The comparison of dimensions and fatigue lives of separate structural parts between Redesign- 1 and -2 indicates that decreasing rib spacing is more effective than decreasing cross- beam spacing to increase fatigue life of structure.

5.6 Results & Discussion

It is numerically proven in this thesis that, there exists an important dimensional change, whether a bridge is designed only as to yield stress or as to desired fatigue life under foreseen design traffic category. It is recommended to determine first rib spacing and then cross- beam spacing, when a bridge is designed for a desired fatigue life under foreseen design traffic category. Subsequently, thicknesses of deck plate and cross- beam web shall be chosen appropriately. The height of longitudinal stringer may be a parameter to reduce the stress range in ribs and weld connecting deck plate to rib. Types and thickness of the wearing surfaces, which disperse wheel load on deck plate, might be a solution to reduce stress ranges developed in structural parts. These will be the research subjects of the author in the future work.

CHAPTER 6

A FE- ANALYSIS STUDY CONFORMING RECOMMEDATIONS OF EUROCODE 3 PART 2 REGARDING RIB DIMENSIONS AND CROSS- BEAM SPACING

Eurocode 3 Part2 recommends a chart in Annex C.1.2.2 for dimensioning of ribs [52]. This chart is based on several researches, calculations, laboratory tests and engineering experience and judgments. This thesis aims to prove the correctness of this chart using FE- analyses, which are not done so far according to the knowledge of author.

6.1 FE- Analysis

In FE- analyses, dimensions of deck plate and ribs are chosen with respect to minimum requirements recommended by Eurocode 3 Part2 Annex C.1.2.2 [52] for cross- beam spacings of 3.5 m, 4.0 m and 4.5 m respectively. Recommendations of Eurocode for choosing rib dimensions as to cross- beam spacings are given in Figure 6.1.

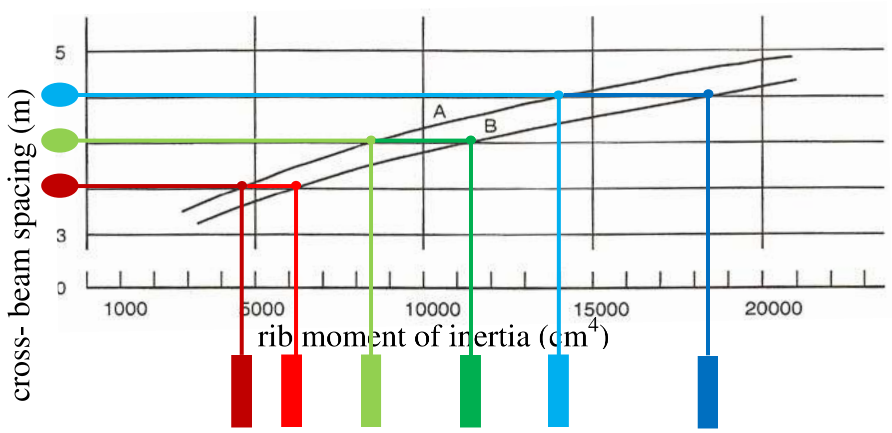

Figure 6.1 Recommendations of Eurocode 3 Part 2 for rib moment of inertia depending on cross- beam spacing.

In Figure 6.1 two curves, namely Curve A and Curve B are given. Curve B is used for the ribs in the 1.20 m vicinity of main girder at both sides as shown in Figure 6.2. In the FE- analyses performed in this thesis there are total four ribs, which shall be dimensioned using Curve B (See Figure 6.3). Curve A is used for all other ribs, which are not encompassed by Curve B. Curve A and Curve B are allowed to be used for all forms of ribs [52].

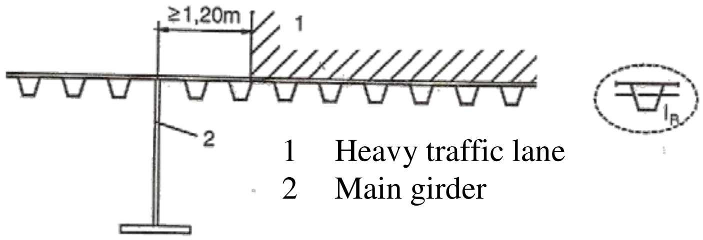

Figure 6.2 Distinction of ribs, for which Curve B is used and are located in the 1.2 m vicinity of main girder [52].

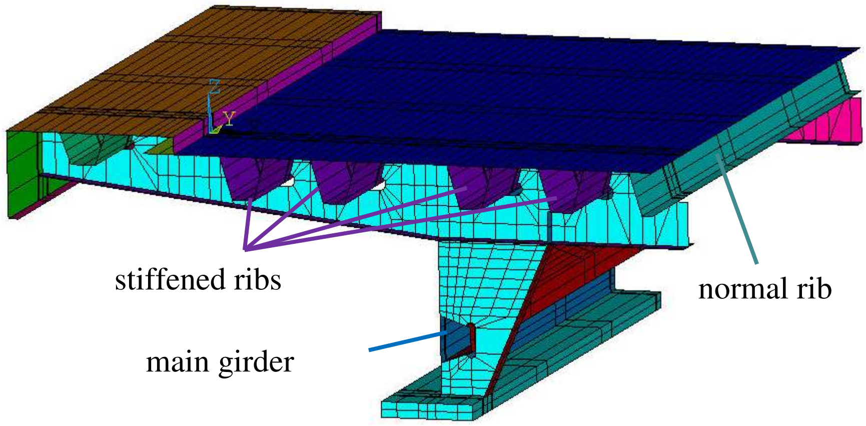

Figure 6.3 Depiction of four stiffened ribs in the 1.2 m vicinity of main girder and one normal rib at the symmetry center of FE- solid model.

Dimensions of deck plate and ribs used in FE- analyses are tabulated in Table 6.1.

Table 6.1 Dimensions of deck plate and ribs used in FE- analyses.

FE- analysis name	Cross- beam spacing (m)	Min. I_R as to EC 3 Part 2 (cm^4)		Selected I_R (cm^4)		Selected dimensions (mm)		
		Normal rib	Stiffened rib	Normal rib	Stiffened rib	Deck plate	Normal rib	Stiffened rib
DINFB3500	3.5	4500	6250	4527.44	6273.18	12	3.8	5.6
DINFB4000	4.0	8500	11500	8584.82	11550.08	16	7.7	11.2
DINFB4500	4.5	14000	18500	14082.84	18506.41	26	12.6	17.8

6.2 Results& Discussion

Results of FE- analyses are presented using figures and tables below. Deformations occurred under wheel loads are presented using pictures of resultant displacements on the bridge structure. Max. resultant displacements are 2.385 mm, 1.719 mm and 1.412 mm for simulations named as DINFB3500, DINFB4000 and DINFB4500 respectively. Values of vectorial stresses as to load bearing steel parts are tabulated in Table 6.2 and interpreted in the subsequent chapter. Afterwards, v.- Mises stress is used to visually present and compare the results both at different points of structure and at same points of different FE- analyses. Since v.- Mises stress is a scalar value and an indicator of yield condition, it is suitable for visually illustration of stress results. In every analyses max. v.- Mises stress rises at the interior stiffened rib next to main girder as shown in Figure 6.4. The close- up view of v.- Mises stress distribution of every analyses are given in Figure 6.7 to Figure 6.9 using non- averaged element results. Here max. v.- Mises stress develops always in the close vicinity of intersection between rib and cross-beam webs.

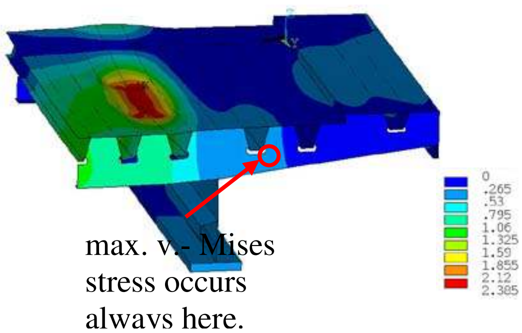

Figure 6.4 Distribution of resultant displacement for DINFB3500.

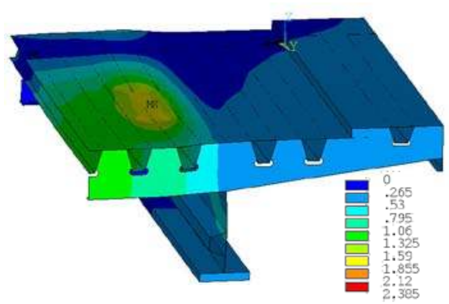

Figure 6.5 Distribution of resultant displacement for DINFB4000.

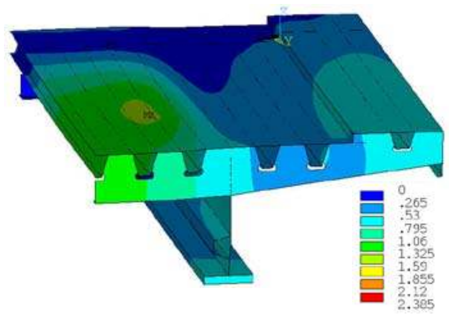

Figure 6.6 Distribution of resultant displacement for DINFB4500.

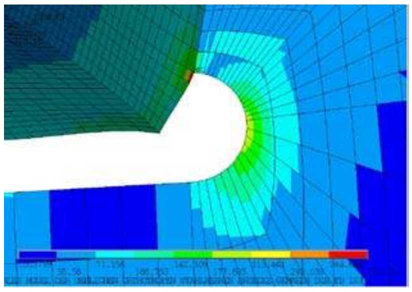

Figure 6.7 Distribution of v.- Mises stress for DINFB3500.

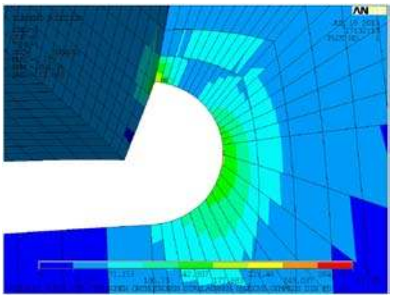

Figure 6.8 Distribution of v.- Mises stress for DINFB4000.

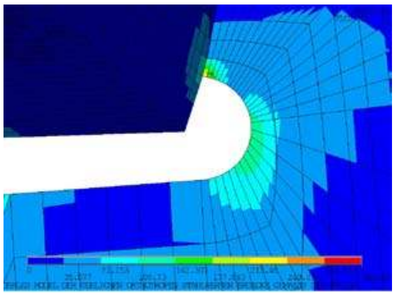

Figure 6.9 Distribution of v.- Mises stress for DINFB4500.

Table 6.2 Stresses developed in structural parts

Type of structure	Type of Stress *(MPa)*	DINFB3500		DINFB4000		DINFB4500	
		max. tens.	max. comp.	max. tens.	max. comp.	max. tens.	max. comp.
Deck plate	σ_{x*}	128.17	127.60	70.77	70.65	35.00	49.40
	σ_{y*}	61.04	78.54	41.44	48.72	23.97	24.38
	σ_{z*}	~ 0					
Cross beam	σ_{x**}	137.73	95.39	219.03	148.86	251.95	184.85
	σ_{y**}	~ 0					
	σ_{z**}	119.92	215.36	115.17	187.87	104.95	146.20
Normal rib	σ_{x***}	0.91	0.85	1.26	1.49	1.63	2.05
	σ_{y***}	11.02	7.98	10.79	8.12	10.94	9.26
	σ_{z***}	6.88	2.86	6.81	4.23	6.85	5.60

Table 6.2 (cont'd)

Stiffened rib	σ_{x***}	104.35	101.48	52.92	47.08	31.36	25.94
	σ_{y***}	180.71	237.14	69.50	133.40	58.56	91.04
	σ_{z***}	312.57	210.79	175.77	113.25	109.62	85.94

*σ_x, σ_y and σ_z are transverse bending stress, longitudinal bending stress and normal stress perpendicular to deck plate plane respectively in deck plate steel material.

**σ_x, σ_z and σ_y are transverse bending stress, vertical bending stress and

Since deck plate forms top flange of rib moment of inertia, thickness of deck plate is increased proportional to cross- beam spacing, in order to meet the recommendation given in Eurocode 3 Part 2[52]. It is seen from Figure 6.4 to Figure 6.6 and Table 6.2, that increasing deck plate thickness results in lower deformation and stress values in deck plate itself. Figure 6.7 to Figure 6.9 reveal that the steel material never yields, in case the min. rib moment of inertia as per Eurocode 3 Part 2 [52] is chosen. It can also be stated that the recommendations of Eurocode 3 Part 2 [52] stipulates more conservative design for cross- beam spans of 4 m and 4.5 m. Transverse stress (σ_x) rises proportional to cross- beam spacing, whereas vertical stress (σ_z) reduces in cross- beam itself as given in Table 6.2. Since the wheel load is far enough from the normal rib, stresses developed in normal rib remain in a very low values, which can be ignored for the assessment. Extreme values of shear stresses developed in steel parts are also very low, so that they are not used in the evaluation of results. Holding the recommendations of Eurocode 3 Part 2 [52] causes always lower normal stresses in stiffened ribs for higher cross- beam spans as indicated in Table 6.2. In DINFB3000 FE- analysis max. v.- Mises stress develops in the rib steel part, whereas in DINFB4000 and DINFB4500 it develops in the cross- beam steel part. Because the thickness of stiffened rib increases from 5.6 mm to 11.2 mm and 17.8 mm in the FE- analyses named as DINFB3500, DINFB4000 and DINFB4500 respectively, while the web thickness of cross- beam remains constant, this result is as expected.

CHAPTER 7

ASSESSMENT ON WEB SLOPE OF TRAPEZOIDAL RIB IN ORTHOTROPIC DECK USING FE- METHOD

Ribs can possess several different shapes like strip, bulb, angle, V- shaped, U- shaped, sektkelch or trapezoidal. This thesis focuses on trapezoidal ribs, since they are dominantly used in industry. Three different slopes of trapezoidal rib web are assessed using FE- method, while rib width, height, spacing and thickness are kept constant. Results show that stresses especially of cross- beam and deflections of deck plate change depending on slope of trapezoidal stiffener webs. Ribs are the longitudinal stiffeners, which are welded continuously to deck plate from bottom and to cross beams intermittently at cross beam locations. In this manner deck plate forms flanges of ribs and cross beams and also a supporting base to its wearing surface, while spreading the load on all structural components. Ribs are referred to as longitudinal stiffener, stiffener or through in some sources and mainly grouped in classes as open and closed ribs. In the progress of orthotropic steel bridges, closed ribs have proved their superiority due to their high torsional and buckling stiffness, less material and welding needs. Nowadays, trapezoidal form of closed ribs is preferred broadly in industry. In the scope of this thesis trapezoidal ribs having three different web slopes shown in Figure 7.1 are compared with each other for the assessment of their efficiency with respect to stresses developed in deck plate, rib and cross beam and resultant displacement developed in deck plate.

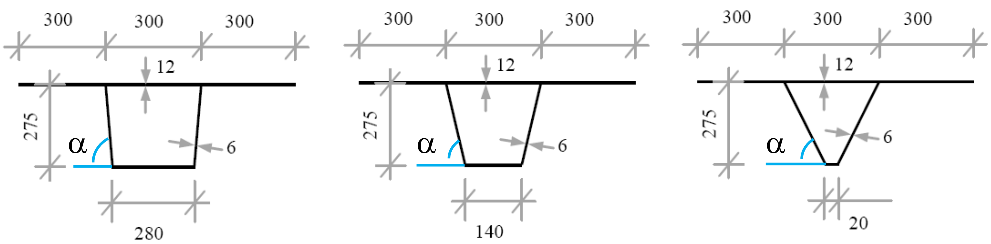

Figure 7.1 Dimensions (in mm) of different rib shapes used in this thesis. The slopes of the rib shapes from left to right are 87.92°, 73.78° and 63.02° respectively.

Design rules and recommendations are given in Eurocode 3 Part 2[52], US Department of Transportation Federal Highway Administration Report No: IF-12-027 [11] and studies conducted by Mangus and Sun [71], Wolchuk [72] and Wolchuk [73] for dimensions of orthotropic steel bridges. In this research the cross section of bridge is chosen as per Eurocode 3 Part 2[52], since it is the most updated information source in comparison with studies done by Mangus and Sun [71], Wolchuk [72] and Wolchuk [73] and a frequently used reference in Europe. In addition, US Department of Transportation Federal Highway Administration Report No: IF-12-027 [11] also sets similar rules and recommendations as Eurocode 3 Part 2 [52] does.

7.1 Comparison of Rib Web Slopes

FE- analyses of steel orthotropic bridge are performed for trapezoidal rib web slopes of 87.92°, 73.78° and 63.02° respectively. First, deformation vectors of whole structure are given in Figure 7.2, Figure 7.3 and Figure 7.4in order to identify which rib web slope results in the best load dispersing of wheel loads on deck plate. It is seen from Figure 7.5 that rib web slope of 73.78° leads to best load dispersing of deck plate with the lowest deformations. According to shape of curve given in Figure 7.5 a moderate rib web slope between two limit situations satisfies the best rib shape so as to obtain min. deformations of wearing surface lying on deck plate. Max. deformation vector values under wheel loads are 1.898 mm ,1.729 mm and 1.966 mm for trapezoidal rib web slopes of87.92°, 73.78° and 63.02° respectively.

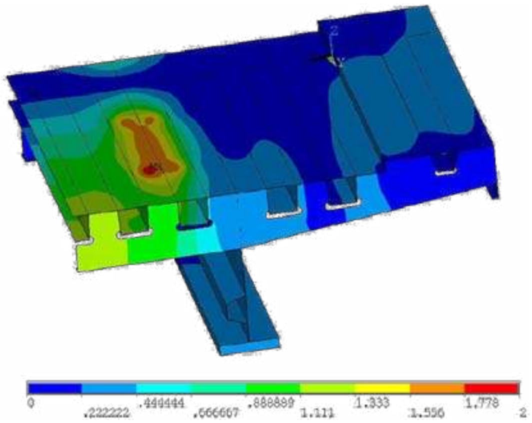

Figure 7.2 Distribution of resultant displacement for rib web slope of 87.92°. Max. value is 1.898 mm.

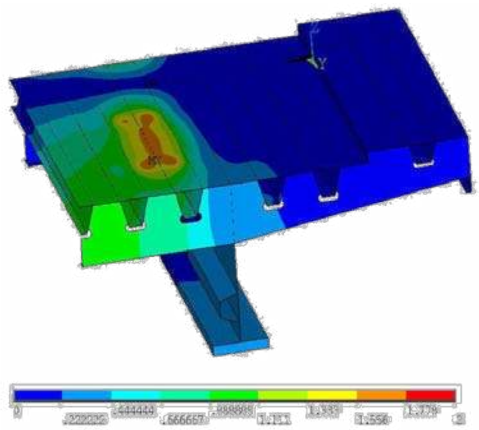

Figure 7.3 Distribution of resultant displacement for rib web slope of 73.78°. Max. value is 1.729 mm.

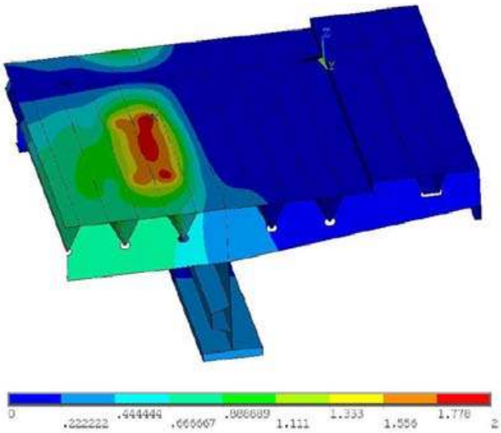

Figure 7.4 Distribution of resultant displacement for rib web slope of 63.02°. Max. value is 1.966 mm.

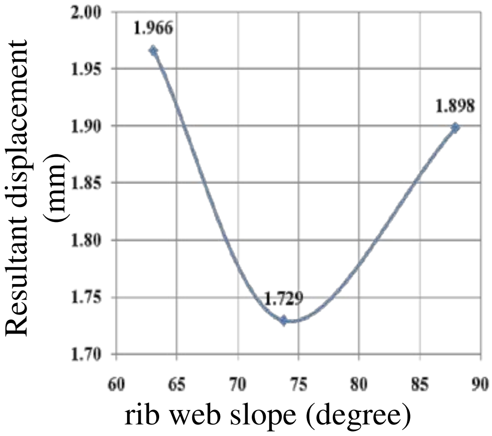

Figure 7.5 Variation of resultant displacement depending on rib web slope.

Second, v.- Mises stress distributions of rib web slopes of 87.92°, 73.78° and 63.02° are given in Figure 7.6, Figure 7.7 and Figure 7.8 respectively. In all these figures v.- Mises stress distributions of the whole structure are given at the top and close- up view of max. v.- Mises stress distributions as per averaged and non- averaged nodal values are given at the bottom. If the max. values of v.- Mises stresses appear in deck plate, ribs and cross- beams for rib web slope of 73.78° are taken as 100 percentage, Figure 7.6 indicates that using rib web slope of 87.92° leads to % 4.04 stress decrease in deck plate, % 2.77 stress increase in ribs and % 30.79 stress increase in cross beams. Likewise, Figure 7.8 indicates that using rib web slope of 63.02° yields to % 5.61 stress increase in deck plate, % 1.98 stress decrease in ribs and % 8.55 stress decrease in cross beams. As a result using rib web slope of 63.02°is the best according to yielding of steel parts of the bridge. Variation of stresses in steel parts is shown in Figure 7.9 for illustration. Third, the extreme values of normal and shear stresses developed in deck plate, ribs and cross beams are examined as to Table 7.1. Max. absolute normal stress value in bridge's transverse direction appears in cross beam as 173.086 MPa, when rib web slope is 87.92°. Using other slopes of rib web concludes in lesser transverse normal stress values. According to normal stresses in bridge' s longitudinal direction max. tension and compression stresses occur always in rib steel parts, whatever rib web slope is used. Min. tensional longitudinal normal stress and max.compressive longitudinal normal stress develop as 89.998 MPa and 200.105 MPa respectively, when rib web slope is 63.02°. From the close examination of longitudinal normal stresses it is concluded that, using lower rib web slope values leads to slight increase of compressive longitudinal normal stresses, but also ~% 50- % 90 decrease of tensional longitudinal normal stresses in rib steel parts. Vertical normal stresses in global Z axis rise in cross beams and ribs, when rib web slope is 87.92°, but lessen in cross beams and ribs, when rib web slope is 63.02°. Values of shear stresses appear in steel structural parts are very much smaller than normal stresses and are of no importance for the assessment of slope of rib web in orthotropic steel bridges.

a)

b)

c)

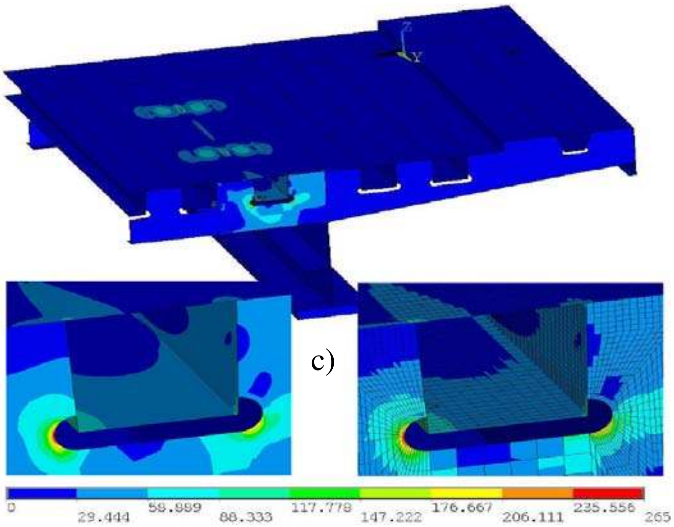

Figure 7.6 a) Distribution of v.- Mises stress with averaged nodal values on the whole structure. b) Close- up view of distribution of v.- Mises stress with averaged element results. c) Close- up view of distribution of v.- Mises stress with non- averaged element results. Both results are for rib web slope of 87.92°. Max. values developed in deck plate, ribs and cross beams are 121.538 MPa, 262.34 MPa and 263.612 MPa respectively.

a)

b)

c)

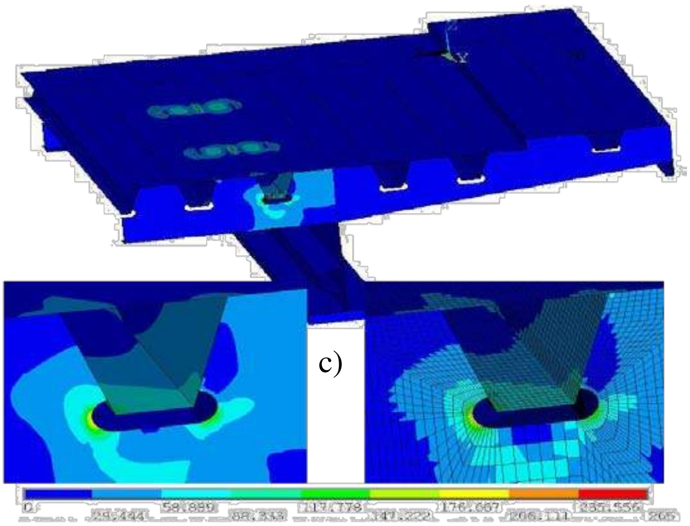

Figure 7.7 a) Distribution of v.- Mises stress with averaged nodal values on the whole structure. b) Close- up view of distribution of v.- Mises stress with averaged element results. c) Close- up view of distribution of v.- Mises stress with non- averaged element results. Both results are for rib web slope of 73.78°. Max. values developed in deck plate, ribs and cross beams are 126.652 MPa, 255.259 MPa and 201.549 MPa respectively.

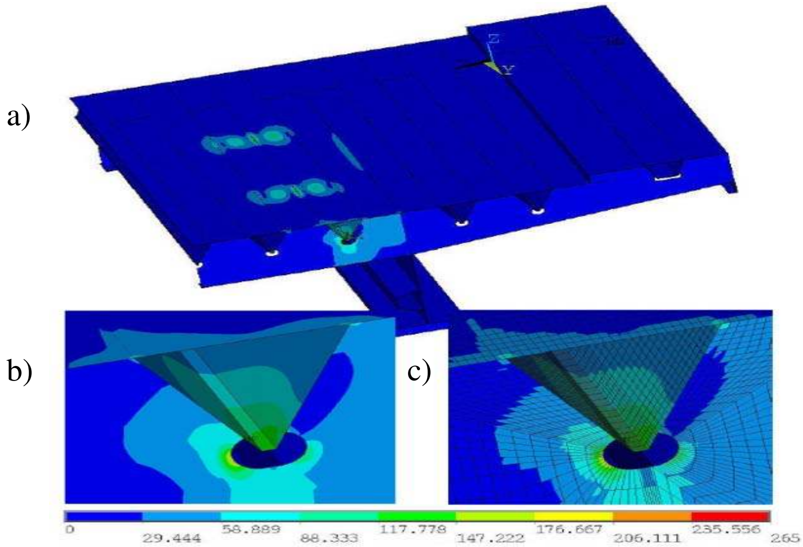

Figure 7.8 a) Distribution of v.- Mises stress with averaged nodal values on the whole structure. b) Close- up view of distribution of v.- Mises stress with averaged element results. c) Close- up view of distribution of v.- Mises stress with non- averaged element results. Both results are for rib web slope of 63.02°. Max. values developed in deck plate, ribs and cross beams are 132.997 MPa, 250.202 MPa and 184.319 MPa respectively.

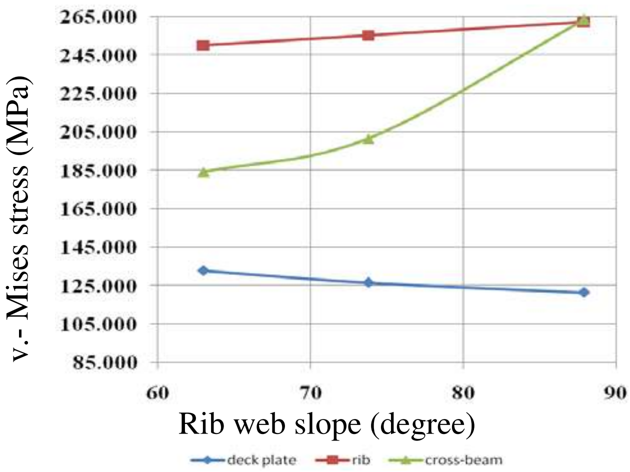

Figure 7.9 Variation of max.v.- Mises stress depending on slope of rib web.

Table 7.1 Comparison of stresses for different slopes of rib webs

Type of stress (Mpa)		Slopes of rib webs					
		87.92°		73.78°		63.02°	
		value & place		value & place		value & place	
σ_{x}*	com	-	deck	-	deck	-	deck
	ten.	173.08	cross	143.55	cross	142.69	deck
σ_{y}*	com	-	rib	-	rib	-	rib
	ten.	188.97	rib	145.48	rib	89.998	rib
σ_{z}*	Com	-	cross	-	cross	-	cross
	ten.	289.72	rib	244.21	rib	189.82	rib
τ_{xy}*	com	-23.904	rib	-21.289	rib	-22.569	deck
	ten.	22.223	deck	21.782	deck	24.892	Rib
τ_{yz}*	com	-51.88	Rib	-46.702	Rib	-37.716	Rib
	ten.	39.141	Rib	54.273	Rib	48.926	Rib
τ_{xz}*	com	-94.819	cross	-69.481	cross	-62.108	cross
	ten.	78.239	cross	71.628	rib	97.041	Rib

*Please refer to Figure 1.3 for explanation of σ_x, σ_y and σ_z on finite elements, with which the whole structure is modeled.

Variation of max.stressesin steel parts depending on slope of rib web is given below in Figure 7.10.

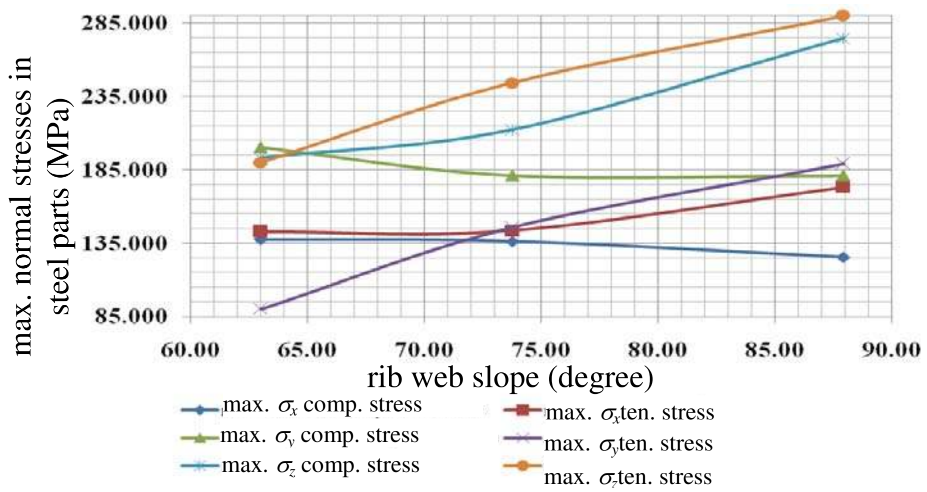

Figure 7.10 Variation of max. stresses in steel parts depending on slope of rib web.

7.2 Results & Discussion

Briefly, usinglimit situations and a moderate value of slope of trapezoidal rib web in orthotropic deckarecompared with each other using FE- method in this thesis.A detailed FE- model is used to assess the effect of slope of rib web on the stresses of steel parts of orthotropic bridge and on the resultant displacement occured at the deck plate. Results of the FE- analyses show that using the lowest slope of rib web is the best, while using highest slope of rib webis the worst as per stresses revealed in rib and cross- beam steel parts of the bridge. This result is especially true for cross- beam stresses. On the other hand max. deck plate resultant displacement and hence max. resultant dislpacement in bridge' s wearing surfaceis obtained, when the lowest slope of rib webis used. Consequently, the lower slope of trapezoidal rib webis used, the lower stresses are obtained in steel parts. However, this slope degree shall be determined according to the permissible displacement value of wearing surface laid on deck plate.

CHAPTER 8

RECOMMENDED PROPERTIES OF ELASTIC WEARING SURFACES ON ORTHOTROPIC STEEL DECKS

Wearing surface on deck plate plays a very important role to avoid or mitigate these damages, since it disperses the load coming on deck structure and increases the bending stiffness of deck plate by forming a composite structure together with it. In this thesis the effect of Elastic moduli, Poisson ratio and thickness of wearing surface on the stresses emerged in steel deck and wearing surface itself is investigated using a FE-model developed to analyze orthotropic steel bridges.In the scope of this thesis wearing surfaces are introduced and the influence of elastic moduli, Poisson ratio and thickness of elastic wearing surface as per stress distribution in orthotropic deck is subsequently handled. Consequently, conclusions and recommendations regarding material properties and thickness of wearing surface are given in the last section.

8.1 Wearing Surfaces

Wearing surface on deck plate plays a very important role to avoid or mitigate the damages of orthotropic deck, since it disperses the load coming from vehicle wheel on deck structure and increases the bending stiffness of deck plate by forming a composite structure together with it. Pouget et al. [74] presented a crucial article about viscous bituminous wearing surfaces on orthotropic decks. In addition several researches are conducted with respect to bituminous wearing surfaces [75- 81]. Buitelaar, Braam and Kaptijn [82] performed researches regarding reinforced high performance concrete (RHPC) as elastic wearing surface on orthotropic decks (See Figure 8.1 and 8.2). They recommend RHPC for renovation of existing damaged wearing surface and construction of new wearing surface as well. They modeled RHPC with linear elastic material properties using their FE- model to estimate stress reduction factors due to RHPC. The elastic module of ultra high performance concrete (UHPC) can vary even between 60 and 100 GPa. The RHPC overlay is a combination of a HPC strength class C110 (based on special pre-blended materials reinforced with both steel and acrylic fibers) and welded mesh reinforcement (consisting of two specially produced mats Ø8 mm # 50 x 100 mm positioned on top of each other such that a total of three layers of Ø8 mm rebars spaced at 50 mm is obtained) [83]. The mesh reinforcement is placed on a Ø8 mm rebar used as a spacer. Thus, the total amount of reinforcement is approximately 24 kg/m^2 traditional reinforcement plus 5 kg/m^2 steel fibers. The total thickness of the RHPC overlay is in this specific case 50 mm. The concrete cover on the reinforcement is thus only 18 mm. If the thickness of the layer should be increased, the reinforcement can be adjusted. To replace the existing wearing surface with a RHPC overlay, the bonding between the steel deck plate (thickness 10 - 12 mm) and the overlay is of crucial importance to secure total deck rigidity and a uniform "monolithic" behavior under all circumstances. For that reason the first investigations were focused on creating a bonding zone that met all requirements. A bonding zone can easily be created by connecting the mesh reinforcement and the steel deck plate by welds, but this might result in undesirable local peak stresses. Therefore research was carried out to find the optimal bonding agent. The best method turned out to be the use of a two-component epoxy based adhesive with sprinkled-in bauxite aggregates. After hardening of the epoxy, the overlay is cast. The surface will be shot blasted. No additional wearing surface will be applied [82].

a) b)

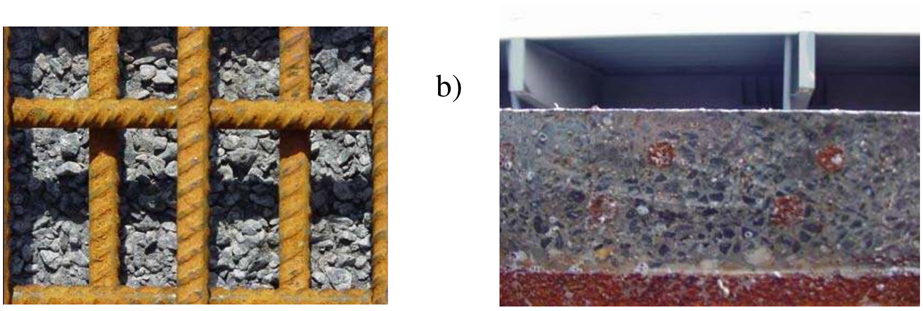

Figure 8.1 a) Reinforcement principle of RHPC. b) RHPC overlay on deck plate [77].

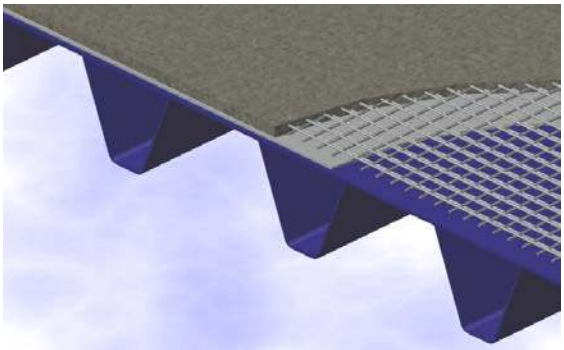

Figure 8.2 RHPC surfacing system [1].

Jong [1] also recommends the same principles and conclusions on the modeling and application of RHPC in his dissertation. The material properties of the linear- elastic modeled wearing surface and bonding layer beneath it are given below;

Material properties of the RHPC surfacing are: Elastic modulus$E$ = 50 000 MPa [39, 40], Poisson ratio ν = 0.3, density ρ = 2400 kg/m^3, thermal expansion coefficient α = 12x10^{-6}. The concrete is modeled as a homogeneous layer. The reinforcement bars and cracks in the tension zones of the concrete are not modeled.

Material properties of the bonding layer between steel and RHPC surfacing are from the product data sheet of Sikadur 30 [84]: Elastic module E = 12 800 MPa, Poisson ratio ν = 0.3, density ρ = 1650 kg/m^3, thermal coefficient α = 90x10^{-6}. Research has shown that Sikadur 30 is a good epoxy bonding layer for RHPC on steel [85]. Therefore in the FE-models the properties of Sikadur 30 were used [1].

As a loading in FE- model of Jong [1] a wheel footprint is used, which is 320 mm long, 220 mm wide, and has a load of 35 kN. This is in fact wheel type A, the so-called single, from Eurocode 1-Part 2. The standard axle load of 70 kN for the steering axle with wheel A is divided by two.

However, in this thesis elastic module of wearing surface is chosen varying between 20 and 35 GPa, which are identical to normal concrete wearing surfaces. The range of Poisson ratio is chosen varying between 0.15 to 0.30 [86]. Because aim of this thesis is determination of the influence of material properties and thickness of normal concrete wearing surfaces on steel decks, high elastic module values possessed by RHPC is not used in this thesis. In the first stage, bonding layer is ignored and a normal concrete wearing surface is considered, which is fully bonded to the top of deck plate. Then stresses developed in orthotropic deck are assessed for different elastic module and Poisson ratio pairs of normal concrete wearing surface. In the second stage, bonding layer is modeled as described by Jong [1] and the results are evaluated depending upon variance of bonding layer's shear module and wearing surface's thickness. It is of great importance to note that, wearing surface term used in this thesis refers to concrete wearing surface plus bonding layer (if considered in FE- model as in the case of second stage). In the first stage of FE- analyses, wearing surface term refers solely to concrete wearing surface, since concrete wearing surface is fully bonded to deck plate without a bonding layer between them. Thus, bonding layer is only involved in the second stage of FE- models.

8.2 FE- Analyses

The variation of elasticity module and Poisson ratio of concrete wearing surface in the first stage of analyses is given in Table 8.1 below. In the first stage of FE- analyses, the thickness of elastic wearing surface is always taken as 40 mm (Here 40 mm is equal to concrete wearing surface's thickness, which rest directly on deck plate without any bonding layer between them) in all FE- analyses. Since 40 mm is the traditional wearing surface thickness value (8 mm rebar spacer at the bottom + 3x8 mm = 24 mm rebar diameters + 8 mm rebar spacer at the top), where wearing surface on deck plate is of concrete, it is chosen as wearing surface thickness value in the first stage of FE- analyses.

Table 8.1 Variation of elasticity module and Poisson ratio as per first stage FE- analyses.

FE- analysis name	Elasticity module (MPa)	Poisson ratio	FE- analysis name	Elasticity module (MPa)	Poisson ratio
T4E20P15NL*		0.15	T4E30P15		0.15
T4E20P15		0.15	T4E30P20	30 000	0.20
T4E20P20	20 000	0.20	T4E30P25		0.25
T4E20P25		0.25	T4E30P30		0.30
T4E20P30		0.30	T4E35P15		0.15
T4E25P15		0.15	T4E35P20	35 000	0.20
T4E25P20	25 000	0.20	T4E35P25		0.25
T4E25P25		0.25	T4E35P30		0.30
T4E25P30		0.30			

*This FE- analysis is same as T4E20P15, however geometrical non- liearity is considered to assess its influence on the results. All materials used in Fe-analyses obey Hooke's Law.

In the second stage of FE- analyses, elasticity module and Poisson ratio of concrete are 30 GPa and 0.3 respectively, which is explained in detail in Table 8.2.

Table 8.2 Variation of bonding layer's shear module and thickness of wearing surface as per second stage FE- analysis.

FE- analysis name	Shear module of bonding layer (MPa)	Thickness of wearing surface (mm)	FE- analysis name	Shear module of bonding layer (MPa)	Thickness of wearing surface (mm)
T25MS5	5		T25MS4923		25
T25MS500	500	25	T50MS4923	4923*	50
T25MS50000	50 000		T75MS4923		75

*This is the shear modulus of Sikadur 30 [84].

Before the first and second stage of FE- analyses, the analysis named T4E20P15NL is performed, whether geometrical non- linearity is effective on results. It is seen from Table 8.3 below that FE- analyses done without considering any non- linearity do not influence the results. Averaged nodal values of results are also tabulated in Table 8.3 for comparison with non- averaged results. As a conclusion, there is almost no difference between the results of three FE- analyses in all both cases.

Table 8.3 Displacement and stresses developed in orthotropic deck.

Type of structure	Resultant displacement (mm)	T4E20P15NL		T4E20P15		T4E20P15^{nodal}	
Whole structure	U_{sum}	1.159		1.160		1.160	
Type of stress		max. tens.	max. comp.	max. tens.	max. comp.	max. tens.	max. comp.
Concrete surface	σ_{x*}	4.563	5.962	4.561	5.969	4.532	5.955
	σ_{y*}	4.250	4.180	4.247	4.185	4.246	4.180
	σ_{z*}	2.234	5.879	2.238	5.875	2.184	5.805
	σ_v	9.720		9.712		8.642	
Deck plate	σ_{x*}	41.023	97.482	41.117	97.452	29.223	64.778
	σ_{y*}	24.626	32.534	24.613	32.502	24.363	16.322
	σ_{z*}	18.057	45.522	18.067	45.597	15.455	39.801
	σ_v	157.492		157.391		110.759	
Cross-beam at field	σ_{x**}	97.039	65.071	97.178	64.999	95.106	63.985
	σ_{y**}	~ 0.000					
	σ_{z**}	92.630	146.686	92.632	146.737	91.531	145.986
	σ_v	141.799		141.826		141.519	

Table 8.3 (cont'd)

Rib	σ_x***	49.702	46.931	49.907	47.121	49.163	46.476
	σ_y***	91.502	89.074	91.872	89.576	52.641	68.402
	σ_z***	120.924	90.631	121.402	91.030	88.323	69.494
	σ_v	122.178		122.588		87.628	

*σ_x, σ_y and σ_z are transverse bending stress, longitudinal bending stress and normal stress perpendicular to deck plate plane respectively in deck plate steel material.

**σ_x, σ_z and σ_y are transverse bending stress, vertical bending stress and normal stress perpendicular to cross- beam plane respectively in cross- beam steel material.

***σ_x, σ_y and σ_z are transverse bending stress, longitudinal bending stress and normal stress perpendiculat to rib material parts respectively in rib steel material.

8.3 Influence of Elastic Moduli, Poisson Ratio and Thickness of Elastic Wearing Surface on Orthotropic Deck

8.3.1 General Deformation Behavior of Bridge

With respect to Figure8.3 the change of wearing surface's Poisson ratio effects max. resultant displacement of bridge very slightly, that the effect of Poisson ratio on it can be neglected. The max. change of max. resultant displacement (U_{sum}) depending on Poisson ratio is only 1.2 %. According to Figure 8.3, U_{sum} is much more influenced by the elasticity module of wearing surface, when there exists a full bond between concrete wearing surface and deck plate. The rise of wearing surface's elasticity module from 20 GPa to 35 GPa leads to 8- 11 % decline of U_{sum} . If the bonding layer is modeled and not a full bond between concrete wearing surface and deck plate is considered, we can state that any increase of bonding layer's shear module or in wearing surface' s thickness elicits to decrease of U_{sum} (See Figure8.4 and 8.5). It is seen from Figure8.5 that increasing wearing surface' s thickness from 25 mm to 75 mm results in 44.44 % fall of U_{sum} . Finally, wearing surface's thickness is recommended as a controlling parameter on U_{sum} , not the material properties of normal concrete wearing surface.

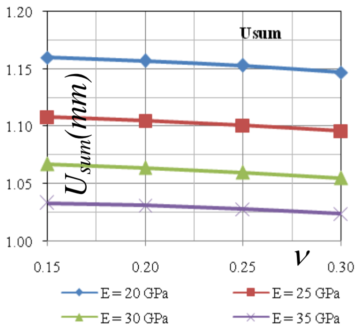

Figure 8.3 Max. resultant displacement as per wearing surface Poisson ratio for varied elastic moduli of wearing surface, in case of full bond.

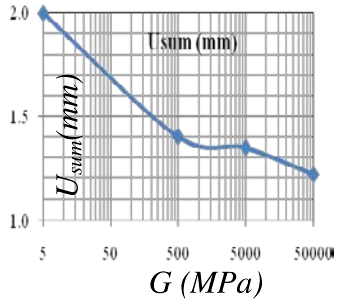

Figure 8.4 Max. resultant displacement as per bonding layer shear module (on logarithmic scale) risen in the bridge.

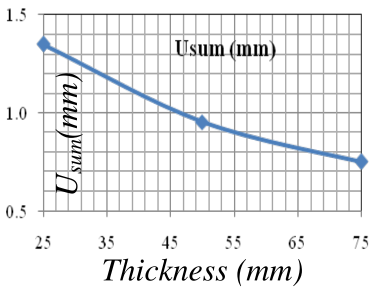

Figure 8.5 Max. resultant displacement as per wearing surface elastic module (on logarithmic scale) risen in the bridge.

8.3.2 Concrete Wearing Surface

Regarding Figure8.6, 8.7, 8.9 and 8.10 increasing bonding layer's shear module or wearing surface's thickness leads in general decreasing of stresses in concrete wearing surface. When bonding layer is ignored and concrete wearing surface is assumed as fully bonded to deck plate, v.- Mises stress decreases depending on material properties of concrete wearing surface as illustrated in Figure 8.8. As a thumb rule it can easily be stated that the parameters to decline the stresses in wearing surface from strongest to weaks are: Thickness and elasticity module of concrete wearing surface, shear module of bonding layer and Poisson ratio of concrete wearing surface respectively.

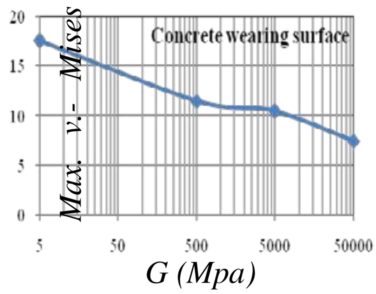

Figure 8.6 Max. v.- Mises stress as per bonding layer's shear module (on logarithmic scale) risen in concrete wearing surface.

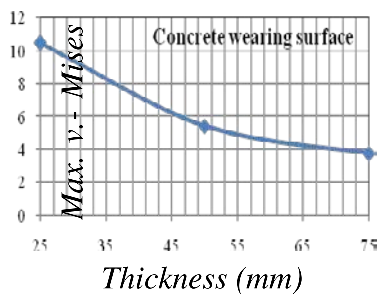

Figure 8.7 Max. v.- Mises stress as per wearing surface's thickness risen in concrete wearing surface, in case of full bond.

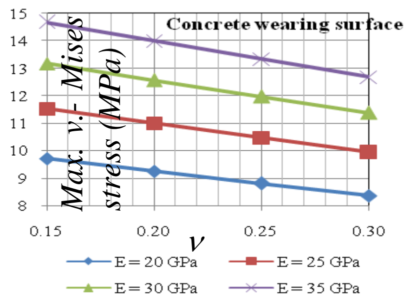

Figure 8.8 Max. v.- Mises stress in concrete surface as per concrete wearing surface's Poisson ratio for its different elasticity moduli, in case of full bond.

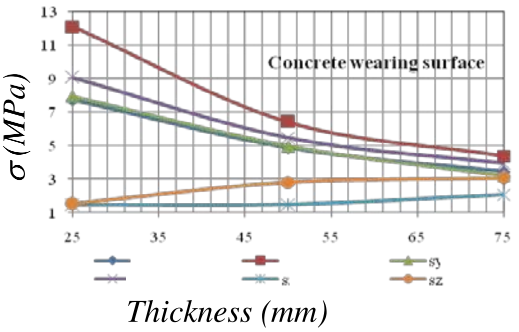

Figure 8.9 Max. stresses as per wearing surface's thicknesses risen in concrete wearing surface, in case of full bond.

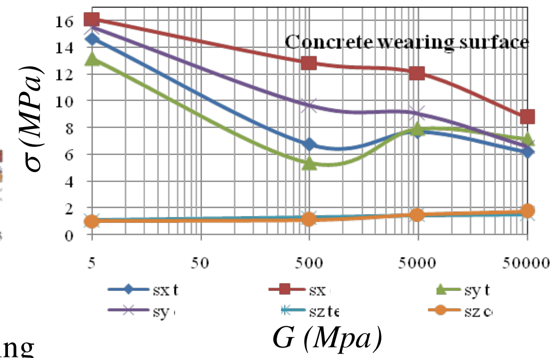

Figure 8.10 Max. stresses as per bonding layer's shear module (on logarithmic scale) risen in concrete wearing surface.

8.3.3 Bonding Layer

As to Figure8.11, excessive value of bonding layer's shear module (50 GPa)causes a high value of v.- Mises stress in bonding layer, that is 30.465 MPa and according to Figure 8.12 increasing thickness of wearing surface has a top value of v.- Mises stress in bonding layer as 6.23 MPa. As a results, it is recommended to choose bonding layer's shear module around 5000 MPa and to increase the thickness of wearing surface to design of elastic wearing surface on orthotropic decks. Figure 8.13 and 8.14 depict the variation of normal stresses depending on wearing surface's thickness and bonding layer' s shear module.

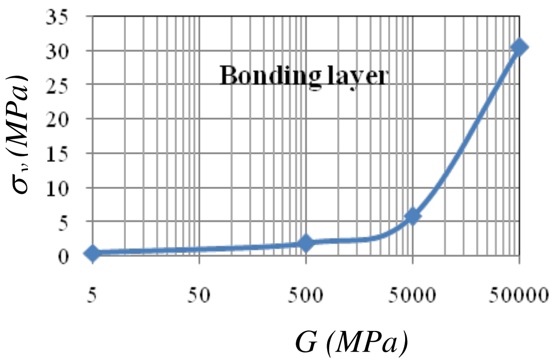

Figure 8.11 Max. v.- Mises stress in bonding layer as per bonding layer's shear module.

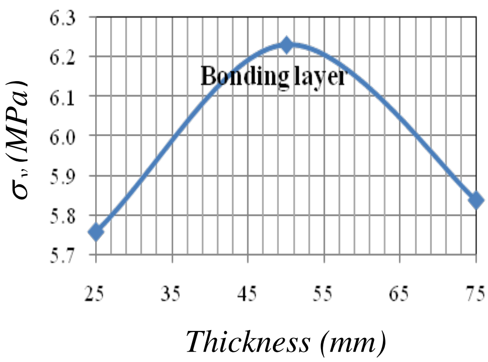

Figure 8.12 Max. v.- Mises stress in bonding layer as per wearing surface's thickness.

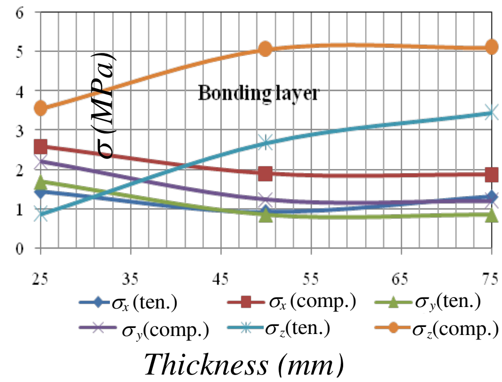

Figure 8.13 Max. stresses in bonding layer as per wearing surface's thickness.

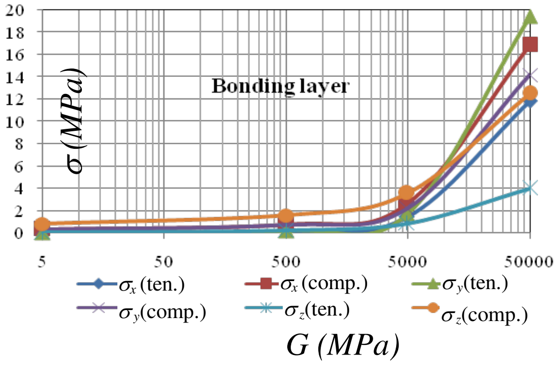

Figure 8.14 Max. stresses in bonding layer as bonding layer's shear module.

8.3.4 Deck Plate

Figure 8.15 shows that Poisson ratio is not effective on stresses emerged in deck plate. Elasticity module of concrete wearing surface has an effect up to approximately 5.5 %, which can also easily be neglected. According to Figure 8.16 the excessive shear module value, 50 000 MPa of bonding layer leads only to 11.35 % decrease of v.- Mises stress in deck plate. With respect to Figure 8.17 and 8.18 increasing wearing surface' s thickness yields in a beneficial decrease of v.- Mises and compressive transverse stress (sx com.) in deck plate. Increasing wearing surface's thickness from 25 mm to 75 mm yields in 30.19 % decrease of v.- Mises stress in deck plate. According to Figure 8.19 increasing bonding layer's shear module effects tensile transverse stress (sx ten.), nevertheless just slightly other normal stresses in deck plate.

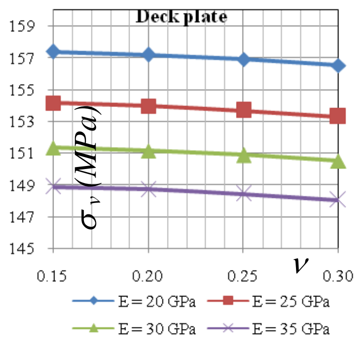

Figure 8.15 Max. v.- Mises stress in deck plate as per concrete wearing surface's Poisson ratio for its different elasticity moduli, in case of full bond.

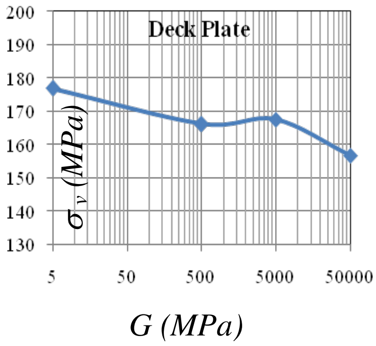

Figure 8.16 Max. v.- Mises stress in deck plate as per bonding layer' shear module.

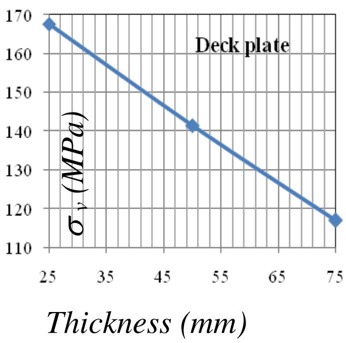

Figure 8.17 Max. v.- Mises stress in deck plate as per concrete wearing surface's thickness, in case of full bond.

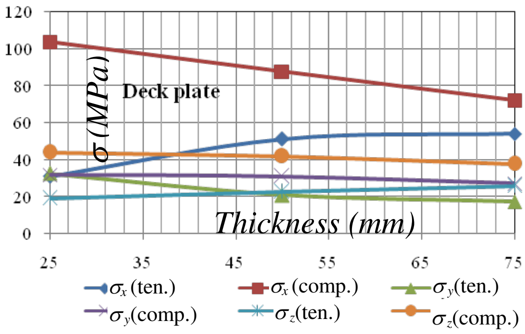

Figure 8.18 Max. stresses in deck plate as per concrete wearing surface's thickness, in case of full bond.

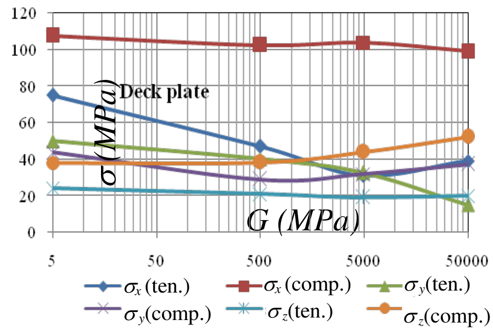

Figure 8.19 Max. stresses in deck plate as per bonding layer's shear module.

8.3.5 Cross- beam

When there exists a full bond between deck plate and concrete wearing surface, max. v.- Mises stress in cross- beam decreases approximately 9.5 %, if concrete wearing surface's elastic module changes from 20 GPa to 35 GPa (See Figure8.20). As per Figure 8.21 and Figure 8.24 rise of bonding layer's shear module causes decrease of v.- Mises stresses and normal stresses in cross- beam, whereas increasing wearing surface's thickness greatly reduces normal and v.- Mises stresses in cross- beam, as given in Figure 8.22 and 8.23.

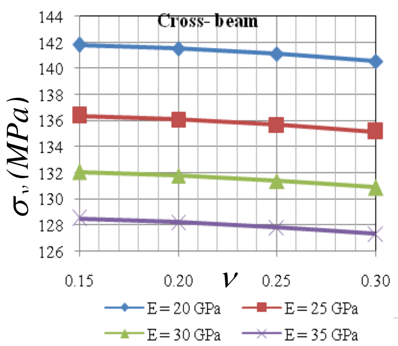

Figure 8.20 Max. v.- Mises stress in cross- beam as per concrete wearing surface's Poisson ratio for its different elasticity moduli, in case of full bond.

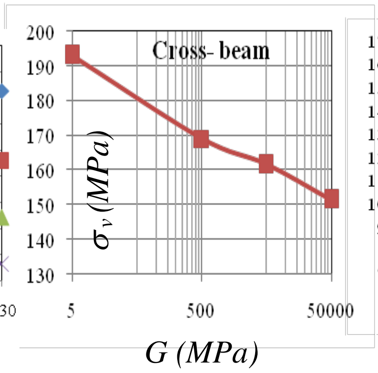

Figure 8.21 Max. v.- Mises stress in cross- beam as per bonding layer' shear module.

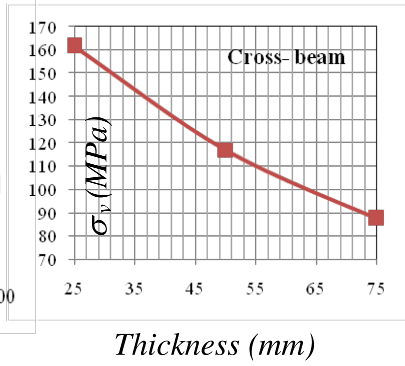

Figure 8.22 Max. v.- Mises stress in cross- beam as per wearing surface's thickess, in case of full bond.

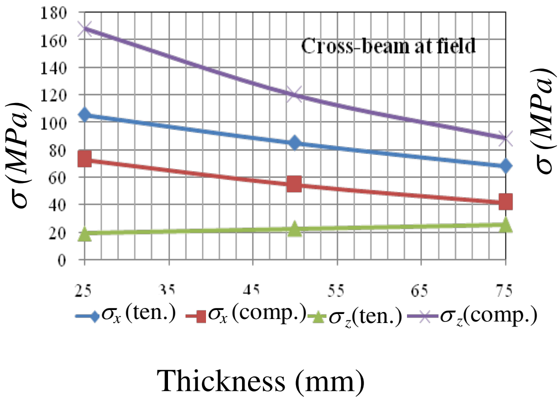

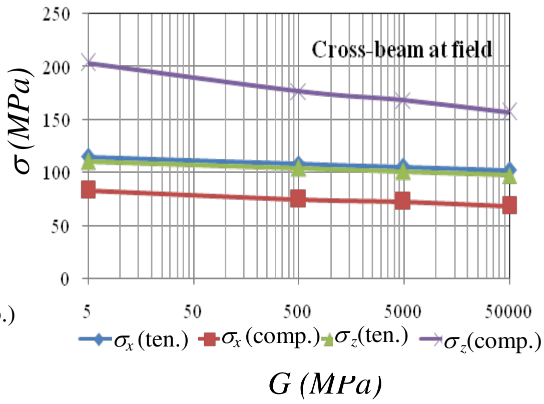

Figure 8.23 Max. stresses in cross-beam as per wearing surface's thickess, in case of full bond.

Figure 8.24 Max. stresses in cross-beam as per bonding layer's shear module.

8.3.6 Ribs

Figure8.25 shows that max. v.- Mises stress developed in ribs is almost not effected by concrete wearing surface' s Poisson ratio, when concrete wearing surface is fully bonded to deck plate. However, increasing concrete wearing surface's elastic module results in approximately 10.2 % decrease of v.- Mises stress in ribs. It is seen from Figure 8.26 and 8.29 that, normal and v.- Mises stresses developed in ribs reduce, when bonding layer' s shear module rises. According to Figure 8.27 and 8.28 max. normal and v.- Mises stresses decrease heavily with the increase of wearing surface's thickness.

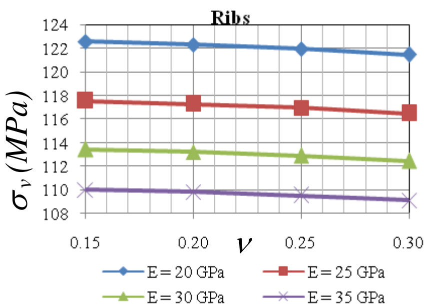

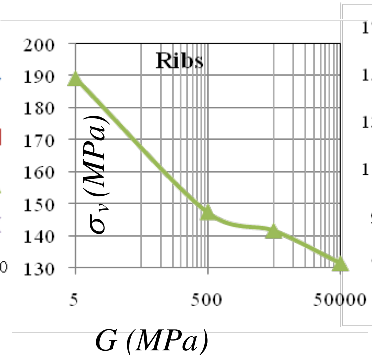

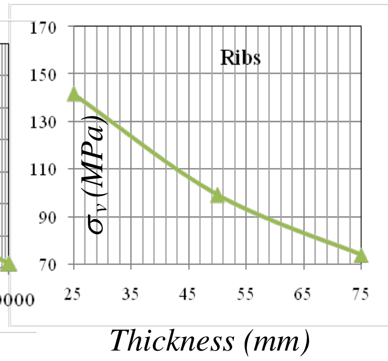

Figure 8.25 Max. v.- Mises stress in ribs as per concrete wearing surface's Poisson ratio for its different elasticity moduli, in case of full bond.

Figure 8.26 Max. v.- Mises stress in ribs as per bonding layer's shear module.

Figure 8.27 Max. v.- Mises stress in ribs as per wearing surface thickness, in case of full bond.

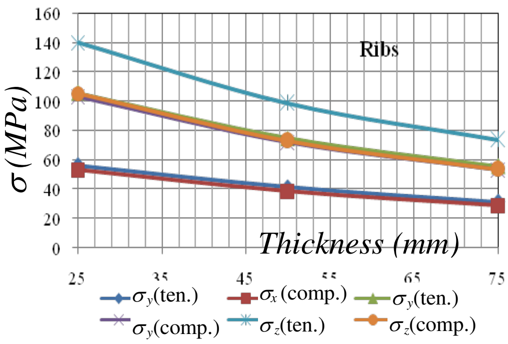

Figure 8.28 Max. stresses in ribs as per wearing surface thickness, in case of full bond.

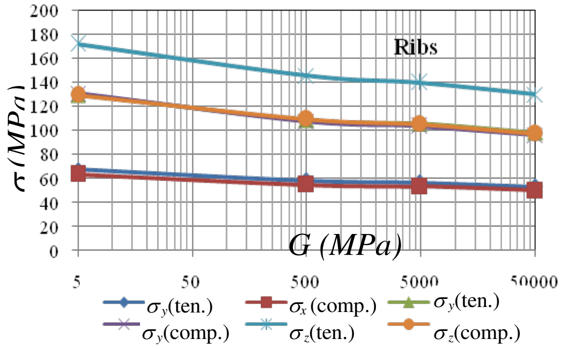

Figure 8.29 Max. stresses in ribs as per bonding layer's shear module.

8.4 Results & Discussion

FE- model established in this thesis is used to evaluate the stresses developing in orthotropic decks. It is investigated the influence of material properties and thickness of linear elastic wearing surface (in the case handled in this article, concrete wearing surface) on the stresses revealed in orthotropic decks. Results can be summarized as follows:

It is seen from the results that Poisson ratio of elastic wearing surface has a vey negligible effect on displacements and stresses developed in any part of orthotropic deck. From this point of view, it is advised utilizing one- dimensional, unconfined tests to obtain elastic module of concrete pavement instead of more expensive confined stress tests. For a Poisson ratio value of concrete pavement any value between 0.15 and 0.30 can be used in FE- analyses.

Thickness of wearing surface is the dominant parameter to really reduce all stresses and displacements in any part of orthotropic decks.

Excessive shear module (50 000 MPa) of bonding layer results in very high v.- Mises stress in bonding layer. As a result a shear module of around 5000 MPa for bonding layer is suitable.

For concrete wearing surfaces fully bonded on deck plate, increasing elastic module of concrete wearing surface from 20 GPa to 35 GPa leads approximately to 50 % increase of v.- Mises stress in concrete wearing surface, 5.5 % decrease of v.- Mises stress in deck plate, 9.5 % decrease of v.- Mises stress in cross- beam and 10.2 % decrease of v.- Mises stress in ribs.

CHAPTER 9

OPTIMIZING RIB WIDTH TO HEIGHT AND RIB SPACING TO DECK PLATE THICKNESS RATIOS IN ORTHOTROPIC DECKS

Necessary FE-analyses are performed to reveal the stresses developed under different rib width to height and rib spacing to deck plate thickness ratios. Based on the results obtained in this thesis, recommendations regarding these ratios are provided for orthotropic steel decks occupying trapezoidal ribs. In this section first, the influence of width to height ratio of trapezoidal rib on stress distribution in orthotropic deck is handled. Subsequently, rib spacing to deck plate thickness ratio is evaluated and results are supplied in this section. Consequently, conclusions and recommendations for the design of orthotropic decks are given.

9.1 Rib width to Height Ratio

Rib width to height ratio of trapezoidal longitudinal stiffener is assessed by means of the stresses revealed for different height of ribs, while the width of rib is always kept as 300 mm. Results are compared with each other to interpret the deformation and stress behavior of the bridge for small, moderate and high values of rib height. Figure 9.1 shows the parameters used in this thesis to evaluate the effect of dimensional ratios on stresses developed in orthotropic deck. Here *a*, *b*, *e* and *t* are rib with, height, spacing and deck plate thickness respectively. Results are illustrated mainly in two different ways, namely using contour graphics and tables. Since they both are scalar values and represent all displacement and stress components well respectively at the point of interest, resultant displacement and v.- Mises stress are chosen to interpret the results using contour graphics. Second, tables are used to present the values of vectorial stress components. Table 2 shows the stresses developed in deck plate, cross-beam and rib separately for different rib width to height ratios. In the FE-analyses all dimensions except rib height are always kept constant to be able to understand the effect of rib width to height ratio on deformation and stress behavior clearly. In the scope of this thesis five different FE-analyses are performed for rib height values of 150 mm, 200 mm, 275 mm, 300 mm and 375 mm, while other dimensions of bridge are kept constant.

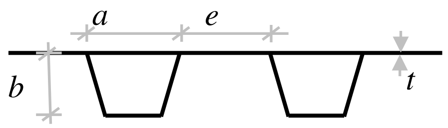

Figure 9.1 Parametric dimensions, which are of interest.

In terms of deformation behavior of the whole structure max. resultant displacement occurs, when the shortest rib height is used as seen in Figure 9.2. Max. resultant displacement developed in deck plate decreases, while rib height increases, that can be seen in Figure 9.2, Figure 9.4, Figure 9.6, Figure 9.8 and Figure 9.10. So rib height is a parameter to limit the resultant displacements rising in deck plate and also in the wearing surface, which lies directly on deck plate and deforms simultaneously together with deck plate. Figure 9.12 indicates that variation of deck plate displacements depending on rib height is not linear. Slope of this variation reduces as the rib height increases. After rib height of 300 mm, which is equal to rib width, the change in displacement is so less, which can be neglected.

Table 9.1 Stresses developed in structural parts for different rib width to height ratios (rib width is 300 mm).

Type of structure	Type of Stress *(MPa)*	b = 150 mm (a / b = 2.00)		b = 200 mm (a / b = 1.50)		b = 275 mm (a / b = 1.09)		b = 300 mm (a / b = 1.00)		b = 375 mm (a / b = 0.80)	
		max. tens.	max. comp.	max. tens.	max. comp.	max. tens.	max. comp.	max. tens.	max. comp.	max. tens.	max. comp.
Deck plate	σ_x	129.	121.	128.	128.	135.	136.	136.	137.	139.	138
	σ_x develops direct under wheel load, due to bending of deck plate. Max. comp. σ_x develops at top, while max. tens. σ_x develops at bottom of deck plate.										
	σ_y	113.12	88.80	79.22	80.88	60.02	73.94	58.09	72.42	55.25	69.21
	σ_y develops under wheel load due to bending of deck plate. Two exceptions are when a/b = 1.5 and 0.8. At these situations max. tens. σ_y at top of deck plate, where deck plate is connected to normal cross-beam.										
	σ_z	~ 0									

Table 9.1 (cont'd)

Cross-beam at field	σ_x	399.	319.1	244.	178.	117.	85.9	130.	92.3	184.	131.78
		σ_x develops at rib web to normal cross-beam connection, where cope hole starts.				σ_x develops at normal cross-beam cope hole rounds.					
	σ_y	12.4	9.62	12.8	10.2	12.3	10.4	11.9	10.3	10.5	11.31
		σ_y develops at the bottom flange of normal cross-beam. Max. comp. σ_y develops at the top of flange plate, while max. tens. σ_y develops at the bottom of flange plate.									
	σ_z	58.9	196.8	78.9	207.	113.	212.	124.	212.	162.	215.79
		Max. tens. and comp. σ_z stresses develop at the rounds of cope hole. This cope hole is located in the interior side next to main-girder.									
Rib	σ_x	190	217.5	127.	137.	84.14	80.4	81.3	77.5	81.16	76.9
		σ_x develops at the rib bottom flange next to main-girder. Max. and min. σ_x stresses are both located in the longitudinal mid of bridge.				σ_x develops at the bottom flange of rib, where rib web connects to stiffened cross-beam.					
	σ_y	193	343.9	164.	265.	145.4	180.	143.	156.	150.5	146.
		Max. tens. σ_y develops at the rib bottom flange, longitudinally at the wheel load position. Max. comp. σ_y develops at the rib, cross- beam and cope hole connection point. This rib is located next to main-girder.				Max. tens. σ_y develops at the rib web closer to stiffened cross-beam. Max. comp. σ_y develops at the rib web to normal cross-beam connection. This rib is located next to main-girder.				Both max. σ_y stresses develop at the rib web closer to stiffened cross-beam longitudinal ly.	

Table 9.1 (cont'd)

Rib	σ_z	294	284.8	330.	238.	244.2	164.	216.	161.	212.3	169.
		Max. tens. σ_z develops at the inner side of rib web, cross--beam and cope hole connection, while max. comp. σ_z develops at the outer side of rib web at the same place. This rib is located next to main girder.		Max. tens. and comp. σ_z stresses develop at the opposite webs of the rib, which is adjacent to main-girder.		Max. tens. σ_z develops at the rib web to normal cross-beam connection, while max. comp. σ_z develops at the rib web to stiffened cross-beam connection. This rib is located next to main girder.				Max. tens. and comp. σ_z stresses develop at the opposite webs of the rib, which is adjacent to main-girder.	

*Please refer to Figure 1.3 for explanation of σ_x, σ_y and σ_z on finite elements, with which the whole structure is modeled.

With respect to v.- Mises stress distribution as rib height increases, the place and value of max. v.- Mises stress changes. For rib heights of 150 mm, 200 mm and 275 mm max. v.- Mises stress rises at the rib web, where it is welded to the web of cross-beam. At this intersection rib is aligned in traffic direction through cut-outs in cross-beam. Therefore, welding between webs of rib and cross-beam is not continuous at the bottom flange of rib, which results in excessive distortion, v.- Mises stress value and so yielding of material as given in Figure 9.3 and 9.5. At rib heights of 275 mm and 300 mm max. v.- Mises stress takes much lesser values below yield stress and develops still at the same point, that is the bottom of welding between rib ad cross-beam (See Figure9.7 and 9.9). At rib height of 375 mm, which is higher than rib width, max. v.- Mises stress takes a slight higher value than the value developed at rib height of 300 mm as given in Figure 9.11 and 9.13. However max. v.- Mises stress occurs at the cross-beam cut-out edge, when the rib height is higher than rib width. From these results it is recommended to select rib height equal to rib width to avoid excessive deformations in deck plate, yielding of steel material and stress concentrations at the intersection point between rib and cross-beam webs under wheel loads used in this thesis.

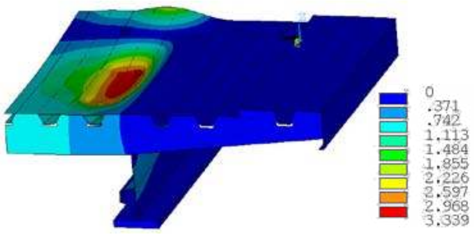

Figure 9.2 Distribution of resultant displacement, when rib height is 150 mm.

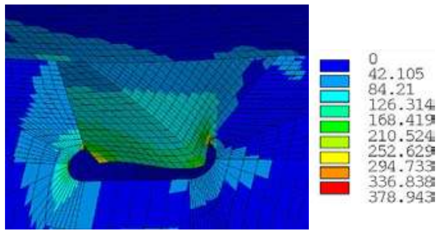

Figure 9.3 Distribution of v.- Mises stress, when rib height is 150 mm.

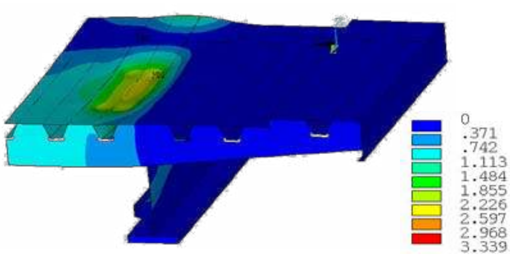

Figure 9.4 Distribution of resultant displacement, when rib height is 200 mm.

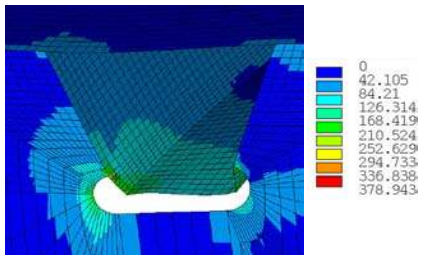

Figure 9.5 Distribution of v.- Mises stress, when rib height is 200 mm.

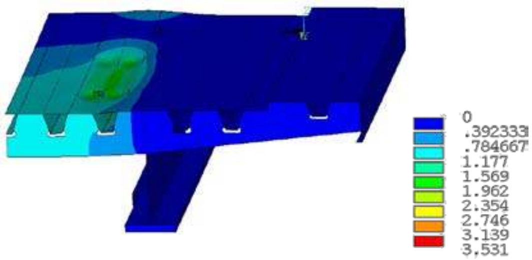

Figure 9.6 Distribution of resultant displacement, when rib height is 275 mm.

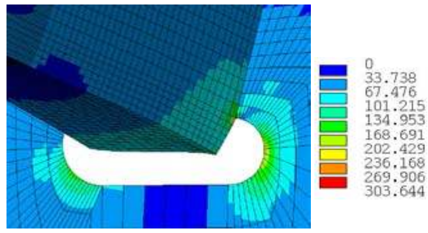

Figure 9.7 Distribution of v.- Mises stress, when rib height is 275 mm.

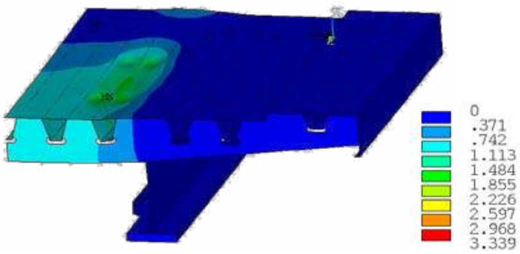

Figure 9.8 Distribution of resultant displacement, when rib height is 300 mm.

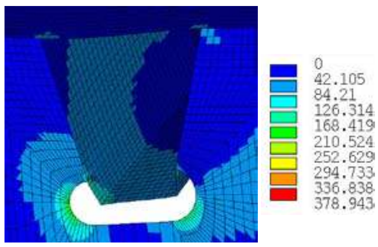

Figure 9.9 Distribution of v.- Mises stress, when rib height is 300 mm.

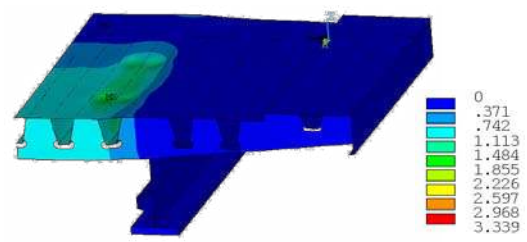

Figure 9.10 Distribution of resultant displacement, when rib height is 375 mm.

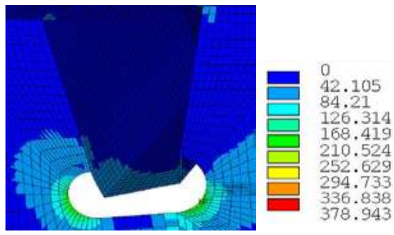

Figure 9.11 Distribution of v.- Mises stress, when rib height is 375 mm.

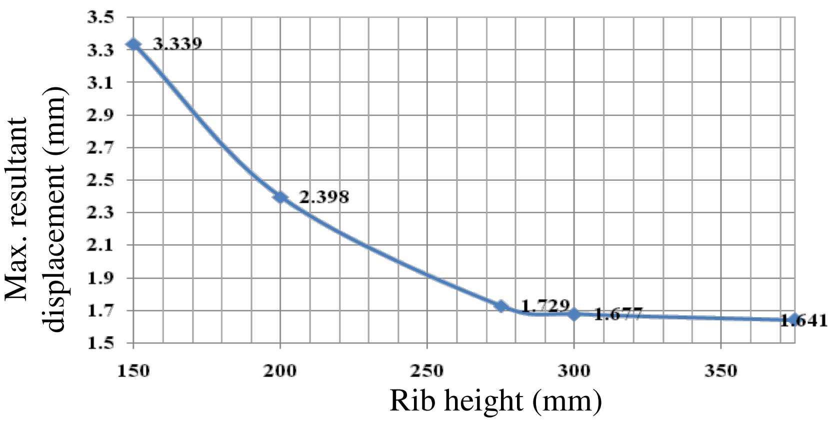

Figure 9.12 Variation of max. resultant displacement as to rib height.

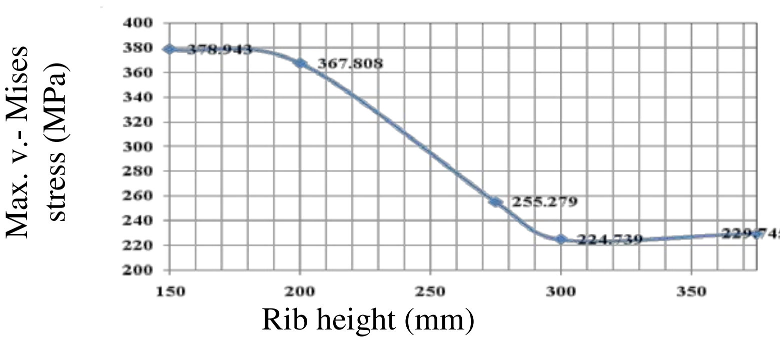

Figure 9.13 Variation of max. v.- Mises stress as to rib height.

Table 9.1 presents normal stress values as per type of structure and rib width to height ratio. Shear stresses developed in structural parts are so less that they are not included in the assessment of results. Regarding normal stresses, variation of rib height effects longitudinal max. tension stress in deck plate, in-plane stresses in cross-beam and normal stresses in ribs according to the stress values given in Table 9.1. Dependence of other stress components on rib height are of no importance as seen in Table 9.1. Increasing rib height results in lesser max. longitudinal tension stress in deck plate as given in Figure 9.14. Nevertheless, this stress decreases rapidly between rib heights of 150 mm and 275 mm and the slope of stress decrease becomes very small and can be assumed constant between rib heights of 300 mm and 375 mm.

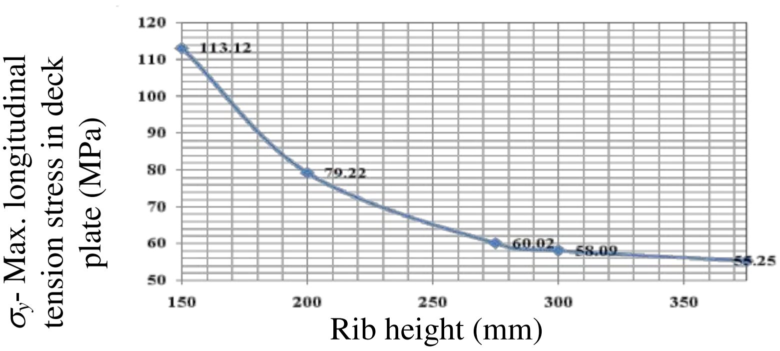

Figure 9.14 Variation of max. longitudinal tension stress in deck plate as to rib height.

Figure 9.15 illustrates the variation of in-plane stresses in cross-beam. Here max. vertical compressive in-plane stress increases steadily proportional to rib height. However this increase has a so small slope that the change of this stress component can be disregarded. Max. vertical tensional in-plane stress increases also steadily proportional to rib height with an almost constant slope and the change of this slope cannot be disregarded. This stress component takes its min. value (58.96 MPa) at the rib height of 150 mm and its max. value (162.08 MPa) at the rib height of 375 mm. Max. transversal both tensional and compressive in-plane stresses first decrease between rib heights of 150 mm and 275 mm, then increase between rib heights of 275 mm ad 350 mm.

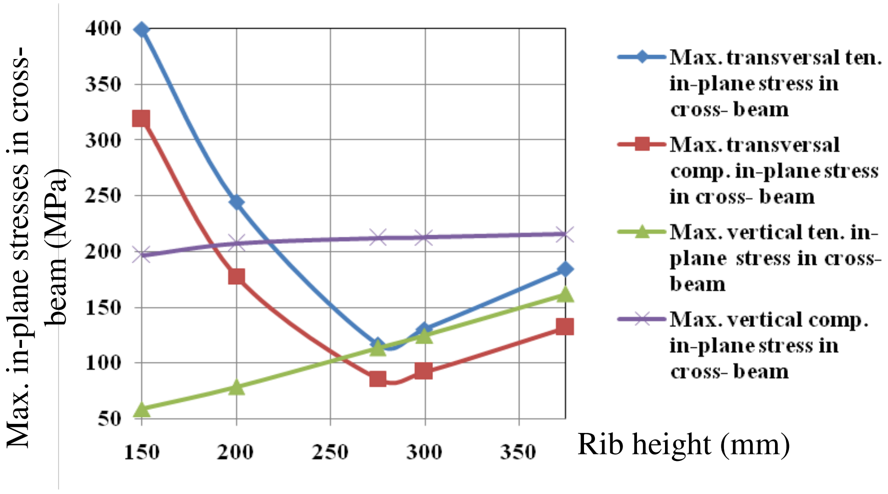

Figure 9.15 Variation of max. in-plane stresses in cross-beam as to rib height.

In trapezoidal ribs variation of all normal stresses is of importance and assessed subsequently as per Figure 9.16. Max. transversal stresses decrease rapidly between rib heights of 150 mm and 275 mm. The decrease of this stress component between 275 mm and 375 mm is almost of no importance. Max. longitudinal tension stress decrease until the rib height of 300 mm and increases between 300 mm and 375 mm. Max. longitudinal compressive stress decreases rapidly between rib heights of 150 mm and 300 mm and slightly between rib heights of 300 mm ad 375 mm. Max. vertical tension stress first increases between rib heights of 150 mm and 200 mm, then decreases rapidly between rib heights of 200 mm and 300 mm and then a slight decrease in this stress component occurs between rib heights of 300 mm and 375 mm. Max. vertical compressive stress decreases rapidly between rib heights of 150 mm and 275 mm and slightly between 275 mm and 300 mm, but afterwards increases slightly between rib heights of 300 mm and 375 mm.

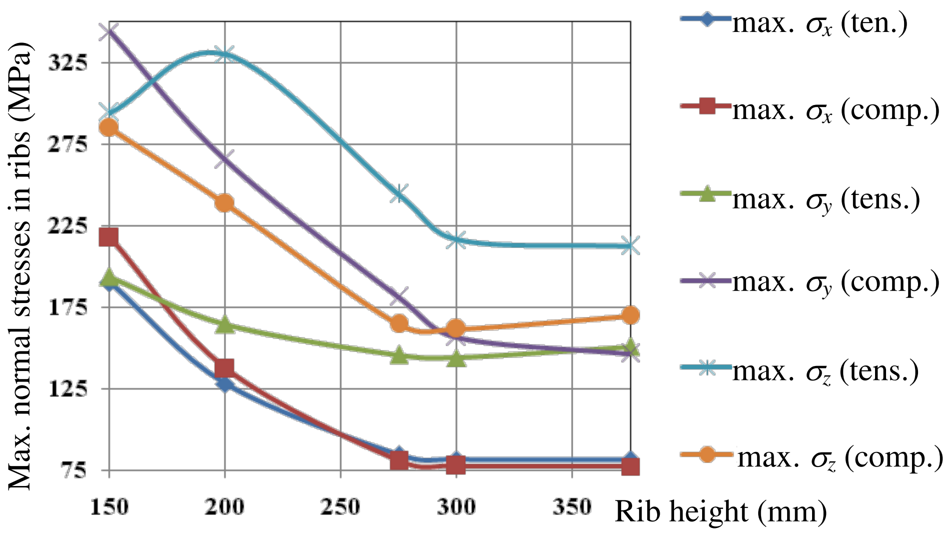

Figure 9.16 Variation of max. normal stresses in ribs as to rib height.

9.2 Rib spacing to deck plate thickness ratio

Table 9.2 and Table 9.3 show the stresses developed in deck plate, cross-beam and rib separately for different rib spacing to deck plate thickness ratios. In the FE-analyses of this parameter study rib width and height are always kept constant as 300 mm and 275 mm respectively, then variation of rib spacing to deck plate thickness ratio is evaluated separately. Initial values of rib spacing and deck plate thickness are 300 mm and 12 mm respectively and results of these FE-analyses for initial dimensional values are given in Figure 9.17 and Figure 9.18. Subsequently, four different FE-analyses are performed, when rib spacing equals 150 mm, 225 mm, 375 mm and 450 mm, while other dimensions of bridge are kept constant. Displacements of steel highway bridge depending on rib spacing to deck plate thickness ratio is assessed using contour graphics, which depict the change in max. resultant displacement. Figure 9.17, Figure 9.19, Figure 9.21, Figure 9.23, Figure 9.25 and Figure 9.35 illustrate the variation of max. resultant displacement on the whole bridge depending on rib spacing. As a result max. resultant displacement develops always in deck plate and increases proportional to rib spacing. In Figure 9.35 it is observed that the value at the rib spacing of 300 mm is out of this trend. The reason of deviation from trend line at this point is the place of wheel loads, which rest on deck plate and rib web at the rib spacing of 300 mm, while wheel loads rest solely on deck plate at the FE-analyses of other rib spacings. While the distance between wheel loads (axle distance of the vehicle) remains always same, the width of bridge changes in transversal direction as rib spacing changes. If wheel loads rested always on rib web and deck plate or only on deck plate, the slope of curve given in Figure 9.35 would always has a positive slope.

In the second set of FE-analyses instead of rib spacing, thickness of deck plate is changed to investigate the variations of displacement and stresses. Initial values of *a*, *b*, *e* and *t* (See Figure 9.1) are same as 300 mm, 275 mm, 300 mm and 12 mm respectively. Afterwards, four different new FE-analyses are done for t = 8 mm, 10 mm, 14 mm and 16 mm, while other dimensions of bridge are kept constant. Results of these FE-analyses are given below.From the assessment of Figure 9.17, Figure 9.27, Figure 9.29, Figure 9.31, Figure 9.32 and Figure 9.36 max. resultant displacement is inverse proportional to the thickness of deck plate and decreases as deck plate thickness increases. Eurocode 3 Part 2 [52] Annex C1.2.2 recommends $e / t \leq 25$ and $e \leq 300$ mm for design of orthotropic deck. According to this recommendation e = 300 mm and t = 12 mm provide min. conditions for design of orthotropic decks. Figure 9.36 shows that deviations from this min. condition by decreasing deck plate thickness results in localized and rapidly increased displacements in deck plate. This result is also valid if deviations from min. condition occur by increasing rib spacing as proven in Figure 9.35. Finally,numerical results obtained under wheel loads used in this thesis support recommendations of Eurocode 3 Part 2 [52] regarding rib spacing to deck plate thickness ratio based on the displacements developed in deck plate in terms of deformation criteria.Increasing rib spacing yields in increasing of v.- Mises stress as seen in Figure 9.37. The slope of the curve given in Figure 9.37 states that max. v.- Mises stress increases rapidly between rib spacing of 150 mm and 300 mm, nevertheless it increases with a decreasing slope after rib spacing of 300 mm, which is a point of inflection, where the sign of curve' s curvature changes. The cause of this "S" shape of curve is the changing of stress behavior between rib spacings of 150 mm and 300 mm. At the rib spacings of 150 mm and 225 mm max. v.- Mises stress rises in deck plate and in cross beam respectively as given in Figure 9.20 and Figure 9.22. At and after rib span of 300 mm max. v.- Mises stress develops always in the connection of rib and cross beam webs as given in Figure 9.18, Figure 9.24 and Figure 9.26. Accordingly, Figure 9.37 shall be seen as two curves before and after rib spacing of 300 mm, which is the min. recommendation of Eurocode 3 Part 2 [52] and satisfies the ratio, e / t = 25. Figure 9.38 reveals that increasing of deck plate thickness causes decreasing of max. v.- Mises stress. At the deck plate thickness of 8 mm, max. v.- Mises stress localized direct under wheel loads takes a very high value close to yield stress (see Figure 9.38). Therefore, deck plate thickness under 10 mm shall not be allowed in orthotropic decks under wheel loads used in this thesis. For deck plates having thickness higher than 8 mm, max. v.- Mises stress develops always in the connection between cross beam and rib webs as given in Figure 9.18, Figure 9.30, Figure 9.32 and Figure 9.34. The magnitudes of shear stresses in comparison with normal stresses developed in orthotropic deck are so less, that they are not involved in the assessment of results. The stress components, which vary essentially depending on rib spacing to deck plate thickness ratio are given in Figure 9.39 through Figure 9.44.

Table 9.2 Stresses developed in structural parts for different rib spacings (a = 300 mm, t = 12 mm, b =275mm)

Type of structure	Type of Stress (*MPa*)	e = 150 mm (e/ t = 12.5 and a / e = 2.00)		e = 225 mm (e/ t = 18.75 and a / e = 1.33)		e = 300 mm (e/ t = 25 and a / e = 1.00)		e = 375 mm (e/ t = 31.25 and a / e = 0.80)		e = 450 mm (e/ t = 37.5 and a / e = 0.67)	
		max. tens.	max. comp.	max. tens.	max. comp.	max. tens.	max. comp.	max. tens.	max. comp.	max. tens.	max. comp.
Deck plate	σ_x	122.88	116.39	137.44	129.40	135.11	136.05	157.61	159.15	182.05	179.53
		σ_x develops direct under wheel load, due to bending of deck plate. Max. comp. σ_x develops at top, while max. tens. σ_x develops at bottom of deck plate						Max. tens. σ_x develops at bottom of deck plate under wheel load closer to normal cross-beam. Max. comp. σ_x develops at top of deck plate under wheel load closer to stiffened cross-beam.		Max. tens. σ_x develops at bottom of deck plate under wheel load closer to stiffened cross-beam. Max. comp. σ_x develops at top of deck plate under wheel load closer to normal cross-beam.	
	σ_y	65.47	75.88	73.2	89.39	60.02	73.94	107.69	121.01	132.69	140.60
		σ_y develops under wheel load due to bending of deck plate.						Max. tens. σ_y develops at bottom of deck plate under wheel load closer to normal cross-beam. Max. comp. σ_y develops at top of deck plate under wheel load closer to stiffened cross-beam.			
	σ_z	~ 0									
Cross beam at field	σ_x	39.14	26.08	73.61	53.21	117.22	85.91	148.90	110.33	160.35	130.72
		σ_x develops at normal cross-beam cope hole rounds.						Max. tens. and comp. σ_x arise at the rib web, normal cross beam and cope hole connection points at opposite sides of cope hole.			
	σ_y	4.93	5.51	9.95	7.88	12.33	10.41	12.70	11.63	12.04	11.78
		σ_y develops at the bottom flange of normal cross-beam. Max. comp. σ_y develops at the top of flange plate, while max. tens. σ_y develops at the bottom of flange plate.									
	σ_z	26.09	81.87	56.60	151.53	113.51	212.20	152.95	221.21	157.21	187.85
		Max. tens. and comp. σ_z stresses develop at the rounds of cope hole. This cope hole is located in the interior side next to main-girder.									

Table 9.2 (cont'd)

	σ_x	27.48 25.00	32.11 32.33	84.14 80.49	108.94 110.66	142.21 140.79
		Both σ_x stresses develop at the bottom flange of rib adjacent to main girder. They arise in the longitudinal mid of bridge.	σ_x develops at the bottom flange of rib, where rib web connects to stiffened cross-beam		Max. tens. σ_x arises at bottom flange of rib, located longitudinally closer to stiffened cross-beam. Max. comp. σ_x arises at bottom flange of rib, located longitudinally closer to normal crossbeam.	Both σ_x stresses develop at the bottom flange of rib adjacent to main girder. They arise in the longitudinal mid of bridge.
Rib	σ_y	41.98 78.19	75.57 106.43	145.48 180.98	167.70 202.93	137.11 229.88
		Max. comp. σ_y develops at the bottom flange of rib adjacent to main girder. They arise in the longitudinal mid of bridge. Max. tens. σ_y develops at the bottom flange of rib adjacent to main girder, closer to stiffened crossbeam.	Max. comp. σ_y develops at the bottom flange of rib adjacent to main girder located longitudinally at normal cross-beam location. Max. tens. σ_y develops at the rib web longitudinally closer to stiffened crossbeam.	Max. tens. σ_y develops at the rib web closer to stiffened cross-beam. Max. comp. σ_y develops at the rib web to normal cross-beam connection. This rib is located next to main-girder.	Max. tens. σ_y arises at the rib web, located longitudinally at stiffened cross-beam position. Max. comp. σ_y arises at the rib web, located longitudinally at normal cross-beam position	Both σ_y develop at the opposite rib webs of the rib adjacent to main girder. Their position is longitudinally at the normal cross-beam location.
	σ_z	69.27 60.63	88.30 77.67	244.22 164.45	299.41 218.40	310.11 231.25
		Max. tens. σ_z develops at the rib web adjacent to main girder. Max. comp. σ_z develops at the rib web to deck plate connection, longitudinally closer to stiffened cross-beam.	Max. tens. σ_z arises at the rib web longitudinally very close to stiffened cross-beam. Max. comp. σ_z arises at the rib to deck plate connection longitudinally almost between normal and stiffened cross-beams.	Max. tens. σ_z develops at the rib web to normal cross-beam connection, while max. comp. σ_z develops at the rib web to stiffened cross-beam connection. This rib is located next to main girder	Max. comp. σ_z arises at the rib web, located longitudinally at stiffened cross-beam position. Max. tens. σ_z arises at the rib web, located longitudinally at normal cross-beam position	Both σ_z develop at the opposite rib webs of the rib adjacent to main girder. Their position is longitudinally at the normal cross-beam location.

*Please refer to Figure 1.3 for explanation of σ_x, σ_y and σ_z on finite elements, with which the whole structure is modeled.

Table 9.3 Stresses developed in structural parts for different deck plate thickness (a = e = 300 mm, b = 275mm)

Type of structure	Type of stress (*MPa*)	t = 8 mm (e/ t = 37.5)		t = 10 mm (e/ t = 30.0)		t = 12 mm (e/ t = 25)		t = 14 mm (e/ t = 21.43)		t = 16 mm (e/ t = 18.75)	
		max. tens.	max. comp.	max. tens.	max. comp.	max. tens.	max. comp.	max. tens.	max. comp.	max. tens.	max. comp.
Deck plate	σ_x	343.22	336.91	208.86	208.80	135.11	136.05	90.38	91.41	69.23	80.50
		Both σ_x arise at deck plate at deck plate under wheel load, longitudinally closer to normal cross-beam. Max. tens. σ_x arises at top, while max. comp. σ_x arises at bottom of deck plate.				σ_x develops direct under wheel load, due to bending of deck plate. Max. comp. σ_x develops at top, while max. tens. σ_x develops at bottom of deck plate		Both σ_x arise at deck plate under wheel load, longitudinally closer to normal cross-beam. Max. tens. σ_x arises at top, while max. comp. σ_x arises at bottom of deck plate.		Max. tens. σ_x arises at the bottom of deck plate, under wheel load, longitudinally closer to stiffened cross-beam, Max. comp. σ_x arises at bottom of deck plate, where deck plate connects to normal cross-beam.	
	σ_y	120.80	138.87	77.79	98.02	60.02	73.94	55.97	58.97	52.30	49.01
		Max. tens. σ_y develops at bottom of deck plate, closer to normal cross-beam, max. comp. σ_y develops at top of deck plate, closer to stiffened cross-beam.				σ_y develops under wheel load due to bending of deck plate.		Max. comp. σ_y arises at top of deck plate under wheel load closer to stiffened cross-beam. Max. tens. σ_y arises at top of deck plate, and deck plate to normal cross-beam connection.		Max. tens. σ_x arises at the bottom of deck plate, under wheel load, longitudinally closer to stiffened cross-beam, Max. comp. σ_x arises at bottom of deck plate, where deck plate connects to normal cross-beam.	
	σ_z	~ 0									
Cross beam at field	σ_x	131.58	90.12	124.04	87.85	117.22	85.91	116.81	84.09	115.91	82.28
		Max. tens. σ_x arises at rib, normal cross-beam and cope hole connection. Max. comp. σ_x arises at round of normal cross-beam's cope hole.				σ_x develops at normal cross-beam cope hole rounds		Both σ_x stresses develop in the round of normal cross-beam's cope hole.			
	σ_y	12.70	11.08	12.55	10.73	12.33	10.41	12.06	10.11	11.77	9.82
		Max. tens. σ_y develops at top of normal cross-beam's bottom flange, while max. comp. σ_y develops at bottom of flange.				σ_y develops at the bottom flange of normal cross-beam. Max. comp. σ_y develops at the top of flange plate, while max. tens. σ_y develops at the bottom of flange plate.		Max. tens. σ_y develops at top of normal cross-beam's bottom flange, while max. comp. σ_y develops at bottom of flange.			
	σ_z	111.94	222.45	113.16	217.83	113.51	212.20	113.24	205.93	112.47	199.28
		Max. σ_z stresses develop at the round of normal cross-beam cope hole.				Max. tens. and comp. σ_z stresses develop at the rounds of cope hole. This cope hole is located in the interior side next to main-girder.		Max. σ_z stresses develop at the round of normal cross-beam cope hole.			

Table 9.3 (cont'd)

Rib	σ_x	90.48	86.96	258.53	171.17	84.14	80.49	81.11	77.53	78.25	74.75
		Both σ_x stresses arise at bottom flange of rib adjacent to main girder and longitudinally at the stiffened cross-beam location.				σ_x develops at the bottom flange of rib, where rib web connects to stiffened cross-beam		Both σ_x stresses arise at bottom flange of rib adjacent to main girder and longitudinally at the stiffened cross-beam location.			
	σ_y	158.24	201.94	151.98	191.58	145.48	180.98	139.14	170.56	133.19	160.64
		Max. tens. σ_y develops at rib web adjacent to main girder, and longitudinally at the stiffened cross-beam location. Max. comp. σ_y develops at the rib web adjacent to main girder and longitudinally at the normal cross-beam location.				Max. tens. σ_y develops at the rib web closer to stiffened cross-beam. Max. comp. σ_y develops at the rib web to normal cross-beam connection. This rib is located next to main-girder		Max. tens. σ_y develops at rib web adjacent to main girder, and longitudinally at the stiffened cross-beam location. Max. comp. σ_y develops at the rib web adjacent to main girder and longitudinally at the normal cross-beam location.			
	σ_z	273.26	178.01	87.28	83.63	244.22	164.45	230.55	157.87	217.78	151.51
		Max.tens. σ_z arises at the rib web adjacent to main girder and longitudinally at the normal cross-beam location. Max. comp. σ_z arises at the rib web adjacent to main girder, and longitudinally at the stiffened cross-beam location.				Max. tens. σ_z develops at the rib web to normal cross-beam connection, while max. comp. σ_z develops at the rib web to stiffened cross-beam connection. This rib is located next to main girder		Max.tens. σ_z arises at the rib web adjacent to main girder and longitudinally at the normal cross-beam location. Max. comp. σ_z arises at the rib web adjacent to main girder, and longitudinally at the stiffened cross-beam location.			

*Please refer to Figure 1.3 for explanation of σ_x, σ_y and σ_z on finite elements, with which the whole structure is modeled.

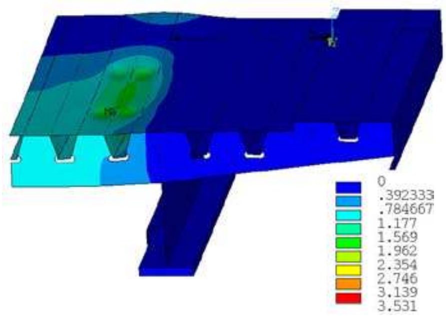

Figure 9.17 Distribution of resultant displacement, when t =12 mm and e = 300 mm.

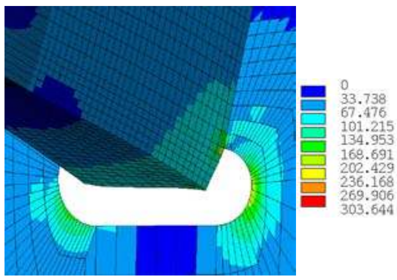

Figure 9.18 Distribution of v.- Mises stress, when t =12 mm and e = 300 mm.

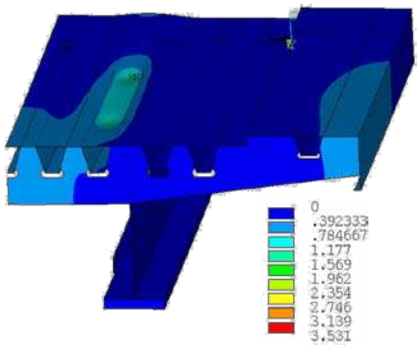

Figure 9.19 Distribution of resultant displacement, when t =12 mm and e = 150 mm.

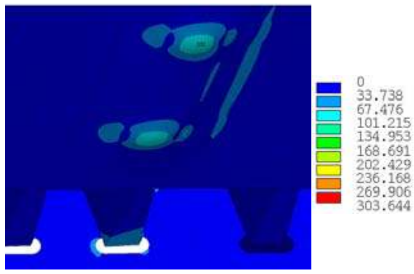

Figure 9.20 Distribution of v.- Mises stress, when t =12 mm and e = 150 mm.

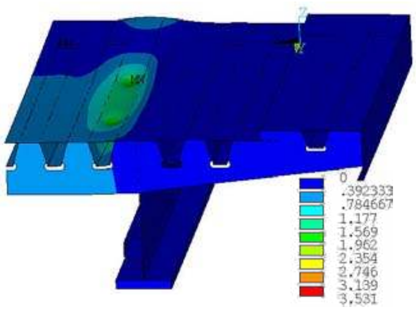

Figure 9.21 Distribution of resultant displacement, when t =12 mm and e = 225 mm.

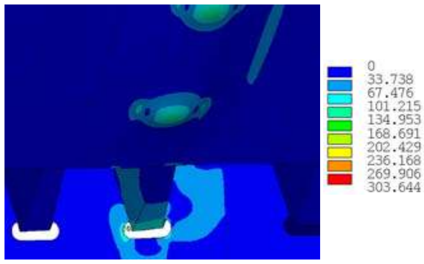

Figure 9.22 Distribution of v.- Mises stress, when t =12 mm and e = 225 mm.

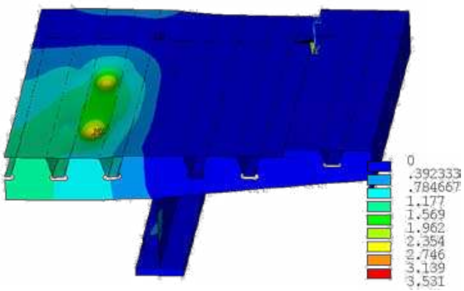

Figure 9.23 Distribution of resultant displacement, when t =12 mm and e = 375 mm.

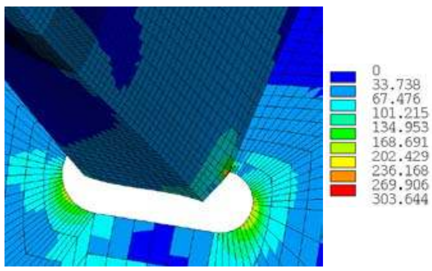

Figure 9.24 Distribution of v.- Mises stress, when t =12 mm and e = 375 mm.

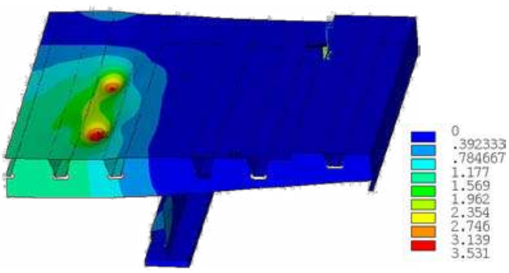

Figure 9.25 Distribution of resultant displacement, when t =12 mm and e = 450 mm.

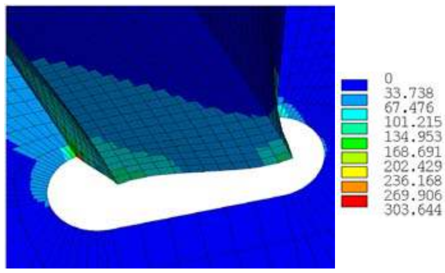

Figure 9.26 Distribution of v.- Mises stress, when t =12 mm and e = 450 mm.

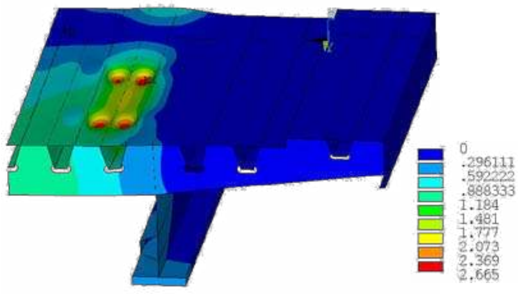

Figure 9.27 Distribution of resultant displacement, when t =8 mm and e = 300 mm.

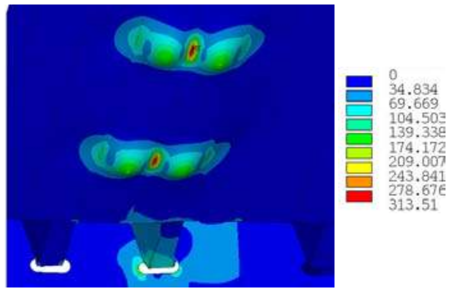

Figure 9.28 Distribution of v.- Mises stress, when t =8 mm and e = 300 mm.

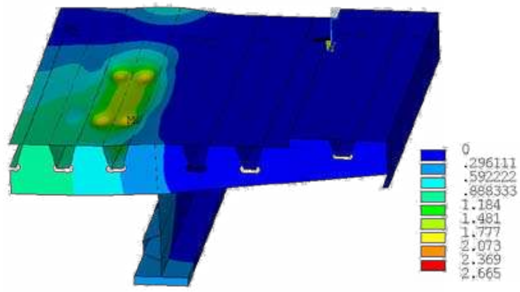

Figure 9.29 Max. disp. vector sum = 2.04 mm, when t =10 mm and e = 300 mm.

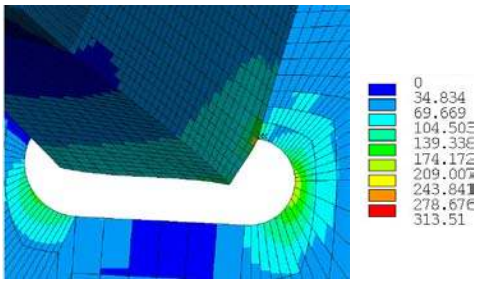

Figure 9.30 Distribution of v.- Mises stress, when t =10 mm and e = 300 mm.

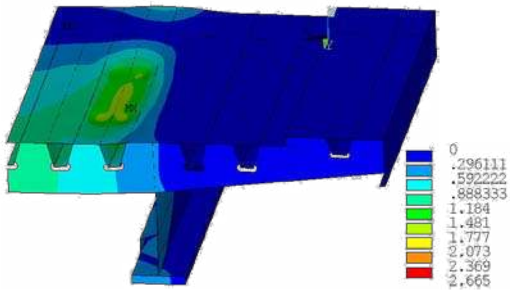

Figure 9.31 Max. disp. vector sum = 1.591 mm, when t =14 mm and e = 300 mm.

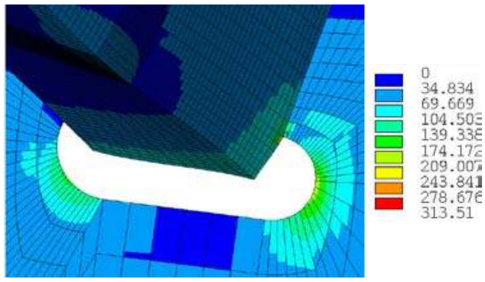

Figure 9.32 Distribution of v.- Mises, when t =14 mm and e = 300 mm.

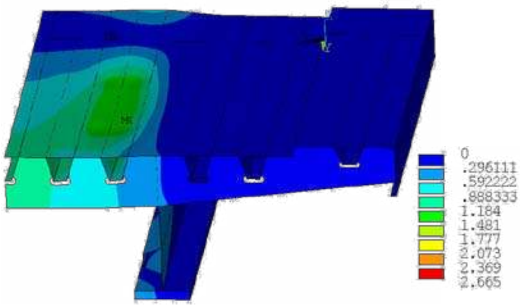

Figure 9.33 Max. disp. vector sum = 1.511 mm, when t =16 mm and e = 300 mm.

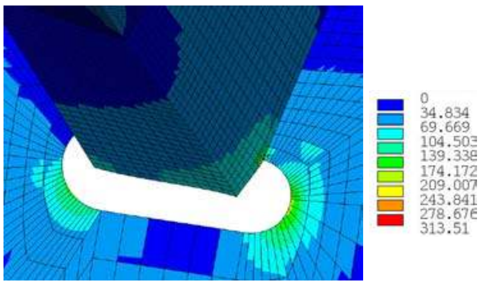

Figure 9.34 Distribution of v.- Mises, when t =16 mm and e = 300 mm.

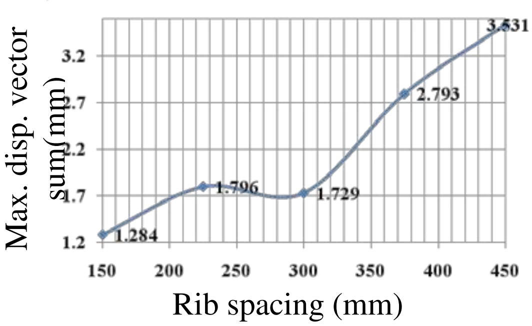

Figure 9.35 Variation of max. resultant displacement as to rib spacing.

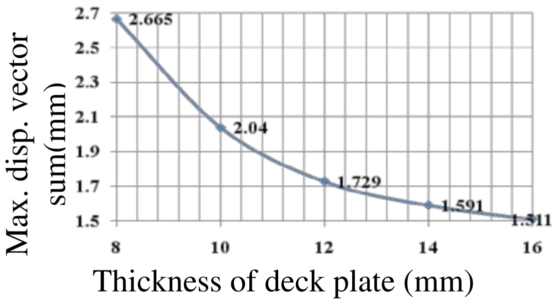

Figure 9.36 Variation of max. resultant displacement as to thickness of deck plate.

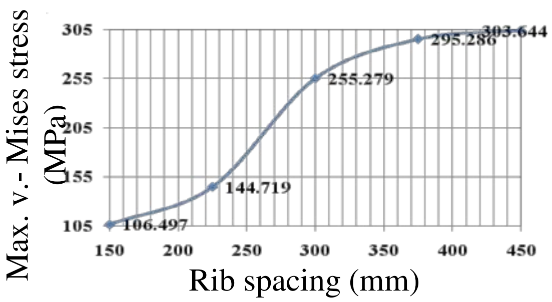

Figure 9.37 Variation of max. v.- Mises stress as to rib spacing.

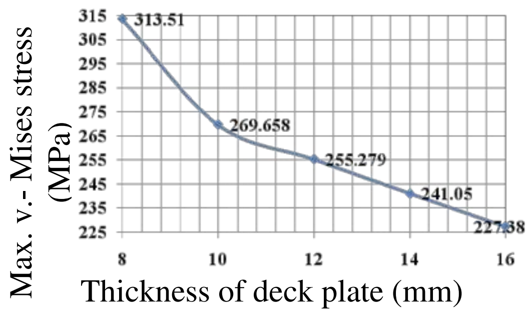

Figure 9.38 Variation of max. v.- Mises stress as to thickness of deck plate.

As seen in Figure 9.39 and in Figure 9.40 max. transversal and longitudinal stresses in deck plate increases with the increase of rib spacing and decrease of deck plate thickness. Variation of deck plate thickness results in slight changes in max. transversal in-plane stresses developed in cross beam and is inverse proportional with transversal in-plane stresses as given in Figure 9.42. However, increase of rib spacing causes rapidly higher transversal and vertical in-plane stresses in cross beam (See Figure 9.41).

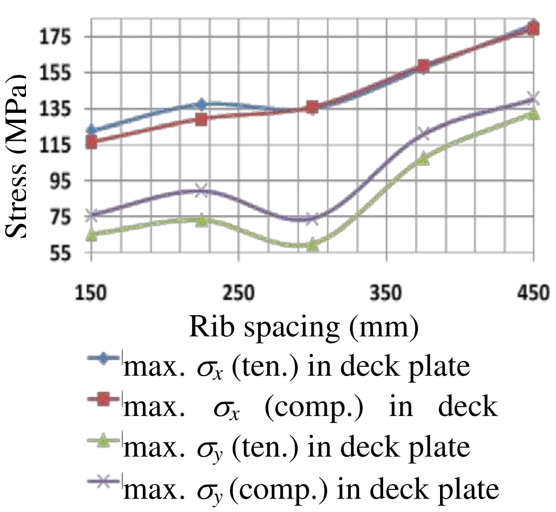

Figure 9.39 Variation of max. stress values in deck plate as to rib spacing.

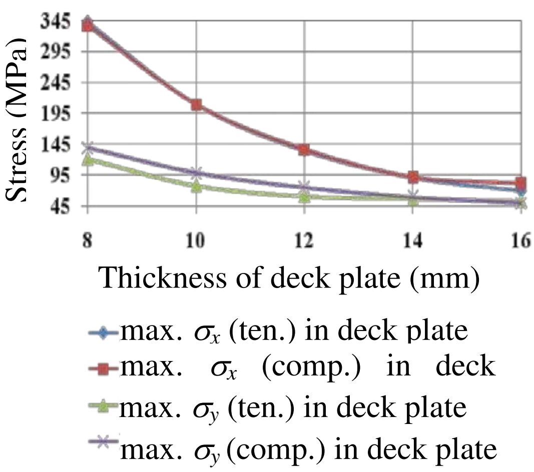

Figure 9.40 Variation of max. stress values in deck plate as to thickness of deck plate.

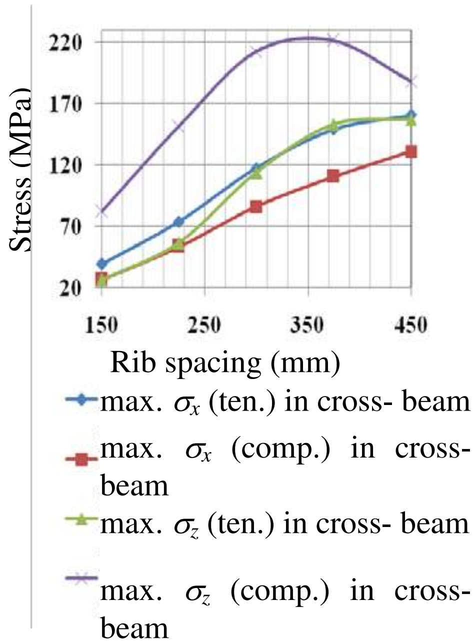

Figure 9.41 Variation of max. stress values in cross-beam as to rib spacing.

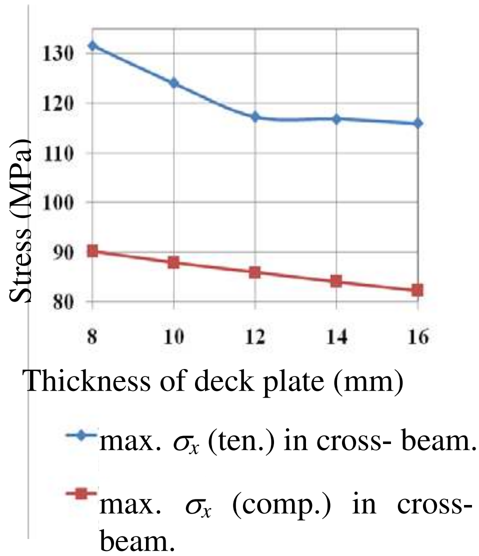

Figure 9.42 Variation of max. stress values in cross-beam as to thickness of deck plate.

All stress components developed in ribs are inverse linear proportional to deck plate thickness as given in Figure 9.44. According to Figure 9.43 transversal stresses in ribs almost do not change between rib spacings of 150 mm and 225 mm, however they increase rapidly proportional to rib spacing between rib spacings of 225 mm and 450 mm. Max. vertical stresses in ribs increase very slightly from rib spacings of 150 mm to 225 mm and from rib spacings of 375 mm to 450 mm. However, vertical stresses in ribs increase enormously from rib spacings of 225 mm to rib spacings of 375 mm. Longitudinal stresses developed in ribs increase also proportional to rib spacing as seen in Figure 9.43.

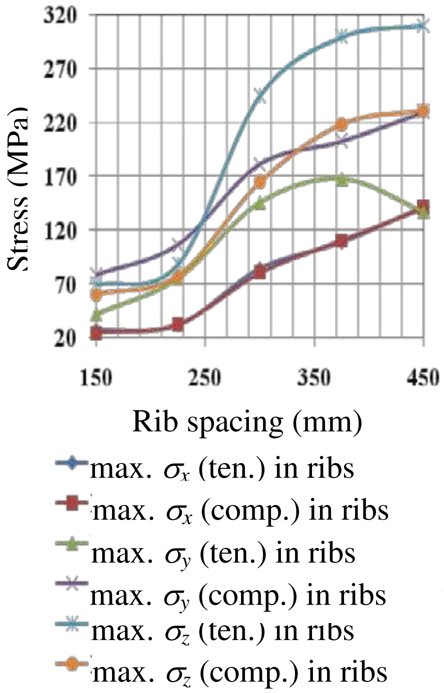

Figure 9.43 Variation of max. stress values in ribs as to rib spacing.

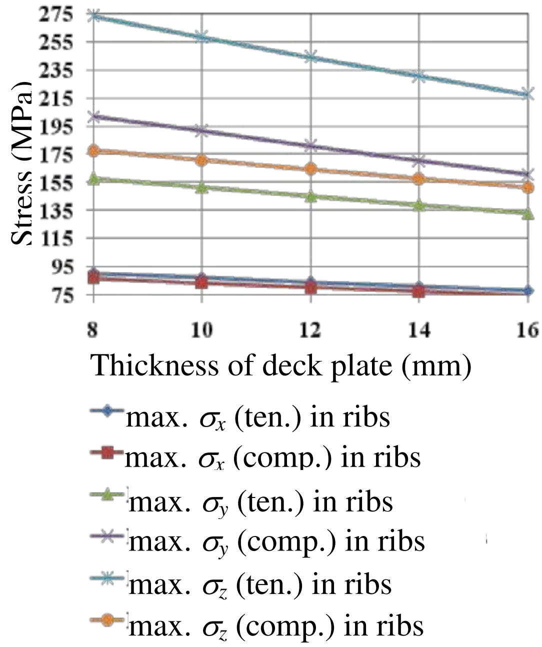

Figure 9.44 Variation of max. stress values in ribs as to thickness of deck plate.

There is an exception, that max. longitudinal (σ_y) tension stress decreases from rib spacings of 375 mm to rib spacing of 450 mm as seen in Figure 9.43, since the point and phenomenon of stress behaviors are different at rib spacing of 375 mm and 450 mm. The cause of this exception is explained in Figure 9.45. While max. tension and compression longitudinal stresses rise in the rib next to main girder at rib spacing of 375 mm, they develop at the second rib away from the main girder at rib spacing of 450 mm. The main reason of this issue is actually increasing the width of deck plate in transversal direction proportional to rib spacing, as the axle distance between wheel loads as to bridge' s midpoint (symmetry center) remains same (See Figure 9.46).

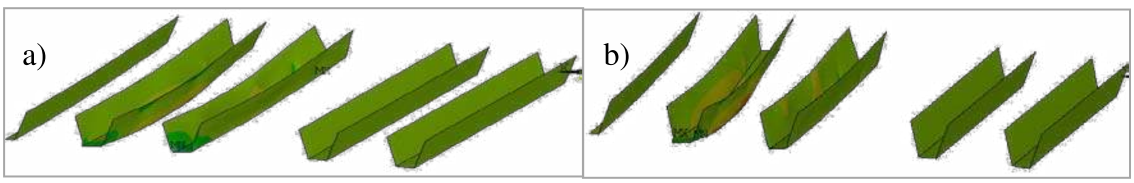

Figure 9.45 a) Max. longitudinal stress develops at rib spacing of 375 mm. b) Max. longitudinal stress develops at rib spacing of 450 mm.

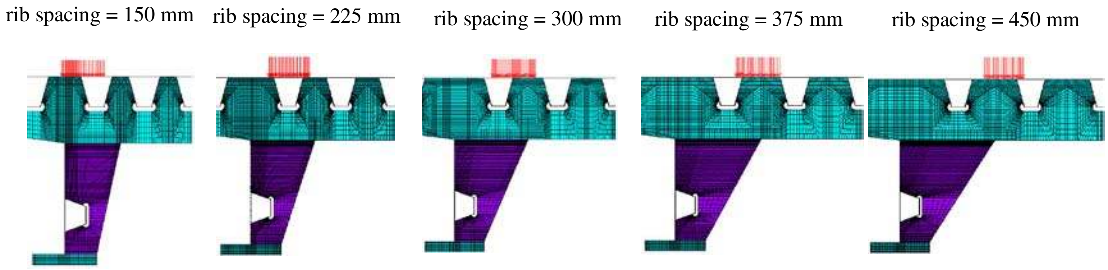

Figure 9.46 Wheel load positions depending on rib spacing.

9.3 Results & Discussion

It is investigated the influence of dimensional parametric ratios on the deformations and stresses developed in orthotropic deck. These dimensional parametric ratios are the rib width to height ratio and the rib spacing to deck plate thickness ratio under wheel loads employed in this thesis. It is concluded from the overall assessment of results that height of trapezoidal rib should be equal to its width with respect to used wheel loads, deck dimensions used in this thesis, deformations and stresses developed in orthotropic decks. Numerical results obtained in this thesis support recommendations of Eurocode 3 Part 2 [52] regarding rib spacing to deck plate thickness ratio as $e / t \leq 25$ and $e \leq 300$ mm under wheel loads used in this thesis. Deck plate thickness less than 10 mm leads to localized high stress concentrations direct under wheel loads and should not be allowed to be used for designing orthotropic decks. To avoid high to moderate stresses or stress concentrations in cross beam or in ribs, dimensional parametric ratios should be as $e / t \leq 225/ 12 = 18.75$ and $a / e \geq 300/ 225 = 1.33$ under wheel loads used in this thesis. To allow moderate stress values in orthotropic deck structure dimensional parametric ratios should be as $25 > e / t \geq 18.75$ and $1.33 > a / e \geq 1$. If $e / t >> 25$ and $a / e << 1$, stress concentrations at the intersection between rib and cross-beam webs together with yielding of material can occur under wheel loads used in this thesis. Of course, dimensions of orthotropic deck should be determined as per fatigue strength, however instead of repeating fatigue calculations after every FE-analysis, it is preferred in this thesis using v.- Mises stress, which is a function of stress phenomena at every structural point and a scalar value. As a result, v.- Mises stress is used for comparison of results of FE-analyses with each other. Consequently, dimensional parametric ratios investigated in this research are of great importance to define the places and values of max. stresses and so control the stresses developing in orthotropic deck.

CHAPTER 10

CONCLUSIONS AND RECOMMENDATIONS

In this thesis, the quantitative reasons of damages in steel highway bridges under conservative static wheel loads were investigated using FE- method by changing one chosen unique dimension, while keeping others costant. So as to make this investigation possible, all dimensions and spans of orthotropic steel bridge were defined as variables in well known commercial FE- method programme ANSYS by means of APDL (Ansys Parametric Design Language). Conclusions and recommendations of the thesis are given below.

Several researches from industry and academic world mention that orthotropic deck has a huge load carrying capacity beyond its yield point because of its integrated structure, in which deck plate forms top flanges of ribs, cross- beams and main girders, since it is welded to those structural parts. In this thesis this fact is numerically proven in chapter 2, because considering kinematic hardening in stress calculations proves that the structure does not fail and continues to carry load thanks ductile material property of steel, while plastic strains develop. However, if the overall results obtained from this thesis is evaluated, it is recommended that orthotropic deck shall be dimensioned as per its fatigue strength and load carrying capacity due to plasticity shall not be considered, if an orthotropic deck is requested to exhibit 100 years service life under foreseen design traffic category.

It is well known and expected that increasing deck plate thickness yields in less stress values in deck plate. Nevertheless, the degree of this effect and the influence of increasing deck plate thickness on the ribs and cross- beams were not numerically obtained so far to the knowledge of author, when the full geometry of the bridge is included in the FE- model. The numerical degree of v.-Mises stress relief for the investigated bridge geometry in deck plate is 31.5 %, when the deck plate thickness is increased from 12 mm to 14 mm. However, increasing deck plate thickness from 14 mm to 16 mm reduces v.-Mises stress only 10.6 % in deck plate. Therefore, increase in deck plate thickness does not linearly reduce v.-Mises stress in deck plate. Other numerical results obtained in chapter 3 proves that the increasing deck plate thickness has very little effects on ribs and cross- beams. Therefore it is recommended using deck plate thickness only to reduce the stresses in itself without considering stresses in other structural parts.

It is evaluated the effect of cross- beam spacing and web thickness on the deck plate, ribs and cross- beams in chapter 4. Numerical results indicated that decreasing cross- beam spacing mainly reduces rib stresses and deck plate deflections, on which wearing surface lies. Therefore it is recommended adjustment of cross- beam spacing is done as per rib stresses and max. deflection values stipulated by the manufacturer of wearing surface, which will be used in the construction of orthotropic deck. A max. permissible deflection value of wearing surface cannot be given here, because it depends on the wearing surface material type, and hence shall be taken from its manufacturer. Another recommendation extracted rom the numerical results of chapter 3 is determining web thickness of cross- beam for reducing stresses in cross- beam itself without any concern regarding dimensions of other load carrying steel member, since any change in cross- beam web thickness effects only stresses in cross- beam not other load- carrying members.

It is numerically proven in chapter 5, that there is a huge variation, when an orthotropic deck is designed as per material limit states and its fatigue strength. Steel ortotropic deck should be designed using fatigue calculation methods and fatigue strengths to obtained 100 years service life fot the foreseen design traffic category.

There was a lack of numerical foundation for the chart, which is given in Eurode 3 Part 2 and used for determination of deck plate thickness and rib dimensions without any need of making calculations. The numerical results of this thesis presented in chapter 6 comply with the correctness of this chart, if the limit stress analysis is used. Nevertheless, this thesis also indicates that design of ortotropic decks should be done using FE- models and fatigue calculation methods. As a result it is highly recommended building FE- model of the orthotropic deck, which is intended to be constructed, and evaluating its stress results as per fatigue strength to supply 100 years fatigue life instead of using the chart given in Eurocode 3 Part 2.

According to the results obtained in chapter 7, it is recommended using lowest web slope for ribs to the extent that the deflections in wearing surface are in permissible values as per its manufacturer’ s information.

Based on the numerical results obtained in chapter 8, it is recommended using Sikadur 30 as a bonding agent with bauxite aggregates in 10 mm thickness between steel deck plate and reinforced concrete wearing surface of 40 or 50 mm. After using the proposed wearing surface type it is recommended to increase the thickness of reinforced concrete wearing surface to decrease the stresses in deck plate, cross- beams and ribs, if the stresses shall be reduced. Apparently, the final value of wearing surface’s thickness shall be determined as per FE- analyses.

Based on the numerical results provided in chapter 9, it is recommended to set rib height to rib width in design phase of an orthotropic deck. Second, rib spacing should not be higher than rib width and should be used as a design parameter to determine the values of cross- beam stresses. It is recommended to use the design ratios given in this thesis for the initial design of orthotropic deck and check the final stress values using a FE- model used to analyze the orthotropic bridge, which is planned to be constructed.

Consequently, as overall recommendations for design of an orthotropic deck, it is recommended the steps given here are followed. First, the unsuitable wheel load and load cycle per year shall be determined. Second, the design category of bridge for 100 years service life shall be selected. Third, the initial dimensions of orthotropic deck shall be chosen as described here. That is a rib width equal to its height and not less than 300 mm, and a rib spacing not higher than 300 mm, preferable 200 mm. Cross- beam spacing shall be 3 m or less, whereas deck plate thickness shall not be less than 14 mm. Wearing surface shall be of reinforced concrete having thickness of at least 50 mm with 10 mm bonding agent of Sikadur 30. Other dimensions may be chosen from conventional design values. Fourth, the full geometry of the bridge shall be modeled coarsely using 1-D finite elements. The orthotropic steel deck under wheel loads shall be modeled using 2-D or 3-D finite elements. Between 1-D finite elements and 2- D or 3- D finite elements contact elements may be used, if it is necessary. After the FE- analysis is performed, stresses developed in the FE- model shall be used with S- N curves to calculate the fatigue life of bridge' s structural life. If the deflection in wearing surface is high, the thickness of wearing surface may be increased or the cross- beam spacing may be reduced. If the deck plate stresses are high, mostly the increasing of deck plate thickness would be beneficial, additionally; wearing surface's thickness may be increased. If the rib stresses are high, cross- beam spacing shall be decreased. If the cross- beam stresses are high, rib spacing shall be reduced and web slope of rib shall be reduced additionally. Fifth, the dimensions, spacings and spans of the orthotropic steel deck shall be revised and FE- analysis and subsequent fatigue life calculations shall be done. Finally, this last step shall be repeated, until the bridge provides 100 years service life as per fatigue calculations.

REFERENCES

[1] Jong, F.B.P.de, (2007). Renovation Techniques for Fatigue Cracked Orthotropic Steel Bridge Decks, Ph.D. Dissertation, Delft University of Technology, Delft.

[2] Honshu Shikoku Bridge Authority, www.hsba.go.jp, 17 January 2005.

[3] Fujino, Y. and Yoshida, Y., (2002). “Wind- Induced Vibration and Control of Trans- Tokyo Bay Crossing Bridge”, Journal of Structural Engineering, 128(8): 1012-1025.

[4] Virlogeux, M., (2004). “The Viaduct Over the River Tarn”, Conference Proceedings Steelbridge, OTUA, 23- 25 June 2004, Paris.

[5] Kennedy, D. J. L., Dorton R. A. and Alexander S. D. B., (2002). “The Sandwich Plate System for Bridge Decks” International Bridge Conference, 10- 12 June 2002, Pittsburgh.

[6] Troitsky, M.S., (1987). Orthotropic Bridges Theory and Design, Second Edition, The James F. Lincoln Arc Welding Foundation, Cleveland, OH.

[7] Huang, C. and Mangus, A., (2008). “Redecking Existing Bridges with Orthotropic Steel Deck Panels” Proc. of 2008 Orthotropic Bridge Conference, ASCE, 25- 29 August 2008, Sacramento, CA.

[8] Hoorpah, W., (2004). “Orthotropic Decks for Small and Medium Span Bridges in France– Evolution and Recent Trends” Proc. of 2004 Orthotropic Bridge Conference, ASCE, 23- 27 August 2004, Sacramento, CA.

[9] Korniyiv, M., (2004). “Orthotropic Deck Bridges in Ukraine.”, Proc. of 2004 Orthotropic Bridge Conference, ASCE, 23- 27 August 2004, Sacramento, CA.

[10] Choi, D., Kim, Y., Yoo, H. and Seo, J., (2008). “Orthotropic Steel Deck Bridges in Korea”, Proc. of 2008 Orthotropic Bridge Conference, ASCE, 25- 29 August 2004, Sacramento, CA.

[11] Connor, R. et al., (2012). Manual For Design, Construction, And Maintenance Of Orthotropic Steel Deck Bridges, US Department Of Transportation Federal Highway Administration, Publication No. FHWA-IF-12-027, Washington, D.C., USA.

[12] De Corte, W. and Philippe, V.B., (2007). "Improvements to the Analysis of Floorbeams with Additional Web Cut- outs for Orthotropic Plated Decks with Closed Continuous Ribs", Steel and Composite Structures, 7(1): 1- 18.

[13] Eggert, H., (1980). Vorlesungen über Lager im Bauwesen, Wilhelm Ernst & Sohn Press, Berlin, München.

[14] Giencke, E., (1960). "Die Berechnung von Hohlrippenplatten", Der Stahlbau, 1: 1-11 and 47- 59.

[15] Giencke, E., (1963). "Die Hohlplatte, eine Schubweiche Platte", ZAMM, 43(7/8): 311- 324.

[16] Pelikann, W. and Esslinger, M., (1957). Die Stahhfahrbahn, Berechnung und Konstruktion, MAN- Forchungsheft 7, Augsburg.

[17] BAST, (2005). Manuskript zum Expertengespräch: Instandsetzung orthotroper Fahrbahnplatten, Bundesanstalt für Straβenwesen, Bergish, Gladbach.

[18] Leendertz, J.S., (2008). Fatigue Behavior of Closed Stiffener to Cross- beam Connections in Orthotropic Steel Bridge Decks, Ph.D. Dissertation, Delft University of Technology, Delft.

[19] Sedlacek, G., (1971). "Einfaches Näherungsverfahren zur Berechung von Hohlplatten", Die Bautechnik, 1(6): 196- 201.

[20] Haibach, E. and Plasil, I., (1983). "Untersuchungen zur Betriebsfestigkeit von Stahlleichtfahrbahnen mit Trapezhohlsteifen im Eisenbahnbrueckenbau", Der Stahlbau, 9: 269- 274.

[21] Falke, J., (1983). Zum Tragverhalten und zur Berechnung von Querträgern orthotroper Platten, Ph.D. Dissertation, Technischen Universität Carolo-Wilhelmina zu Braunschweig.

[22] AISC, (1963). Design Manual for Orthotropic Steel Plate Deck Bridges, American Institute of Steel Construction, Chicago, USA.

[23] Eurocode 3 Part 1-9, (2003). Design of Steel Structures-Fatigue, European Committee for Standardization, Brussel.

[24] Kuhl, D. and Meschke, G., (2005). Finite Element Methods in Linear Structural Mechanics, Lecture Notes Ruhr University Bochum, Bochum.

[25] Kuhl, D. and Meschke, G., (2005). Advanced Finite Element Method, Lecture Notes Ruhr University Bochum, Bochum.

[26] Zienkiewicz, O.C. and Taylor, R.L., (2000). The Finite Element Method Volume 1: The Basis, Butterworth- Heinemann Press, Bristol.

[27] Zienkiewicz, O.C. and Taylor, R.L., (2000). The Finite Element Method Volume 2: Solid Mechanics, Butterworth- Heinemann Press, Bristol.

[28] Zienkiewicz, O.C. and Taylor, R.L., (2000). The Finite Element Method Volume 3: Fluid Dynamics, Butterworth- Heinemann Press, Bristol.

[29] Chrisfield, M.A., (2000). Nonlinear Finite Element Analysis of Solids and Structures Volume 1: Essentials, John Wiley & Sons Press, Chichester.

[30] Chrisfield, M.A., (2000). Nonlinear Finite Element Analysis of Solids and Structures Volume 2: Advanced Topics, John Wiley & Sons Press, Chichester.

[31] Belytschko, T. and Liu, W.K., (2001). Finite Elements for Continua and Structures, John Wiley & Sons Press, Chichester.

[32] Segerlind, L.J., (1984). Applied Finite Element Analysis, John Wiley & Sons Press, Chichester.

[33] Stolarski, T., Nakasone, Y. and Yoshimoto, S., (2006). Engineering Analysis with ANSYS software, Butterworth- Heinemann Press, Oxford.

[34] Moaveni, S., (1999). The Finite Element Analysis, Theory and Applications with ANSYS, Prentice Hall Press, New Jersey.

[35] Akin, J.E., (2005). Finite Element Analysis with Error Estimators, Butterworth & Heinemann Press, Oxford.

[36] Chen, Z., (2005). Finite Element Methods and Their Applications, Springer Press, Berlin, Heidelberg.

[37] Hutton, D.V., (2004). Fundementals of Finite Element Analysis, McGraw Hill, New York.

[38] Woolfson, M.M. and Pert, G.J., (1999). An Introduction to Computer Simulation, Oxford University Press, New York.

[39] Zimmermann, W.B.J., (2004). Process Modelling and Simulation with Finite Element Methods, World Scientific Publishing, Singapore.

[40] Hartmann, F. and Katz, C., (2007). Structural Analysis with Finite Elements. Springer Press, Berlin, Heidelberg.

[41] Munjiza, A., (2004). The Combined Finite- Discrete Element Method. John Wiley & Sons Press, Chichester.

[42] Liu, G.R. and Quek, S.S., (2003). The Finite Element Method, a Practical Course, Butterworth- Heinemann Press, Oxford.

[43] Rao, S.S., (2004). The Finite Element Method in Engineering, Elsevier Science & Technology Press, Miami.

[44] Kwon, Y.W. and Bang, H., (1997). The Finite Element Method, CRC Press, London.

[45] ANSYS, (2010). ANSYS: User Manuals, USA.

[46] Huurman et.al., (2002). “3D-FEM for the Estimation of the Behaviour of Asphaltic Surfacings on Orthotropic Steel Deck Bridges”, 3rd International Symposium on 3D Finite Element for Pavement Analysis, Design & Research, 2- 5 April 2002, Amsterdam.

[47] Fettahoglu, A. and Bekiroglu, S., (2012). “Effect of Kinematic Hardening in Stress Calculations”, Advanced in Civil Engineering, 17- 19 October 2012, Ankara.

[48] Fettahoglu, A., (2012). “Effect of Deck Plate Thickness on the Structural Behaviour of Steel Orthotropic Highway Bridges”, Advanced in Civil Engineering, 17- 19 October 2012, Ankara.

[49] Fettahoglu A., (2013a). “Arranging Thicknesses and Spans of Orthotropic Deck for Desired Fatigue Life and Design Category”, International Journal of Advances in Engineering & Technology, 6(4):1512- 1523.

[50] Fettahoglu A., (2013b). “A FEA Study Conforming Recommendations of DIN FB 103 Regarding Rib Dimensions and Cross-beam Span”, International Journal of Civil Engineering Research, 4(3):197- 204.

[51] Fettahoglu, A., (2013c). “Assessment on Web Slope of Trapezoidal Rrib in Orthotropic Decks Using FEM”, Sigma, Journal of Engineering and Natural Sciences, 32(1):52- 59.

[52] Eurocode 3 Part 2, (2006). Design of Steel Structures-Steel Bridges, European Committee for Standardization, Brussel.

[53] Eurocode 3 Part 1-1, (2001). Design of Steel Structures-General Structural Rules, European Committee for Standardization, Brussel.

[54] Paschen, M., (2008). Untersuchung zum Ermüdungsverhalten orthotroper Fahrbahnplatten, Ph.D. Dissertation, RWTH Aachen.

[55] Eurocode 3 Part 3, (2006). Actions on Structures, European Committee for Standardization, Brussel.

[56] PLANUNG UND ENTWICKLUNG IM BAUWESEN GmbH, ING.- BÜRO PROF. SEDLACEK & PARTNER, (2005). Untersuchung zur nachhaltigen Instandsetzung von orthotropen Fahrbahnplatten von Stahlbrücken unter Berücksictigung des Belagsystem. 2. Zwischenbericht FE 15.405/2004/CRB, Aachen.

[57] Sedlacek, G.; Paschen, M., (2005). Untersuchung zur Nachhaltigen Instandsetzung von Orthotropen Platten. In: BASt (Hrsg.): Manuskript zum Expertengespräch Instandsetzung Orthotroper Fahrbahnplatten.

[58] Medani, T.O., (2006). Design Principles of Surfacings on Orthotropic Steel Bridge Decks, Ph.D. Dissertation, Delft University of Technology, Delft.

[59] Bathe, K. J., (1996). Finite Element Procedures, Prentice-Hall, Englewood Cliffs.

[60] Mendelson, A., (1968). Plasticity: Theory and Application. The Macmillan Company, New York.

[61] Cook, D.R., Malkus, D.S. and Plesha, M.E., (1989). Concepts and Applications of Finite Element Analysis, John Wiley & Sons Press, New York.

[62] Simo, J. C. and Taylor, R.L., (1985). “Consistent Tangent Operators for Rate-Independent Elastoplasticity”, Computer Methods in Applied Mechanics and Engineering, 48:101- 118.

[63] Eurocode 1 Part 2, (2003). Actions on structures-Traffic Loads on Bridges, European Committee for Standardization, Brussel.

[64] Günther, G.H., Bild, St. and Sedlacek, G., (1985). “Zur Frage der Haltbarkeit von Fahrbahnbelägen auf Stählernen Straßenbrücken”, Der Stahlbau. 11:336-342.

[65] Klöppel, K. & Roos, E., (1960). “Statische Versuche und Dauerversuche zur Frage der Bemessung von Flachblechen in Orthotropen Platten”, Der Stahlbau, 29(12): 361- 373.

[66] Dowling, P.J., (1971). “The Behaviour of Orthotropic Steel Deck Bridges”, Conference, University of Cardiff, United Kingdom.

[67] Beales, C., (1979). Severn/Wye Bridge Project - Tests on Crossbeam Joints, Working Paper WP/BD 44, Transport Research Laboratory, Crowthorne, Berkshire, United Kingdom.

[68] Fisher, J.W., (1977). Bridge Fatigue Guide, Design and Details, American Institute of Steel Construction Inc., New York.

[69] Kolstein, M.H. and Back, J.de, (1989). Measurement and Interpretation of Dynamic Loads on Bridges, Phase 3, Fatigue Strength of Orthotropic Steel Decks, Part 2, Trough to Crossbeam Connections, Research sponsored by European Community of Steel and Coal, Delft University of Technology, Faculty of Civil Engineering, The Netherlands.

[70] Bruls, A., Caramelli, S., Cuninghame, J.R., Jacob, B., Kolstein, M.H., Lehrke, H.P.and Pautremat, E. Le, (1997). Measurement and Interpretation of Dynamic Loads on Bridges, Phase 4, Fatigue Strength of Orthotropic Steel Decks, Research sponsored by European Community of Steel and Coal, Report Delft University of Technology, Faculty of Civil Engineering, The Netherlands.

[71] Mangus, A.R. and Sun, S., (2000). Bridge Engineering Handbook: Orthotropic Deck Bridges, CRC Press, Boca Raton.

[72] Wolchuk, R., (1963). Design Manual for Orthotropic Steel Plate Deck Bridges, American Institute of Steel Construction, Chicago.

[73] Wolchuk, R., (1967). Structural Engineering Handbook: Steel-plate-deck bridges and steel box girder bridges, 4th ed., McGraw Hill, New York.

[74] Pouget, S., Suzéat, C., Di Benedetto, H., Olard, F., (2012). “Modelling of Viscous Bituminous Wearing Course Materials on Orthotropic Steel Deck”, Materials and Structures, 45:1115- 1215.

[75] Hanzik, V. and Luxemburk, F., (1978). "Die Eigenschaften von Guβasphalt bei Dauerbelastung", Bitumen, 40: 9- 13.

[76] Hondros, G., (1959). "Evaluation of Poisson' s Ratio and Modulus of Materials of a Low Tensile Resistance by the Brazilian (Indirect Tensile) Test with Particular Reference to Concrete", Australian Journal of Applied Science, 10(3): 243- 268.

[77] Fettahoglu, A., (2015). “,Assessment of stiffness moduli obtained from IDT test”, International Conference on Civil And Environmental Engineering, 20-23 May 2015, Nevsehir.

[78] Park, S.W., Kim, Y.R. and Schapery, R.A., (1996). "A Viscoelasting Continuum Damage Model and its Application to Uniaxial Behavior of Asphalt Concrete", Mechanics of Materials, 24: 241- 255.

[79] Schindler, K., (2008). Untersuchung des Verformungsverhaltens von Asphalt zur Bestimmung von Materialkennwerten für die Dimensionierung, Ph.D. Dissertation, Technischen Universitaet Carolo- Wilhelmina zu Braunschweig.

[80] Sedlacek, H., (1966). "Beläge auf Stahlfahrbahnen", Der Bauingenieur, 41(4): 121- 132.

[81] Sedlacek, H., (1968). "Vergleichende Studie über Verschiedene Belaege auf Stahlfahrbahnen von Bruecken in Relation zum Asphaltbelag", Der BAUINGENIEUR, 43(6): 199- 206.

[82] Buitelaar, P., Braam, R., and Kaptijn, N., (2004). “Reinforced High Performance Concrete Overlay System for Rehabilitation and Strengthening of

Orthotropic Steel bridge decks", Proc. of 2004 Orthotropic Bridge Conference, ASCE, Sacramento, 23- 27 August 2004, CA.

[83] Buitelaar, P., (2002). "Ultra Thin Heavy Reinforced High Performance Concrete Overlays", 6th International Symposium on Utilization of High Strength / High Performance Concrete, 16- 20 June 2002, Leipzig.

[84] Sika, www.sika.nl/tds_sikadur30_nl.pdf, 13 January 2006.

[85] Poulis, J.A., Borger, D.P., de Regt, P., (2000). Metingen Rijkswaterstaat, Het verlijmen van diverse materialen op staalplaten ten behoeve van brugdekversteviging, Delft, Rapport HI 2079.

[86] Erdogan, S., T. and Erdogan, T., Y., (2006). Sorular ve Yanitlariyla Beton, T.H.B.B., Istanbul.

CURRICULUM VITAE

PERSONAL INFORMATION

Name Surname : Abdullah FETTAHOĞLU

Date of birth and place :15.02.1979, Trabzon

Foreign Languages :English and German

E-mail :abdullahfettahoglu@gmail.com

EDUCATION

Degree	**Department**	**University**	**Date of Graduation**
Master	Structural Engineering	Istanbul Technical University	2003
Undergraduate	Civil Engineering	Istanbul Technical University	2001
High School	Natural Sciences	Trabzon Kanuni Anatolian High School	1996

WORK EXPERIENCE

Year	**Corporation/Institute**	**Enrollment**
2015	Avrasya University	Lecturer
2014	Freelancer	Dedicated to doctoral study

2013	Alsim Alarko	QA/ QC Chief
2012-13	Polat Joint Stock Company	Deputy Site Chief
2011-12	Trabzon Chamber of Commerce & Industry	Project Coordinator
2010	Saudi Arabian Baytur	QA/ QC Engineer
2008-09	Ferchau	Stress Engineer
2007	Enka	QA/ QC Engineer
2004-07	TU- Dortmund	Research Engineer (DAAD fellowship)
2002-2004	Istanbul University	Teaching Assistant

PUBLISHMENTS

Papers

1. Fettahoglu A., (2013). “Arranging thicknesses and spans of orthotropic deck for desired fatigue life and design category”, International Journal of Advances in Engineering & Technology, 6(4): 1512- 1523.

2. Fettahoglu A., (2013). “A FEA study conforming recommendations of DIN FB 103 regarding rib dimensions and cross-beam span”, International Journal of Civil Engineering Research, 4(3): 197- 204.

3. Fettahoglu, A., (2013). “Assessment on web slope of trapezoidal rib in orthotropic decks using FEM”, Sigma, Journal of Engineering and Natural Sciences, 32(1): 52-59.

4. Fettahoglu, A., (2015). "Effect of Cross- Beam on Stresses Revealed in Orthotropic Steel Bridges", Steel and Composite Structures, 18(1): 149- 163.

5. Fettahoglu, A., (2015). "Recommended Properties of Elastic Wearing Surfaces on Orthotropic Steel Decks", Steel and Composite Structures, 18(2): p.357-374.

6 Fettahoglu, A. and Bekiroglu, S., (2015). "Optimizing Rib Width to Height and Rib Spacing to Deck Plate Thickness Ratios in Orthotropic Decks", Gazi University Journal of Science, under review.

7 Fettahoglu, A., (2015). "Effect Of Time Step Size On Stress Relaxation", Sigma Journal of Engineering and Natural Sciences, under review.

8 Fettahoglu, A., (2015). "Selection Of Regression Function For Indirect Tensile Test Results", Sigma Journal of Engineering and Natural Sciences, under review.

Conference Papers

1. Fettahoglu A. and Omurtag M.H., (2003).“Vlasov Zemin Parametrelerinin İncelenmesi”, Mühendislik Bilimleri Genç Araştirmacilar I. Kongresi, 17- 20 February 2003, İstanbul.

2. Omurtag M.H, and Fettahoglu A., (2003). “Zeminle etkileşim içindeki ayrik plaklarda Vlasov parametrelerinin belirlenmesi”, XIII. Ulusal Mekanik Kongresi, 8- 12 September 2003, Gaziantep.

3. Fettahoglu, A. and Bekiroglu, S., (2012).“Effect of kinematic hardening in stress calculations”, Advanced in Civil Engineering, 17- 19 October 2012, Ankara.

4. Fettahoglu, A., (2012).“Effect of deck plate thickness on the structural behaviour of steel orthotropic highway bridges”, Advanced in Civil Engineering, 17- 19 October 2012, Ankara.

5 Fettahoglu, A., (2015). “Assessment of stiffness moduli obtained from IDT test”, International Conference On Civil And Environmental Engineering, 20- 23 May 2015, Nevsehir.

6 Fettahoglu, A., Bekiroglu, S., Bal, I. E., (2015). “Response spectral analysis of orthotropic steel deck as perTurkish local design spectrums”, International Conference On Civil And Environmental Engineering, 20- 23 May 2015, Nevsehir.

7 Fettahoglu, A., (2015). “Error Amount in Viscoelasticity Analysis Depending on Time Step Size and Method used in ANSYS”, ICCCGE 2015: 17th International Conference on Civil,Construction and Geological Engineering, 21- 22 May 2015, Istanbul.

8 Fettahoglu, A., (2015). “A Guide for Using Viscoelasticity in ANSYS”, ICCCGE 2015: 17th International Conference on Civil, Construction and Geological Engineering, 21- 22 May 2015, Istanbul.

AWARDS

1.2005-2006 DAAD fellowship